``

Self-assembled Photo-responsive Nanostructures for Smart Materials Applications

DISSERTATION

Presented in Partial Fulfillment of the Requirements for the Degree Doctor of Philosophy in the Graduate School of The Ohio State University

By

Mengmeng Liu

Graduate Program in Chemistry

The Ohio State University

2017

Dissertation Committee:

Professor Jonathan R. Parquette, Advisor

Professor Jovica D. Badjic

Professor Psaras L. McGrie

Abstract

Self-assembly is an important strategy of building materials at nanoscale from the "bottom up" pathway. Self-assembly of peptides and peptide derivatives has provided great inspiration for the design of functional materials ranging from biological engineering to optoelectronics. The design of successful self-assembly materials involve the comprehensive interaction and balance of attractions and repulsions in solution. Peptides and peptides hybrids are exceptional candidates for self-assembly structure design due to their great biocompatibility and bioactivity, versatile sequences and capacity to form various secondary structures.

We have designed and synthesized a type of spiropyran tetrapeptides conjugate. This smart material can undergo photo- and thermo- responsive self-assembly via ring closing/opening process on nanoscale and moreover, it can achieve the conversion between solution and gel states on macroscale under light and thermo- triggers. The conjugate can change into the closed spiropyran form and self-assemble into amyloid β-sheet fibrils and form networks that further gelation under visible light. When heated to over 60℃ in 0.75% TFA condition, the spiropyran moiety undergo ring-opening isomerization and changed into the protonated merocyanine form. This hydrophobic to hydrophilic conversion renders the disassembly of fibrils and the gel changes back into

solution state. Thus we have developed a novel smart photo- and thermo-controlled assembly and gelation material.

We have also prepared a series of simple spiropyran monopeptide and dipeptides hybrids. The spiropyran piece is a versatile photo-responsive chromophore as it can convert among three different states. The three designed spiropyran monopeptide conjugates adopt different assembly structures through visible light irradiation. The Fmoc-dipeptide conjugates also have photo-controlled assembly and thermo-controlled disassembly via ring closing/opening process. Although the transformation of the ring-opening process was not ideal in water solvent, this type of compounds is simple and convenient to synthesis, and can shed light to future photo-controlled smart material study.

Dedication

This document is dedicated to my parents Fan Liu and Hui He, to my husband Wei Wang, and to my family and friends.

Acknowledgments

I would like to express my sincere appreciation to my advisor, Dr. Jon R. Parquette, who has been my mentor that assists me and guides me through the graduate study. You are always so nice, kind and responsive to us and always encourage us when I am confused. Your scientific vision and knowledge greatly inspired and enlightened me when I encounter difficulties in research. Besides, your support and encouragement to my every little progress are very precious to me. I would never be able to make this far without your kind guidance and encouragement.

I would also like to thank the Parquette group members, both in the past and present. My thanks go to Dr. Se Hye Kim and Dr. Nicholas A. Bewick for teaching and training me on plenty of devices and fundamental operations. I would also like to thank Dr. Yuan Sun, Dr. Aileen Shieh and Dr. Mingyang Ji for your kindness support and great assistance in solving problems during the research. I would like to thank all my colleagues and I'm so glad to work with you and be a member in the nice Parquette group.

I would especially thank Dr. Jovica D. Badjic, Dr. Psaras L. McGrier and Dr. Carlos Ernesto Castro for their kind instructions and generous assistance.

This material is based upon work supported by the U. S. Army Research Laboratory and the U. S. Army Research Office under contract/grant number W911NF1410305.

Vita

2007.....Wuhan Foreign Languages School

2011.....B.S. Chemistry, College of Chemistry and Molecular Science, Wuhan University

2011 to present .....Graduate Teaching Associate, Department of Chemistry and Biochemistry, The Ohio State University

Fields of Study

Major Field: Chemistry

Table of Contents

List of Tables

List of Schemes

List of Figures

Chapter 1: Self-assembly of Peptides Derivatives

1.1 Introduction

Self-assembly is by definition, the process of automatic arrangement of components into ordered structures or patterns without outside forces or guidance.[1-2] It is one of the most common phenomena in nature world and can be discovered in various aspects, ranging from the tiny molecular arrangement to large scale planetary movement[1]. Generally, self-assembly is classified into two types: the static self-assembly and the dynamic self-assembly. In, static self-assembly, after components form an ordered structure, the system tend to stabilize and hardly release any energy when reach equilibrium. Typical examples are ionic crystals,[3] liquid crystals and phase-separated polymers.[4] On the contrary, dynamic self-assembly are assemblies that formed by local interactions of different structures in a pre-organized pattern to reduce energy.[5-6] Bacteria colony and solar system are examples of dynamic assemblies. Various types of self-assembly are closely related to the living creatures on earth, like the double helix of deoxyribonucleic acid (DNA) and the secondary, tertiary and quaternary structures of proteins (Figure 1). The self-assembly strategy has been applied to many fields in real life. In particular, plenty of chemists are interested in molecular self-assembly, which is

defined as the process of molecules arrange into defined patterns without outside human interference or management.[2, 7-8]

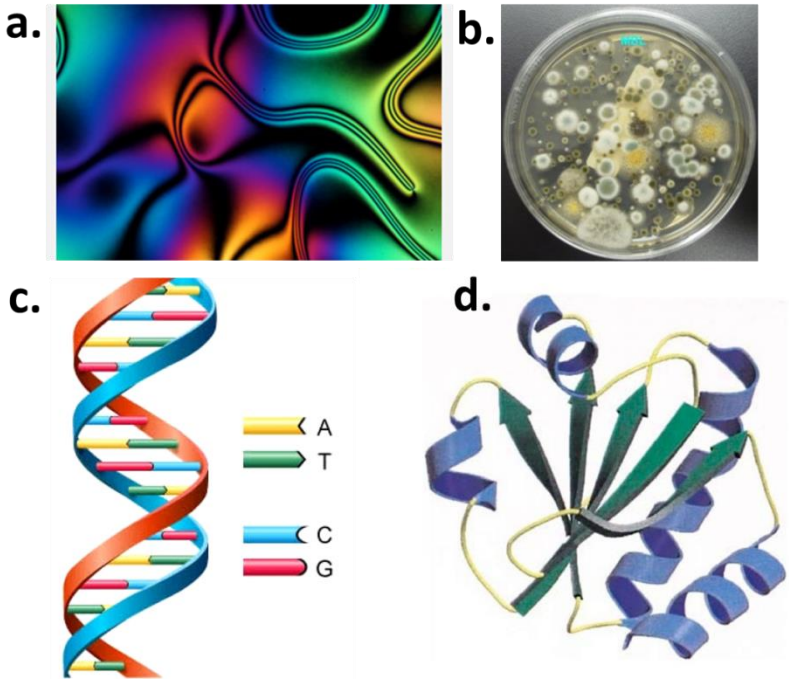

Figure 1. Examples of self-assembly in nature. a) liquid crystal; b) bacterial colony; c) double helix structure of DNA; d) secondary and tertiary structures of protein.

The self-assembly strategy has given important insights to the development of nanotechnology since well-ordered structures in nanoscale can be established from single molecules as building blocks. This is known as the "bottom up" process to construct the nanostructures within anticipated scale range, which is from 1 nm to 100 nm (Figure 2). [9-14] The "bottom up" strategy is a completely different pathway of generating nanostructures within this range as opposed to the "top down" approaches such as lithographic patterning.[15-16] During the molecular self-assembly process, the molecules interact with each other as small units and then associate and generate larger structures

from one-dimension to three-dimensions.[17] These self-assembly nanostructures can be applied to a great number of aspects such as drug-delivery,[18-20] 3-D scaffold,[21-23] tissue engineering,[24-26]optoelectronics[27-28] and optical graphing.[29]

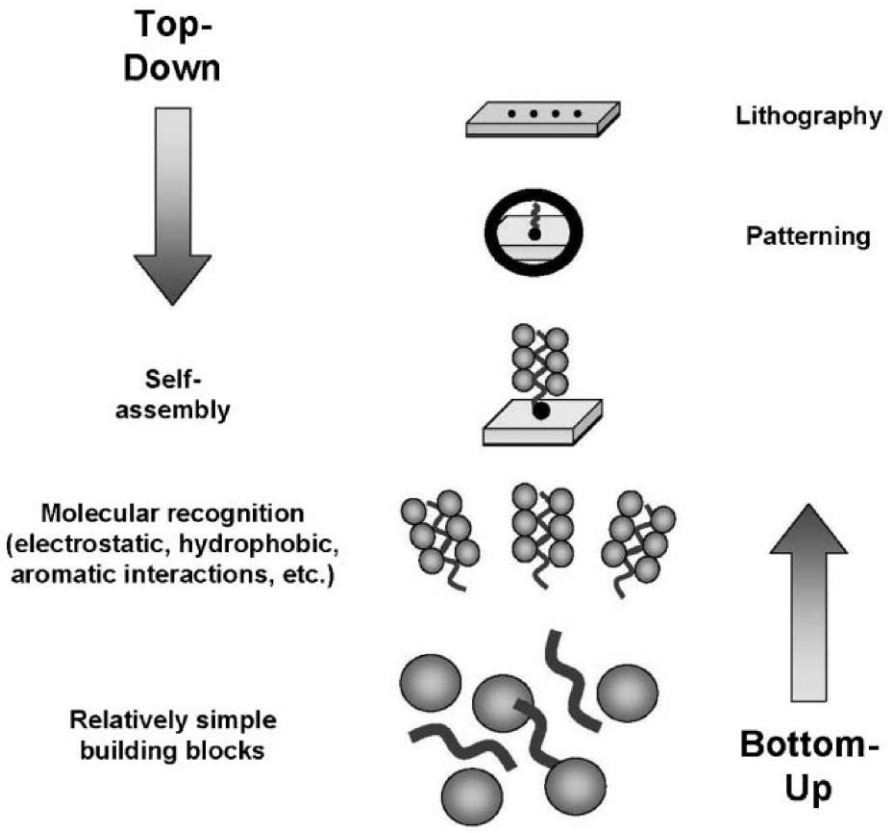

Figure 2. The process of "top-down" as compared to "bottom-up" self-assembly. Copyright 2007 The Royal Society of Chemistry**.**[11]

To achieve this spontaneous association, the small building blocks need to have specific recognition between each other, which is various types of non-covalent forces, such as hydrogen-bonding, hydrophobic interactions, electrostatic interactions, π-π interactions and Van der Waals force.[30] Nature also offers a wide selectivity of

building blocks changing from inorganic pieces to organic structures. On one hand, carbon structures such as carbon nanotubes and buckminsterfullerene were the building materials in early nanotechnology study. Later, increasing numbers of inorganic materials were involved in the selection pools, such as silicon nanotubes and fullerene-like structures formed by NbS_2 and WS_2. On the other hand, diverse organic compounds also offer a plethora of possible choices. A great number of different polymeric materials were designed and synthesized in industry for daily need, such as polyethylene, nylon, polytetrafluoroethylene (Teflon) and polyvinylchloride (PVC). Polypeptides and proteins are also widely used in many industries.

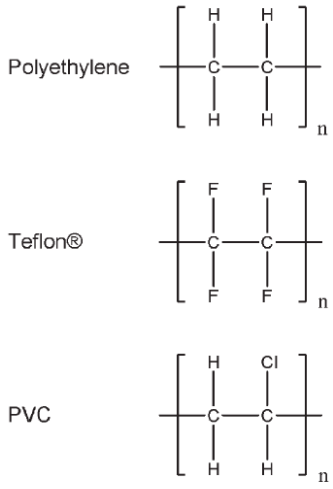

Figure 3. Structures of some common commercially available polymers: Polyethylene, Teflon and PVC.[11] Copyright 2007 The Royal Society of Chemistry.

Although a wide range of inorganic and organic compounds have been chosen as building blocks to design self-assembly nanostructures, the detailed mechanism and

precise manipulation of the assembly process remain unclear for a number of cases. Herein, a brief introduction is given to discuss the principle in designing self-assembly structure and some applications of self-assembled nanostructures, especially nanostructures consisting peptides structures.

1.2 The forces behind the self-assembly

The forces involved in the self-assembly process are non-covalent interactions rather than strong covalent bonding. The noncovalent are generally weak (2–250 kJ mol^{-1}) in comparison with the covalent bond energy (100–400 kJ mol^{-1}).[31] However, upon accumulation, the non-covalent forces, including hydrogen-bonding, hydrophobic effects, electrostatic interactions, π-π interactions, Van der Waals force and metal coordination, are adequate to induce the self-assembly behavior.

1.2.1 Hydrogen bonding

Hydrogen bonding is the attraction between an electronegative atom and a hydrogen atom which is in close distance and connected to another atom. In the hydrogen bond system, the electronegative atom that attracts nearby hydrogen is defined as hydrogen-bond acceptor (Figure 1.4). The hydrogen-bond acceptors are usually electronegative atoms such as halogens (F, Cl, Br, I), oxygen (O) and nitrogen (N) can offer lone pairs to attract hydrogen.[32] The hydrogen attached to the other atom being attracted is referred as the hydrogen bond donor.[33] This interaction can be either intermolecular or intramolecular. This attraction is much weaker than the regular covalent bonding forces, but is cumulative in the construction of assembly structure. For instance, in DNA, there

are three hydrogen bonding structures between one of the base pairs: guanine and cytosine, which help stabilizing the DNA double-helix structure in general.[34]

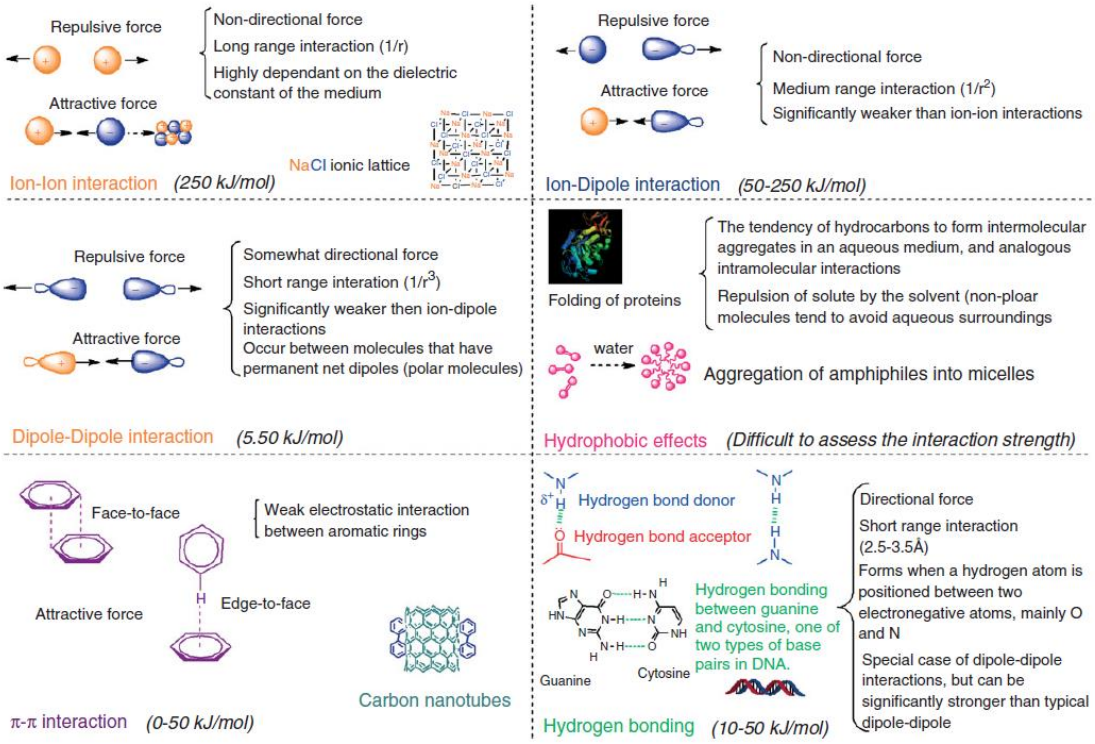

Figure 4. Examples of some noncovalent interactions involved in self-assembly and their corresponding strength. [31, 35-36] Copyright 2013 Wiley Periodicals.

1.2.2 Hydrophobic effect

Hydrophobic effect is a type of interaction induced in polar solvent.[37] In polar solvent, the hydrophobic components inside the molecules have the tendency of gathering together to reduce the surface that interacts with the polar solvent. This aggregation process is usually favored as the free energy ΔG decreases.[38] Although the entropy S is also decreased as the system changes from a less-ordered state to a more defined state

with the hydrophobic parts aggregating together and the hydrophilic or less hydrophobic part on the surface, the change in enthalpy can still enables the decrease of free energy in general.[39] The hydrophobic interaction is a strong contributor for a great number of amphiphilic structure assemblies in aqueous solvent.[40-41]

1.2.3 Electrostatic interactions

Electrostatic interactions are also called the coulombic forces. These interactions can be either attractions or repulsions according to the charges. If the two components carry the same type of charges, then the electrostatic interaction will be repulsion. In contrast, if one component carries the positive charge(s) or partially positive with the other carries negative charge(s) or partially, the interaction will be attraction.

Attractive Force	**Repulsive Force**
Van der Waals	Electric repulsion (same charge)
Hydrophobic	Steric Interaction
π- π stacking	
Hydrogen Bonding	
Coordination bond	
Electric repulsion (opposite charge)	

Table 1. Representative intermolecular attractive and repulsive forces for self-assembly.[30] Copyright 2008 John Wiley & Sons.

These forces decrease dramatically as the distance increase. The effect can be discovered between ion and ion, ion and dipole. Electrostatic interactions provide

effective assistance in tuning the assembly and disassembly process by adjusting the charged components in each building block.

1.2.4 Aromatic stacking

Aromatic Stacking is also referred to as π-π interaction. It is the attraction between the aromatic rings and results from the p-orbital interactions in the aromatic systems. The aromatic ring is an electron rich system, the conjugated π-orbitals can attract nearby electropositive or partially positive molecules or other aromatic π-orbitals. In a benzene ring, the polar bond C-H makes the benzene ring plane partially positive as carbon (C) is more electronegative than hydrogen (H). Correspondingly, there are two negative electron cloud formed both on top and blow the benzene ring. There are two types of most well-known aromatic interactions between two aromatic components. The first type is a face-to-face parallel displaced interaction,[42] the interaction arisen from the quadrupoles of aromatic rings.[43] The second type is the T-shape interaction. One benzene ring has a positive-negative-positive sandwich quadrupole alignment, it can attract the nearby benzene ring in two these fashions. When benzene rings are aligned on parallel position, the positive middle part is placed close to the negative electron cloud of the other one. For the second type, the positive middle part attracts the electron cloud of the other benzene ring in the perpendicular direction, which forms T-shape structure. π-π interactions have placed an important role in molecular recognition, protein-folding and material science.[44]

1.2.5 Van der Waals forces

Van der Waals forces are the attractions and the repulsions between molecules that generated from neither covalent bonds nor electrostatic interactions, including dipole-dipole interaction, dipole-induced dipole interaction and London forces.[45] Dipole-dipole interaction is a directional force between the two dipoles, namely attractive between a positive and a negative dipole and repulsive between two same types of dipoles. It decreases drastically as the distance increase ($1/r^3$) and is much weaker than the ion-dipole interaction.[31] Dipole-induced dipole force is even weaker than the dipole-dipole interaction. London dispersion force is the attraction between a pair of molecules as their temporary multipoles attract each other. It is the weakest intermolecular force. In general, Van der Waals forces are rather weak and short-range forces.[46] Therefore, they are only effective between the closest molecules. Except for dipole-dipole interaction, Van der Waals forces are non-directional. Van der Waals interaction does not place a significant influence in many self-assembly process. Nevertheless it is a contributory factor in some assembly cases like the self-assembly of the oligopeptides.[47]

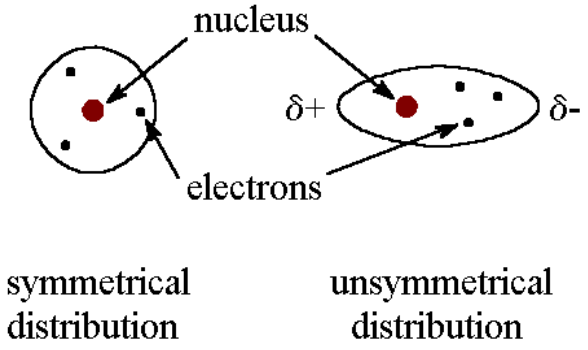

Figure 5. Illustration of generating London dispersion force. Copyright www.chem.purdue.edu

In summary, the successful self-assembly system requires the balance between the attraction and repulsion. As displayed in table 1.1, Hydrogen Bonding, Van der Waals forces, hydrophobic interactions, π- π stacking, electrostatic interaction between opposite charges are the possible attraction forces during the self-assembly process. The electric repulsion between same charges and the steric interaction are the possible repulsion forces during the self-assembly process. If there is too much attraction, the sample will tend to form oversized aggregates and further precipitate out rather than dissolve in the solution. If there is too much repulsion among the monomers, the building blocks will not associate together to establish larger aggregates. Hence, both attraction and repulsion are essential and need to be involved in the design of self-assembly systems.

1.3 Protein and peptides based self-assembly nanostructures.

Peptides and proteins are the common and irreplaceable components of living creatures on earth, from tiny single cell animal, paramecium, to the largest mammals, whales. The proteins perform a huge variety of diverse functions in living organisms in biological world. They are the structural elements of creatures' body, responsive to outside stimuli, involving in DNA replication process and assist the metabolism as catalyst in numerous reactions. Amino acids are the building blocks of proteins and peptides. Therefore, peptides and protein derivatives generally have great biocompatibility and bioactivity. There are about 500 known different amino acids, which provide an immense poll of possible selections of peptides sequences for the self-

assembly nanostructure materials. Among them, there are 20 types of common proteinogenic amino acids that are straightly involved in the protein synthesis in human body. Having the carboxylic acid and amine groups, all amino acids are capable of carry charges even slightly basic or acidic conditions to provide the electrostatic interactions. The different charge repulsion or attraction can be achieved by alternating amino acid sequences or adjusting pH. A considerable number of amino acids have hydrophobic side chains that can offer hydrophobic interactions. Several amino acids have aromatic benzene rings that may provide aromatic stacking. By arranging differently into certain sequences, amino acids can generate different peptides structures that can form hydrogen bonding. For instance, hydrogen bonding can be discovered in a number of common peptides secondary structures, such as α-helix, β-sheets or β-hairpins. All above mentioned merits render amino acids and peptides excellent materials for the design of self-assembly nanostructure.

1.3.1 Peptides assembly based on α-helix/ coiled-coil formation

A plethora of assemblies based on one of the common secondary structures, α-helix, have been studied.[48-52] It is widely-accepted that different amino acids favor different secondary structures. In a α-helix structure, there are 3.6 residues per turn in average, which means that a hydrophobic amino acid (H) is placed between three or four hydrophilic amino acids residues (P)[48] (Figure 6a, the 1 and 2 labeled the hydrophobic core). In this structure, one driving force of assembly is the hydrophobic interaction that tends to form the hydrophobic phases and wraps around. This pattern is repeated with

seven residues in cycle as $(HPPHPPP)_{n \geq 4}$, and usually marked as adcdefg. A considerable number of structures following this pattern form rope-like coiled-coil structure.[53] These helices are in left-handed twist as these structures have 3.5 residues per turn, slightly less than the 3.6 residues per turn right-handed α-helix structure in nature. The salt-bridge interactions between the coils facilitate the aggregation of two or multiple coils.

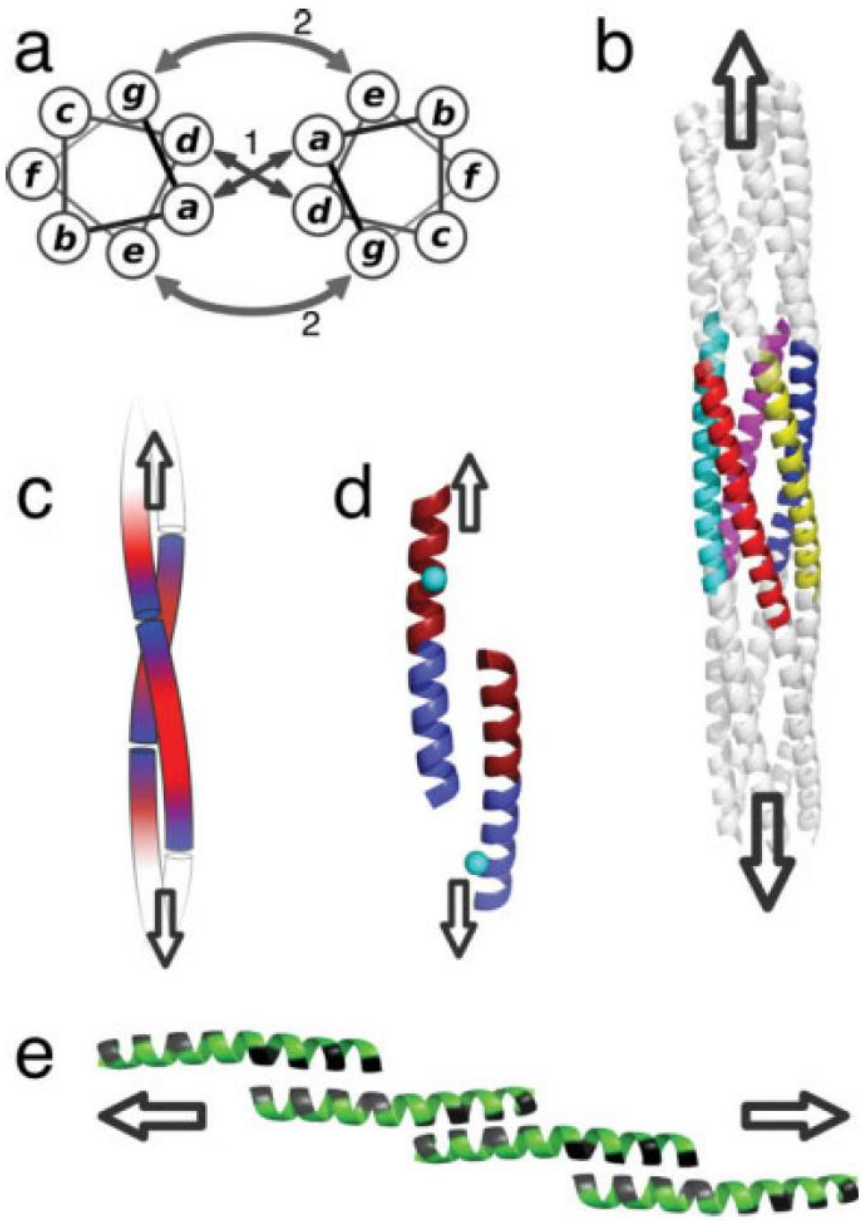

Figure 6. Principles of fibrous coiled-coil assembly: a. The heptad sequence repeat (abcdefg) configured on a dimeric helical wheel; b. Slipped assembly based on a coiled-coil pentamer (colored) as proposed by Kajava and coworkers;[49] c. Designed single peptide, sticky end assembly implement by the Conticello and coworkers and Woolfson and coworkers;[48, 52] d. The SAF design;[54] e. Assembly of coiled coils with out-of-phase hydrophobic faces by Fariman and coworkers[50-51]. Copyright 2010 Wiley Periodicals.

In 1997, Kojima and coworkers firstly designed the peptides sequences $(LETLAKA)_3$ that acquired α-helix structure.[55] Kajava's group used this strategy to build more α-helix peptides with this frame, such as $QLAREL(QQLAREL)_4$ (Figure 6b) that can form nanofiber structures.[49] Conticello and coworkers further proposed that fiber structure can be formed upon staggered coilded-coil structure (Figure 6c).[52] Woolfson and coworkers has concluded a self-assembly fibler (SAF) system with two coils twist around each other.[50]

Furthermore, Conticello's group[56] and Hartgerink group[57] have successfully designed structures that mimic the collagen helices with heterotrimeric amino acids triptes $(Pro\text{-}Arg\text{-}Gly)_n$, $(Glu\text{-}Hyp\text{-}Gly)_n$, (Pro-Hyp-Gly)n insider of the peptides chains. These sequences together can form triple helix structure in order to form fibers and further hydrogel based on Hartgerink's study.[58] All these structures are peptide self-assembly designs based on α-helix structures.

1.3.2 Peptides assembly based on β-sheet structure

Not only for studies on α-helix secondary structures, there are plenty of peptide assembly structures designed based on the β-sheet structure. There are various types of peptides or peptide derivative assemblies involved β-sheet structure. A great portion of them include the alternating arrangement of hydrophobic amino acid and hydrophilic amino acids.

Tubular structure peptides

One of the earliest examples of designed peptides self-assembly nanostructure was the cyclic peptide nanotubes by Ghadiri and coworkers.[59-61] Ghadiri's group has designed a cyclic peptides consists of alternating D- and L- amino acids. This peptides monomer is a generally planar ring structure. During the assembly process, the ring can stack on top of each other in order to form a tubular structure collectively (Figure 7). The hydrogen bonding between amide bonds in two neighbor rings helps to stabilize the tubular structure. The anti-parallel β-sheet structure of this stacking was confirmed by a series of studies. The diameter of nanotube structures can be modified by the number of peptides involved in the monomer. Besides, different residues can be incorporated into the side chains of the nanoring. For example, 1,4,5,8-naphthalenetetracarboxylic acid diimide (NDI) have been connected to the lysine side chain and successfully form nanotube assembly structure in later work.[61]

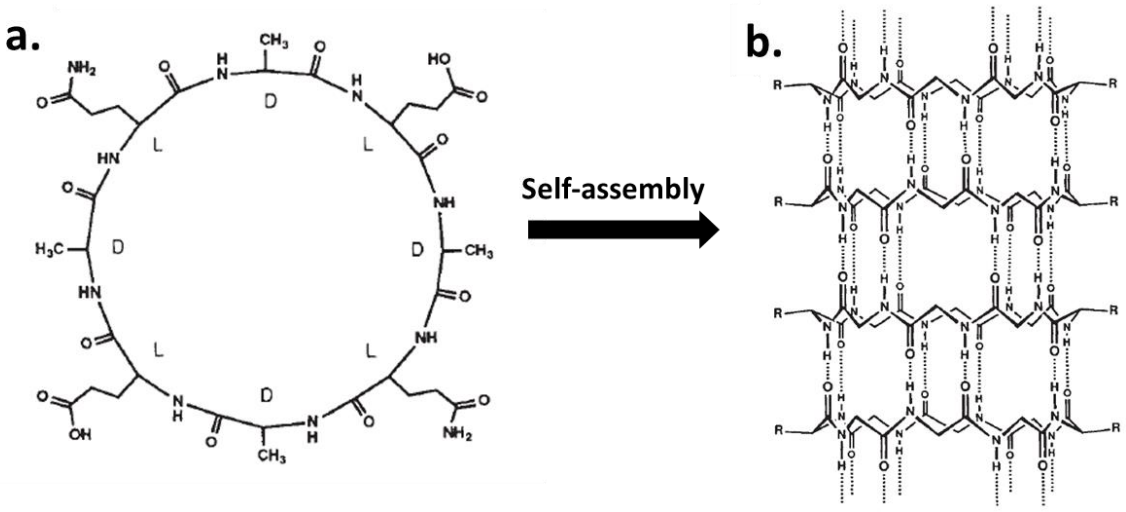

Figure 7. a. Structure of the cyclic peptides b. Nanotube formed by stacking of the cyclic peptides.[59] Copyright 1993 Nature Publishing Group.

Self-Complementary peptides

In 1993, Zhang and coworkers[62] have discovered a type of complementary ionic peptides, under the inspiration of motif, $(RERERKRK)_2$. This motif was found in peptide EAK16-II which has AEAEAKAKAEAEAKAK 16 amino acids sequence, in the Z-DNA binding protein, zoutin. They found that this sequence have adopted a β-sheet configuration as the ionic sidechains face one direction and the hydrophobic chains face the opposite directions. When two monomer peptides present in aqueous solvent at neutral pH, they tend to form face to face dimers with their ionic face attracting with each other (the positive charged lysine residues attached to the negative charged glutamate side chain), or the hydrophobic alanine sides facing each other.

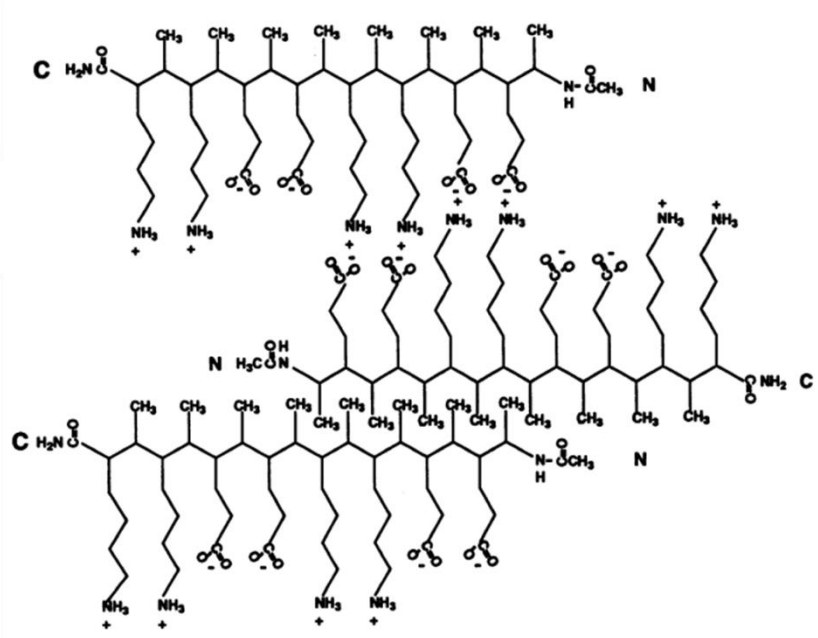

Figure 8. Self-assembly structure of peptides EAK16-I and into nanofiber.[62] Copyright 1993, CrossMark

In further study, peptides sequences named as RAD16-I,[63] which is Ac-$(RADA)_4$-$CONH_2$, and RAD16-II (Ac-RARADADARARADADA-$CONH_2$) and KLD-12 ($(LKLD)_3$) were designed and synthesized. These structures all possess the similar motif of alternating hydrophilic and hydrophobic amino acids.[64-65] The alternating hydrophilic amino acids also carry opposite charges in order to complement and attract the other monomer. Those peptides can form β-sheet configuration in aqueous solvent with the backbone hydrogen bonding. Peptides RAD16-I were discovered to form stable nanofiber structure and further form hydrogel networks. RAD16-II and EAK16-II were found to support cell growth in several mammalian cells.[21] With this insight, those complementary β-sheet peptides have become decent material candidates for 3D scaffold for tissue engineering.

Glutamine-Rich Peptides

Aggelli and coworkers have designed a series of glutamine rich peptides that adopt β-sheet secondary structure and can self-assembly into fibril structure with pH trigger.[66-67]

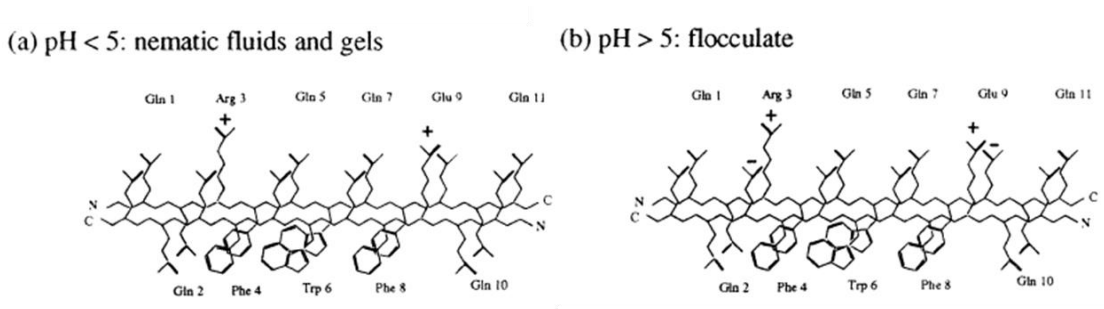

Figure 9. Illustration of glutamine-rich peptides P_{11}-2 under different pH: a. pH < 5, b. pH > 5.[67] Copyright 2002 American Chemistry Society.

This series of peptides are labeled as P_{11}-2 (CH_3CO-Gln-Gln-Arg-Phe-Gln-Trp-Gln-Phe-Glu-Gln-Gln-NH_2) (Figure 8), P_{11}-3 (CH_3CO-Gln-Gln-Arg-Phe-Gln-Trp-Gln-Phe-*Gln*-Gln-Gln-NH_2), P_{11}-4(CH_3CO-Gln-Gln-Arg-Phe-*Glu*-Trp-*Glu*-Phe-Glu-Gln-Gln-NH_2) P_{11}-5 (CH_3CO-Gln-Gln-*Orn*-Phe-*Orn*-Trp-*Orn*-Phe-*Gln*-Gln-Gln-NH_2). All sequences contain rich glutamine residues that constitute the hydrophilic side of the peptides. The core of design is also consists of alternating hydrophobic and hydrophilic amino acids. The hydrophobic amino acids are three aromatic amino acids (two Phe and one Trp) that not only can offer hydrophobic interactions but also π-π interactions for stacking. In P_{11}-2 and P_{11}-4, there are two amino acids carrying opposite charges (Arg and Glu) under neutral condition and facing on the hydrophilic side. This feature helps two peptide chains pack into the anti-parallel β-sheet position with the opposite charged sidechains next to each other. The anti-parallel β-strand structures will further pack into fibril structures. This assembly is also pH-controlled as under certain low pH, the negative charged residues will be protonated and reduce the attractions in between. P_{11}-4 and P_{11}-5 were reported to disassemble under low pH.

1.3.3 Peptides assembly based on β-hairpin structure

Schnider and coworkers have created another class of amphiphilic peptides that can self-assemble into hydrogel based on β-hairpin secondary structure.[68-74] This type of material is a series of 20 residue peptides that formed only by amino acids. The model can be expressed as $(XZXZ)_2V^DPPT(XZXZ)^2$, in which X is hydrophobic amino acid and Z is hydrophilic amino acid. The V^DPPT is incorporated to adopt the

type II’ structure in order to generate the β-hairpin secondary structure for each peptides molecule (Figure 9). Z is mostly positive charged amino acids such as K and R. In this model, water soluble peptides stay as free solution in an unfolded state under acidic conditions with the repulsion of positive charged amino-acids. With the decrease of pH or adding of salt concentration, or increase of temperature, the repulsion is compromised and peptides are triggered to a folded state driven by the hydrophobic interactions. In this state, the hydrophobic amino acids, such as valine, attempt to stay close to each other and as a result, peptides monomer is folded, forming a distinct hydrophobic phase and a hydrophilic phase. With two hydrophobic phases facing each other, hydrophobic interaction is maximized and further creates nanofiber. Not only capable of triggered by pH, salt concentration and temperature, these type of materials is also found to have a shear-thinning property. With an application of shear stress, the non-covalent cross-linked network is disrupted and low-viscosity gel forms; with the cessation of shear stress, both the non-covalent network and hydrogel rigidity are recovered. This property is crucial in minimally invasive delivery, as some study indicates that some hydrogel materials irreversibly lost its mechanical rigidity due to the shear stress during the syringe injection.

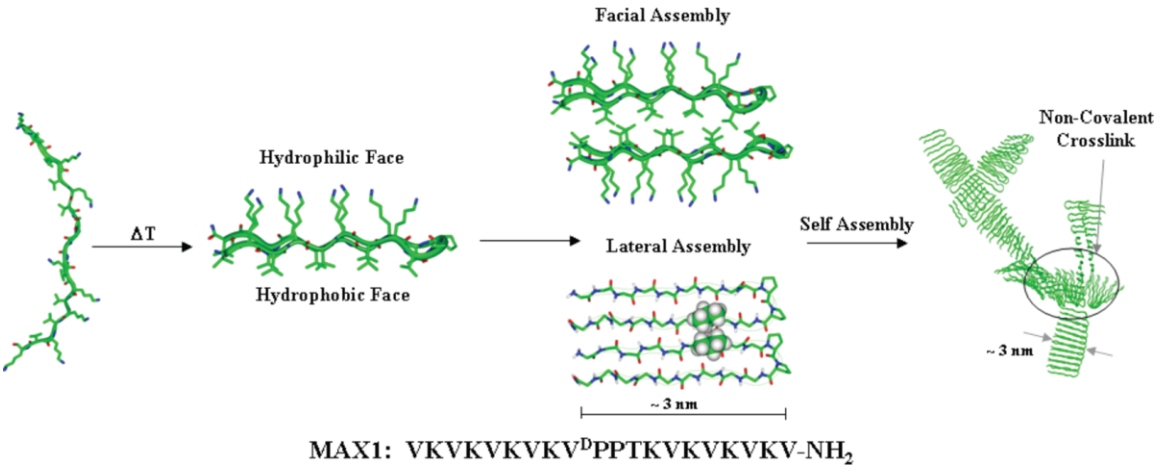

Figure 10. Proposed structure and the β-hairpin assembly model of molecule MAX1 (VKVKVKVKV^{D}PPTKVKVKVKV-NH$_2$) and further formation of fibril.[68] Copyright 2009 American Chemistry Society.

1.3.4 Amphiphilic Peptides

Amphiphilic peptides are the type of peptides or peptides derivatives that contain both hydrophilic component(s) and hydrophobic component(s). This is an extremely versatile type of material and it possesses great potential to construct various bioactive nanostructures.[75] One typical sample is the surfactant-like peptides proposed by Zhang and coworkers.[76]

Zhang's group has first designed and synthesized a series of lipid-like peptides, A_6D, V_6D, A_6D_2 and L_6D_2 (Figure 10). All these peptides have a long hydrophobic tail consists of same type of amino acids with hydrophobic sidechains, such as A, V and L. Besides this long hydrophobic tail, they also have another hydrophilic end which is one or two hydrophilic amino acids D. This type of peptides were found to also assemble in the lipid pattern in aqueous solvent with the bilayer structure of hydrophobic tail buried

inside of walls and hydrophilic ends facing outside. In further study, they expand the hydrophobic amino acids selections to G, I, L and F and hydrophilic amino acid to K.[77-80] Those peptides series were found to self-assemble into nanotubes or nanovesicles structures based on TEM studies. In addition to these mentioned peptides, Zhang's group has proposed another lipid-like peptides sequence of Ac-GAVILRR-NH_2.[81-82] This sequence has a hydrophilic head with two charged arginines connected to hydrophobic tail of amino acids with decreasing sizes.

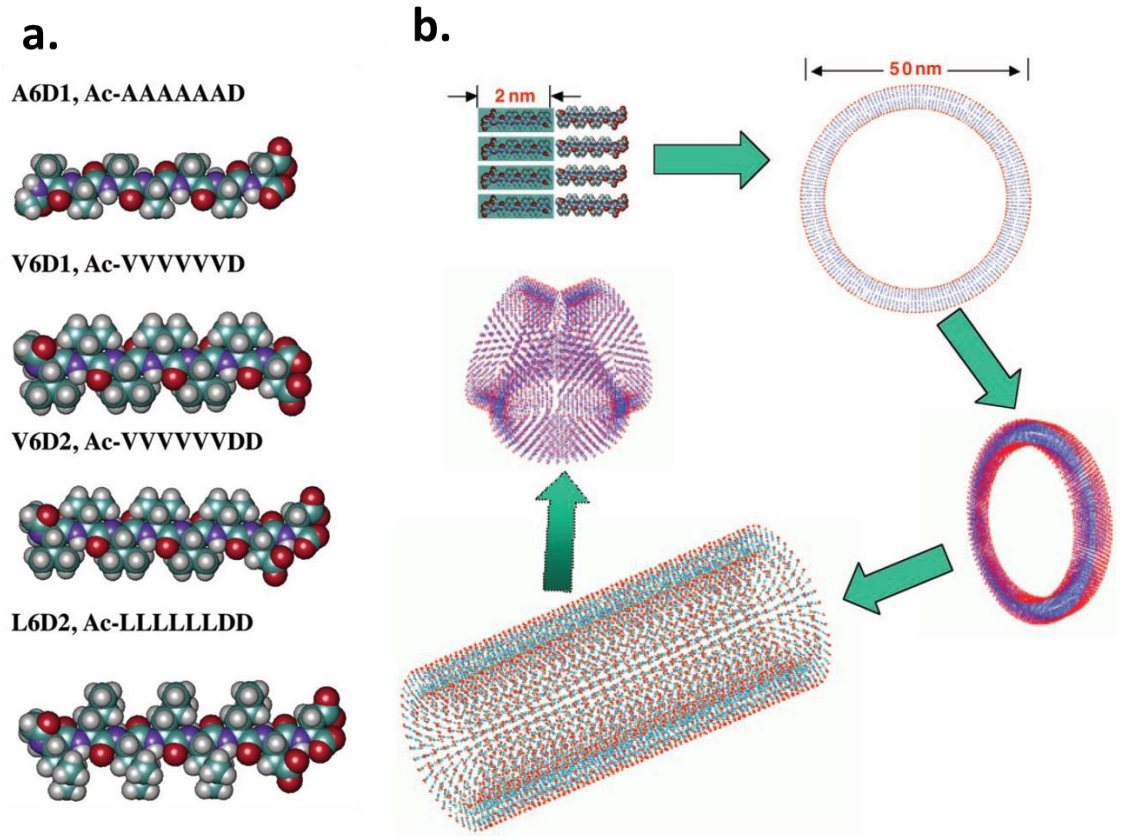

Figure 11. a. Models of surfactant peptides A_6D, V_6D, A_6D_2 and L_6D_2; b. Proposed self-assembly model of V_6D.[76] Copyright 2002 CrossMark.

Aside from these surfactant-like peptides, Stupp and coworkers have established a class of peptides amphiphiles (PA) that can form hydrogel and are able to deliver multiple bioactive motives.[23, 83-89] This class of materials is a hybrid of peptides and alkyl chains. As shown in Figure 11, typically this model consists of four segments: a hydrophobic tail, β-sheet forming short peptides, a charged component (can be amino acid) and a bioactive epitope.[90] It has been discovered that among the four parts, the indispensable two core segments are the hydrophobic tail and the short peptide as hydrophilic site.[91] The peptide region contains sequence that assists the forming of intermolecular hydrogen bonding, charged amino acids to improve solubility and further develop a pH- or salt sensitivity, and bioactive epitope(s) capable of interacting with proteins. This type of material can self-assemble into a cylindrical structure with hydrophobic tail buried inside and hydrophilic peptides domain expressed outside and further form high-aspect-ratio nanofibers. Besides, studies have been shown that more than one cell adhesion RGD epitopes can be functionalized in this model by couple this epitope to amino acid as side chain aside from the main chain, and the cell culture results also demonstrated that the cell adhesion has been further enhanced in this way.[92-94] This class of PA has revealed great versatility in function and pH-, salt sensitivity and the corresponding assembly structures can be tuned by changing the component size and amino acids.[83]

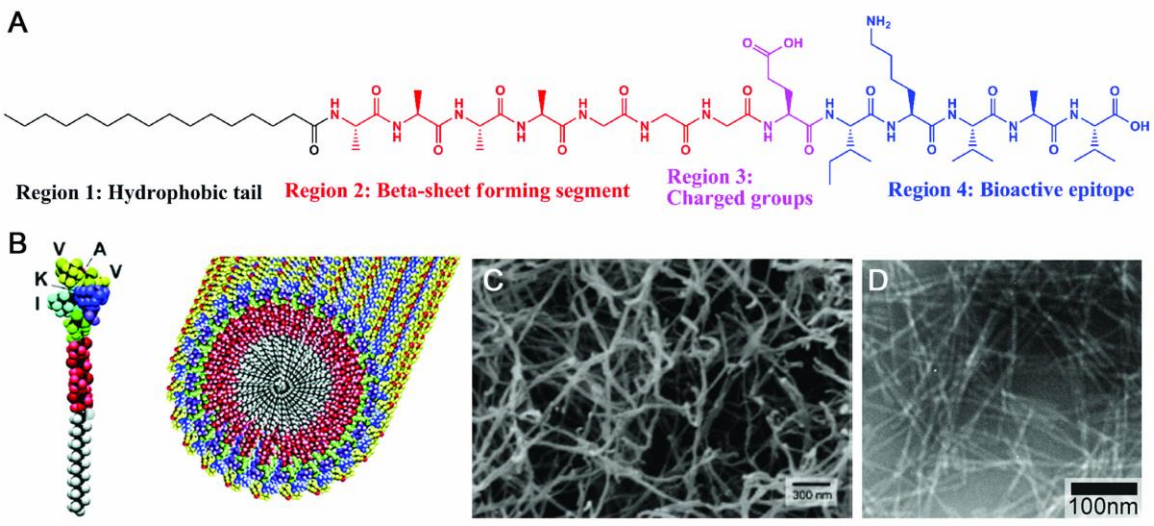

Figure 12. (A) Molecular Structure of representative peptide amphiphile with four rationally designed chemical entities; (B) Molecular model of the IKVAV-containing peptide amphiphile molecule and its self-assembly into nanofibers; (C) SEM picture of IKVAV nanofiber network. (D) TEM picture of IKVAV nanofiber network.[83] Copyright 2010 NCBI.

1.3.5 Aromatic short peptides derivatives assembly

Aromatic short peptides are another class of peptides based on short aromatic peptides or peptides derivatives with aromatic systems. The assembly driving force of this type of assembly was majorly based on short amyloid structure[11]. One of the earliest examples of reported aromatic dipeptides assembly is the hydrogel formation of dibenzoylcystine in water by Gortner and Hoffman in 1921.[95] The structure and the assembly mechanism was unveiled by Menger and coworkers[96-97] after fifty years. Since then, many aromatic short peptides assemblies were discovered and reported. Among those works Gazit and coworkers[98] have revealed the self-assembly of Phe-Phe dipeptides into highly stable nanotubes via the aromatic side chain's π-π interactions and the hydrogen bonding

between the amide groups in the β-strand structure.[99] Different variations of this dipeptides motif have been further studied and reported. The bulky aromatic group fluorenylmethoxycarbonyl (Fmoc) was incorporated into the dipeptides design in later study of Gazit's group (Figure 12).[100] This Fmoc-Phe-Phe peptides were found to self-assemble into fibrils in nanoscale and further form networks into hydrogel.[22] This alternation from nanotube into nanofibers results from the increased π-π interactions.[100] The hydrogel formed was reported to support the growth of Chinese hamster ovary cells with decent viability. Ulijin and coworkers then investigated this assembly mechanism in details with a series of spectroscopy study. Both FT-IR and X-ray results indicated the antiparallel β-sheets secondary structure formation.[101]

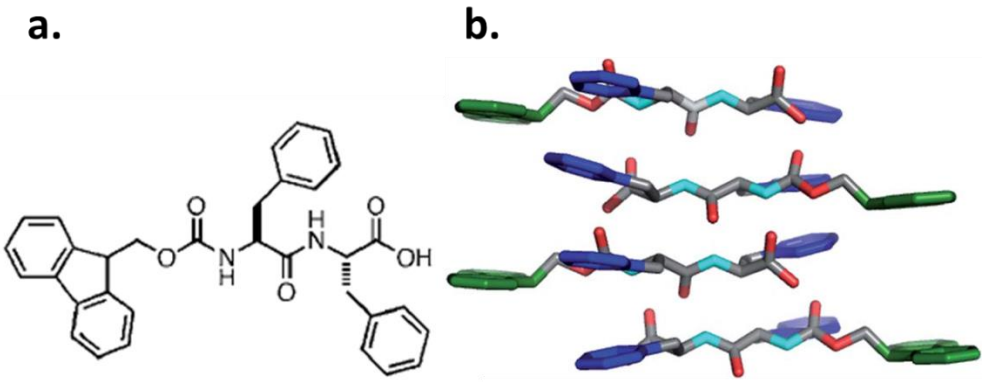

Figure 13. a. Chemical structure of Fmoc-Phe-Phe; b. Packing model of Fmoc-Phe-Phe. Copyright 2012 Royal Chemistry of Society.[100, 102]

In addition to the Fmoc-Phe-Phe, more short peptides or peptide derivatives with different amino acid or modifications have been discovered, such as Fmoc-F-OH, Fmoc-K-OH, Fmoc-AA-OH, Fmoc-LG-OH and Fmoc-FG-OH). Some biological

motifs, such as RGD can also be incorporated into this system with examples of Fmoc-RGD-OH and Fmoc-FRGD-OH.[101-102] This type of peptides is generally simpler with shorter sequences in comparison with other types and can reduce the synthesis production cost.

1.3.6 Self-assembly nanostructures designed by Dr. Parquette's lab

The Parquette's group has developed a series of self-assembly nanostructures in previous research.[103-109] In 2007, Hui and coworkers has designed and synthesized a series of 16 peptide-dendron hybrids (PDH) combining the dendrimer motif to the peptides side chains.[110] The dendron motif was used in the organocatalysis. This series of PDH have the Ac-AAAAKAAAAKAAAAYA-NH_2 peptides backbone, there is one dendron attached to the third A (position *i*) and the other dendron was connected to the other A on the position from *i*+4 to *i*+10. This type of PDH conjugates have charged lysine residues and the hydrophobic dendron components, and were reported to assembly and form nanotube structures in aqueous solvent. The corresponding assembly model for dendrons on (*i*, *i*+10) positions is illustrated in Figure 14. Our group has found that in pure water solvent, this PDH adopts the nanotube assembly structure, with the addition of salt solution or pH change, the assembly structure changed into an amyloid fiber structure on nanoscale. This change was due to the attenuation of the repulsion between the positive-charged side chains when increase salt solution concentration or increase pH.

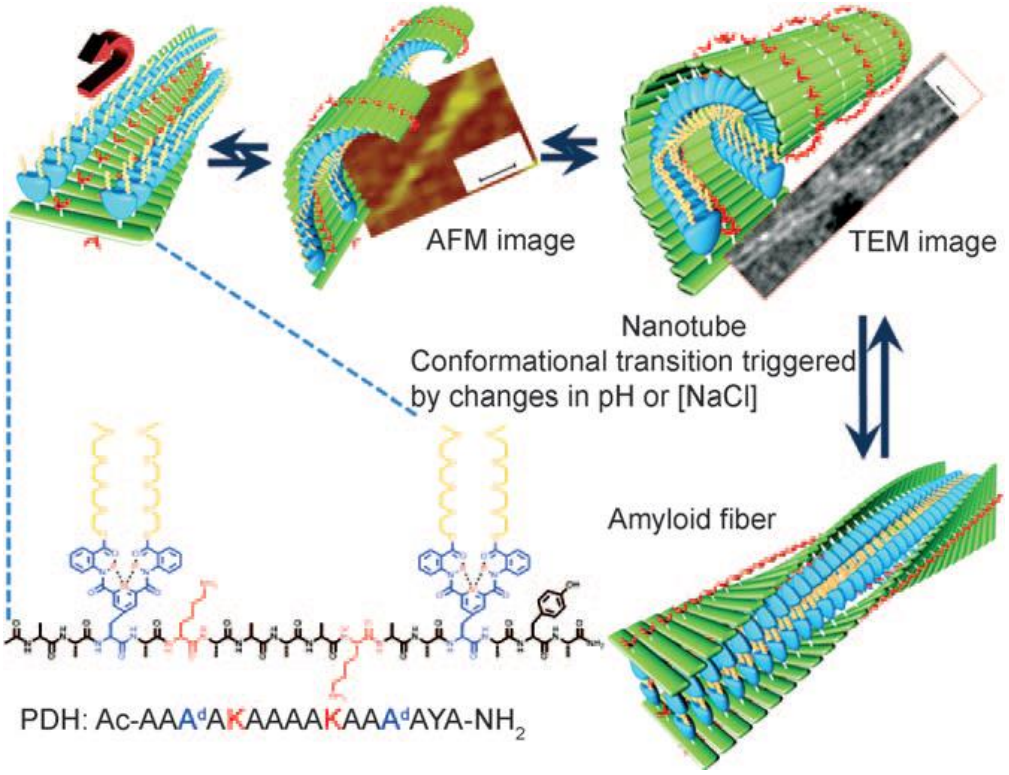

Figure 14. Schematic representation of nanotube and nanofiber formed by PDH self-assembly.[103, 110] Copyright 2009 Wiley Online Library

In 2010, our group has reported the self-assembly behavior of a class of lysine 1,4,5,8-naphthalene-tetracarboxylic acid diimide (NDI) dipeptides hybrid structures. A series of lysine-lysine dipeptides and NDI hybrid were designed and synthesized.[106] The NDI is an organic semiconductor chromophore and it was covalently bonded to one of the lysine side chain. We found that as we changed the P1 group from the least hydrophobic hydrogen to acetyl group to the most hydrophobic Fmoc group, the assembly behavior also changes with it. When P1 is hydrogen, the molecule is too hydrophilic to assemble. No ordered assembly structures were observed. When we

increased the hydrophobicity to acetyl group, nanofibers assembly structures were discovered based on TEM study. When it comes to the Fmoc dipeptides, nanobelt structures were observed and the nanobelts can even form hydrogel networks. The NDI is an aromatic chromophore that can provide π-π stacking interactions as one attraction force for assembly; the dipeptides backbones can form hydrogen bonding in β-sheet pattern, which also helps packing. The positive charge on the amine of the other lysine side chain can provide the necessary repulsion for assembly. In Fmoc-KK(NDI)-NH_2, the Fmoc group also enhanced the π-π stacking (Figure 15).

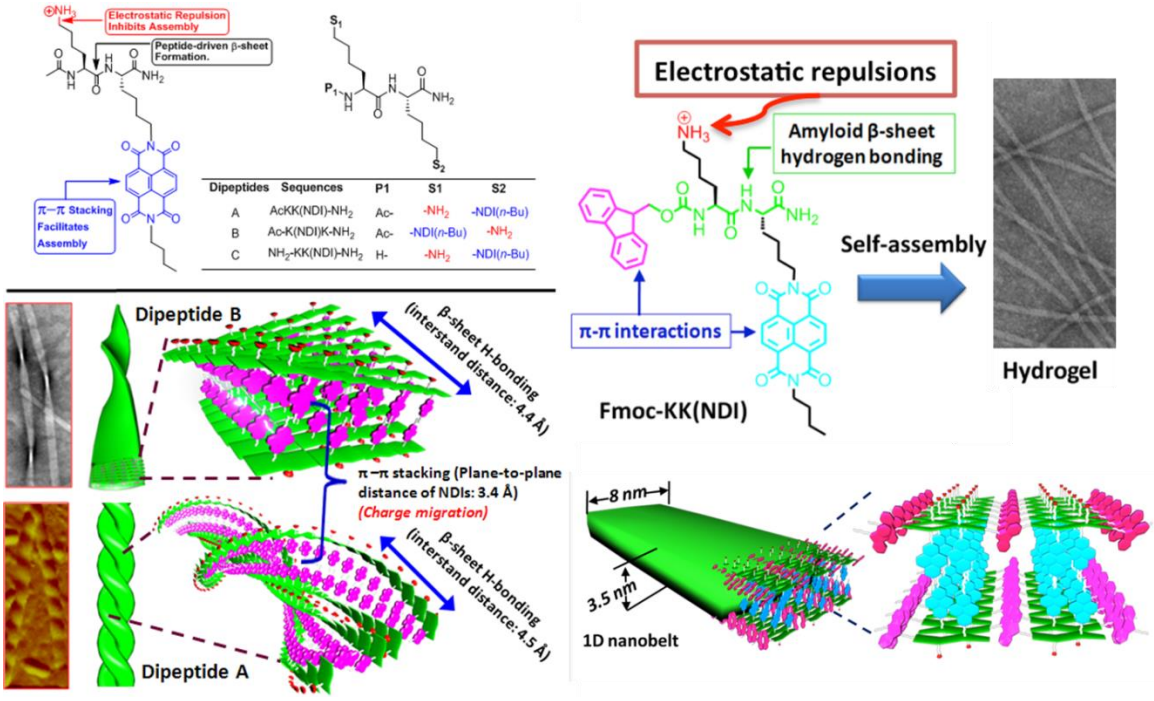

Figure 15. Representation of β-sheet assembly of lysine-NDI dipeptides into nanofiber and nanobelts.[106]

Besides these NDI dipeptides structures, we also designed and examined the assembly behaviors of a class of NDI bolaamphiphile structures[107] and the assembly behaviors of series of NDI with mono-lysine amphiphiles (Figure 16).[105] In the bolaamphiphile design, the NDI was bonded to two lysine residues on both sides. The π-π association among the NDI chromophores serves as the driving force for assembly in water. The lysine headgroups on both sides offer electrostatic interactions.[111-112] When (R = O^-), bolaamphiphile A was reported to self-assemble into monolayer nano-rings first and further pack into 1D (one dimensional) nanotube structures, as shown in the TEM images. This type of amphiphiles has revealed great homogeneity in structure and conformation that leads to rapid energy migration within the nanotubes, which is confirmed by time-resolved fluorescence anisotropy experiments. For the families of NDI-Lysine peptides, NDI chromophore was connected to n-butyl group on the other side. The n-butyl NDI parts together constitute the hydrophobic tail whether the lysine derivative serves as the hydrophilic head. All three compounds adopt one dimentional nanotube assembly conformations under high concentration. Based on the TEM measurement and atomic force microscope (AFM) study, the tubes formed by Lys(NDI)-OH and Lys(NDI)-NH_2 are bilayers, the Lys(NDI)-OCH_3 tube is tetra-layer, this is due to the surfactant-like structure which promotes the packing of the hydrophobic tail-to-tail packing pattern. We raised a hypothesis that the methyl ester group at the interlamellar interface might induce subtle change in bilayer adhesion that further lead to the multilamellar nanotube structure.[113-115]

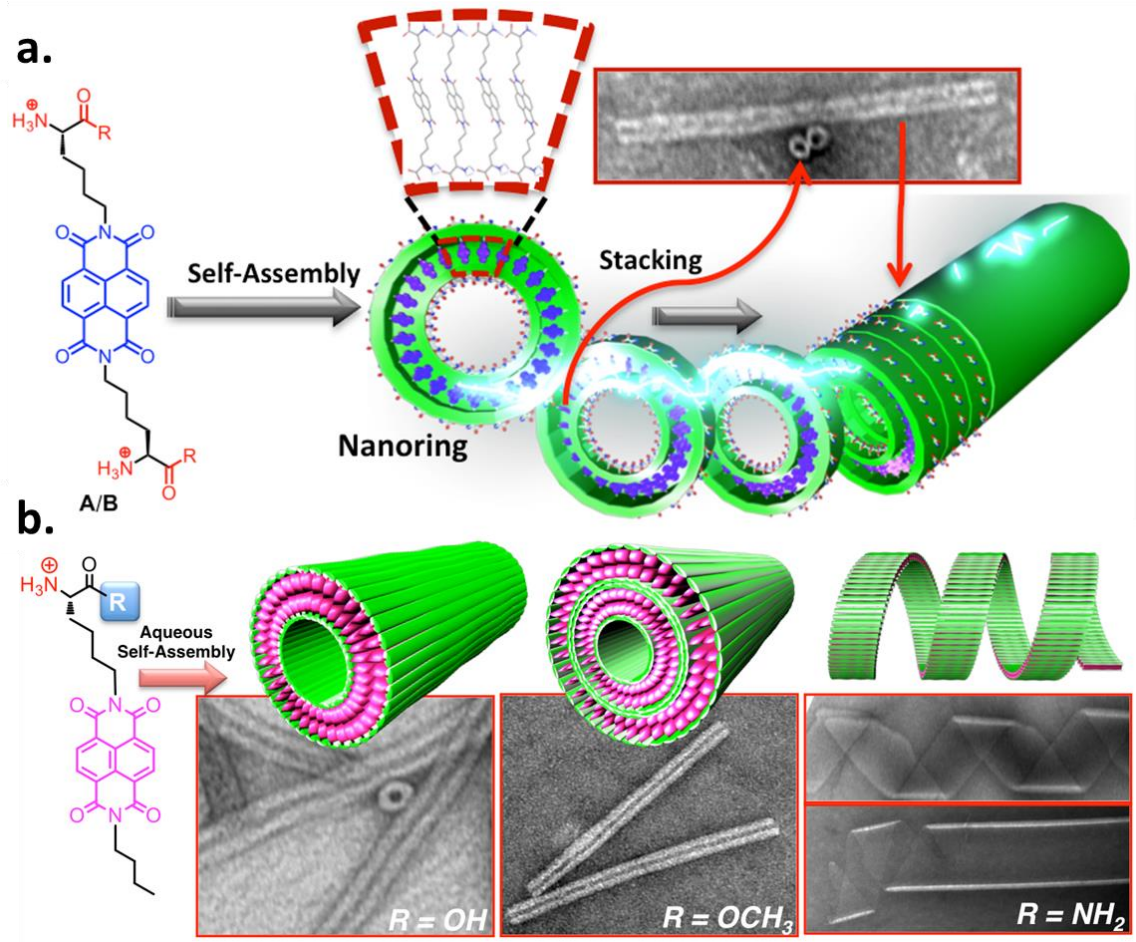

Figure 16. a. The Structures of bolaamphiphiles A (R = O^-) and B (R = OMe) and the proposed assembly model of A.[107] b. Structure of Lys(NDI)-COR and corresponding assembly structures and models (R_1 = OH, R_2 = OCH_3, R_3 = NH_2).[105]

Besides the NDI peptides hybrids, our group has expand the self-assembly design to peptide hybrid systems with other chromophores, such as coumarin,[104] camptothecin[116-117] and 5-fluorouracil pieces.[118] In 2015, our group has reported the photo-crosslinking of a self-assembled coumarin-dipeptide hydrogel.[104] The lysine-lysine dipeptides was functionalized with 7-(dithylamino)-3-coumarin carboxylic acid (7-DAC) chromophore. This DAC-KK(DAC)-NH_2 structure is capable of self-assemble into nice long nanofiber

conformation and form hydrogel structure in both water and phosphate-buffered saline (PBS) solution. Both hydrophobic and π-π interactions were induced by the DAC chromophores. The assembly adopts β-sheet secondary structure attribute to the dilysine backbone. With moderate ultraviolet (UV) light irradiation at 365 nm on the nanofibers, the coumarin groups dimerize and crosslink with neighbor ones and further stabilize the fiber structure (Figure 17). During this process, the mechanical properties of hydrogel are greatly enhanced upon dimerization crosslink according to the rheology study of oscillatory shear. Extensive irradiation interrupts the hydrogel structure and lead to precipitation.

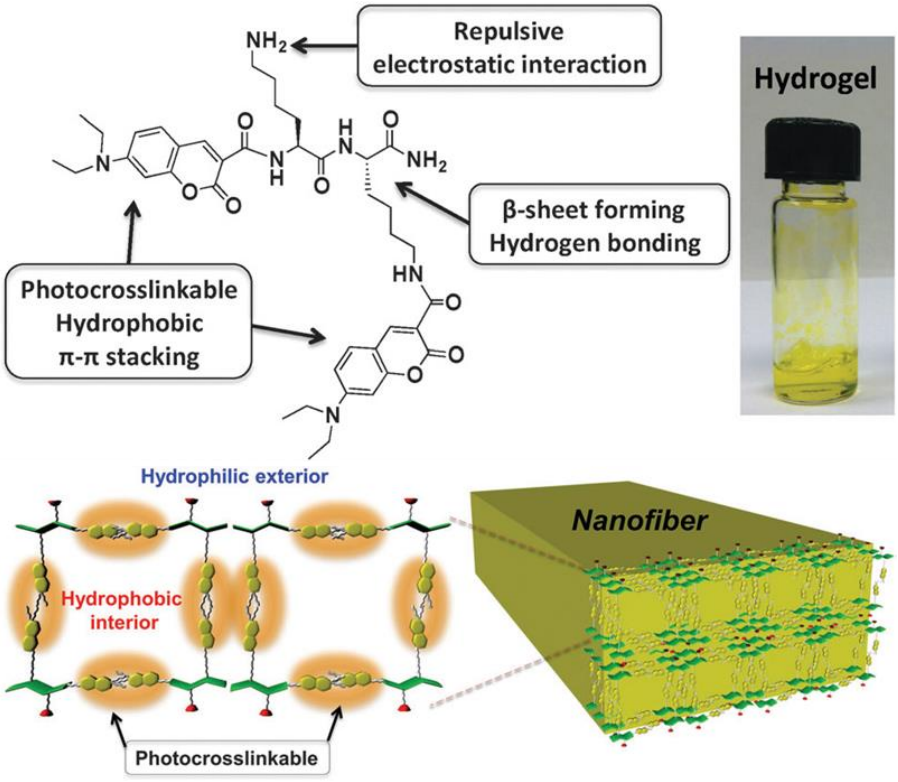

Figure 17. The structural design and the assembly model of coumarin dipeptides hydrogel.[104] Copyright 2015 CrossMark.

Chapter 2: Photo- and Thermo- Responsive Sol-Gel Conversion Based on the Self-Assembly of Spiropyran Derivative

2.1 Introduction

Functional materials that are capable of responsive to different external stimuli like pH, temperature, electric fields and salt concentration,[119] have been a great interest in the field of material.[120-126] Particularly, as one of the most efficient and promising stimulus, light has received much attention as it can be controlled spatially and accurately with ease.[127-131] Photo-responsive materials that can exist in two thermodynamically stable and reversible states with distinctly different properties undergoing photochemical reaction are great candidates for smart materials.[15, 54, 132-135] The incorporation of photo-switching chromophores in development of materials provides valuable insights to further applications in optical storage,[136-138] display devices,[139] molecular recognition,[140-141] drug delivery and wettability.[142-143]

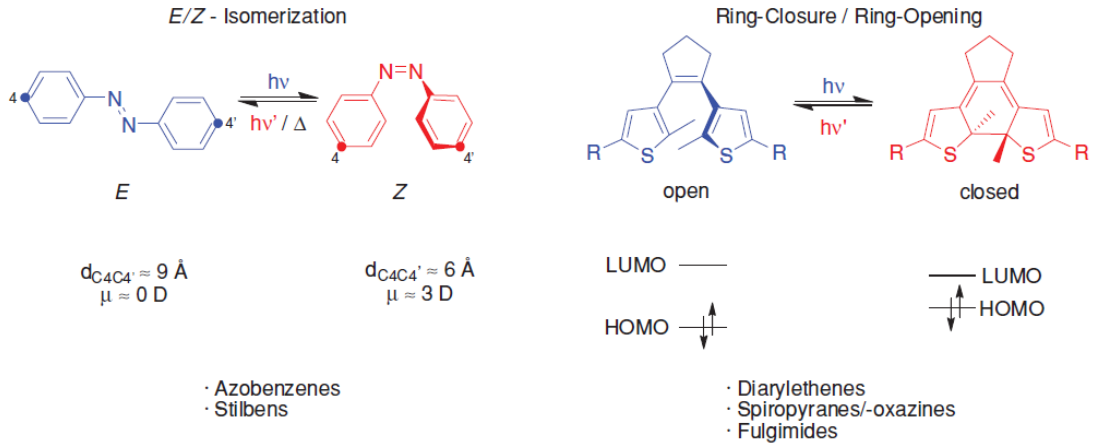

Figure 18. Common photochromic molecules: azobenzene and diarylethenes. Copyright 2010 Wiley Online Library

The photochromism phenomenon was first discovered in 1867 by Fritzsche with a tetracene solution that was organge-colored at night and bleached under sunlight. [144] However, it was not until late 20th century when a series of photo-switching chromophores, such as azobenzene, spirooxazine and diarylethene have been discovered and reported (Figure 18).[145-148] There are two common classes of photo-responsive chromophores; the first type undergoes E/Z isomerization with certain light irradiation, the second type converts between the ring-closure and ring opening states with light triggers.

Typical chromophore examples for the first type are azobenzenes, stilbens, dibenzuberane,[149] and diphenylbutadiene. Among those *trans-cis* changeable chromophores, azobenzene has been widely applied to a considerable number of cases in developing photo-responsive materials.[150] The *cis* and *trans* azobenzene isomers are facing different directions that can change the length of molecules when aligned

vertically and generate self-assembled mololayers (SAMs). Via this process, a photo-switchable surface can be formed. Mayor and coworkers[151] have proposed a azobenzend thiol derivative based on Au(111) film. The *trans-cis* isomerization changed the direction of connected RGD group and further changed the distance between RGD and the cell. The film can only connect to the Hg-drop electrode when azobenzene derivatives are *trans* forms. Similar examples such as the photo- controlled cell-adhesion experiments have also been designed by Shao and coworkers (Figure 19).[152] Besides those mentioned chromophores, this type of photo-triggering E/Z transformation is also discovered in some natural protein structures, such as the 13- and 15- cis-trans configuration change in retinal proteins[153]. However, the designed applications for this type of E/Z isomerization are merely limited to the geometry change, since the chemical properties for E/Z isomers are often very similar. Another drawback for this type of design is, when applied as SAM, sometimes the E isomers assemble in a too crowded fashion that hinders the Z isomerization with limited space.

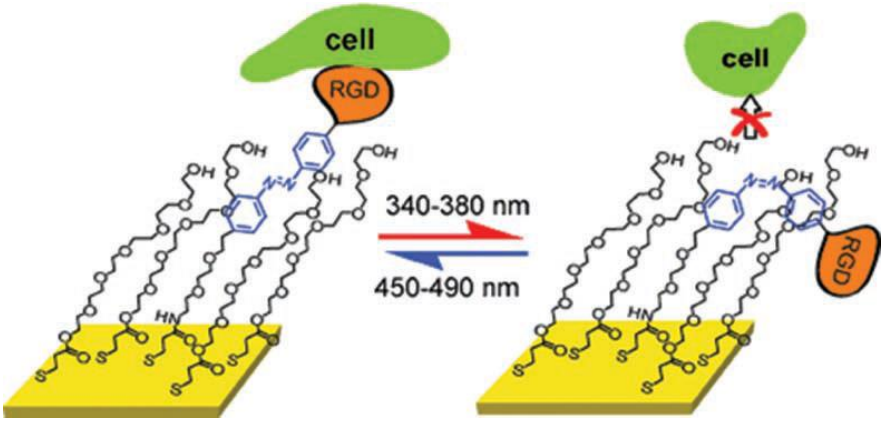

Figure 19. Photocontrolling cell-adhesion based on azobenzene chromophore.[15, 152] Copyright 2010 Wiley Online Library.

The second type of ring-opening/closure chromophores examples are diarylethenes, fulgimides and spiropyran/-oxazines. Diarylethene chromophores have been incorporated into field of liquid crystal study.[154] A type of photoprogrammable organic light emitting diode (OLED) based on diarylethenes has been designed and synthesized by Meerholz and cowerkers.[155] In their design, crosslinkable polymerizable 1,2-dithienylperfluorocyclopentene derivative (XDTE) has been used to prepare a photo-chromic layer to control hole transport. As the XDTE isomers change from ring-open to ring-closed form, a shift of HOMO levels is induced by ca. 0.6 V that enables the hole transportation. Efficient ON:OFF OLEDs with high ratio and electroluminescence can be achieved and may be utilized for signage applications.

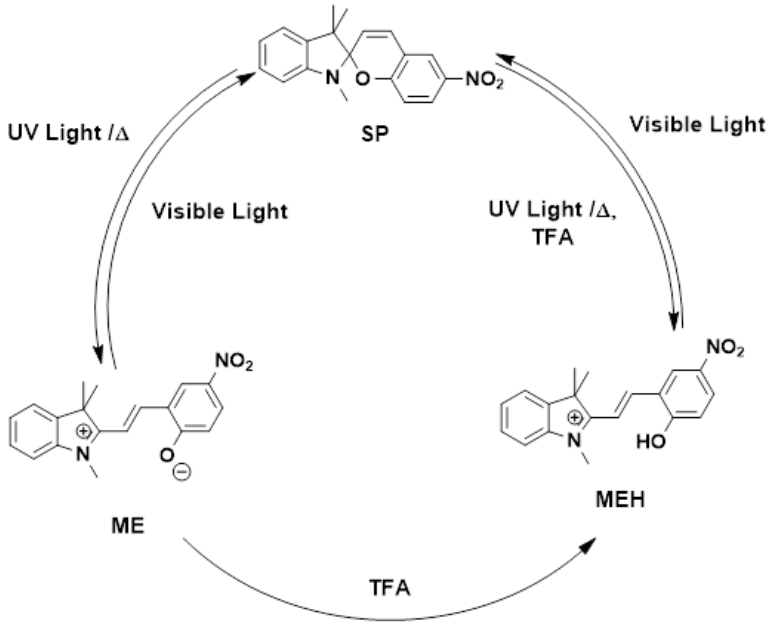

Figure 20. The conversion between spiropyran (SP), merocyanine (ME) and protonated merocyanine (MEH) forms.

Among the second type chromophores, spiropyran (SP) and spirooxazine derivatives has been an effective and well-known class of chromophore.[147] It has been discovered that provided enough heat or under ultraviolet light irradiation, the spiropyran can undergo structural change into the open and deeply-colored merocyanine (ME) form with the photo-cleavage of the C-O bond and change from colorless to an orange color.[142] This process is reversible as with visible light irradiation, the open merocyanine form will convert back to the closed spiropyran form. In addition, with trifluoroacetic acid addition, the open merocyanine(ME) form will be protonated and turn into the protonated merocyanine (MEH) form (Fig. 1). This protonated MEH form can and change back to the spiropyran closed form (SP) with deprotonation under visible light irradiation.[156] The three forms, SP, ME and MEH possess different physical and chemical properties and moreover, exhibit distinctive and signature absorbance band in UV spectrum which can be easily detected.[156-163] These interesting features have been applied to change the permeability of a self-assembly material.[164] As far as we know, very few cases have been reported for materials with photo-responsive tunable rheology property. Only several cases of photo-switch solution-gelation transformation were reported, in 2013 with supramolecular structure through non-covalent and covalent bonding change.[130] Herein, we report a photo-controllable gel-sol spiropyran derivative material based on merely non-covalent interactions of small organic molecules which are more dynamic and are possible to be tuned by various conditions or outside stimulus.

Determine amyloid fibril structure experiment

Amyloid fibrils have been discovered in many protein-misfolding diseases, such as Alzheimer's disease, Parkinson's disease and type-II diabetes.[165-166] A wide range of proteins have adopted amyloid fibril deposits, which is known to have a long and ribbon-like appearance and consisting of "cross-β" architecture.[167-168] Based on this morphology, the β-strands of the protein lie perpendicularly with the long axis of the fibrils. Throughout the centuries, scientists have discovered several dyes to specifically identify this type of structure, such as "Congo red" and Thioflavin-T (ThT).[169] In comparison to "Congo red", Thioflavin-T has become a widely accepted standard to diagnose the existence of amyloid fibrils with great convenience and high accuracy of recognizing peptides structures with various different amino acids sequences.[170]

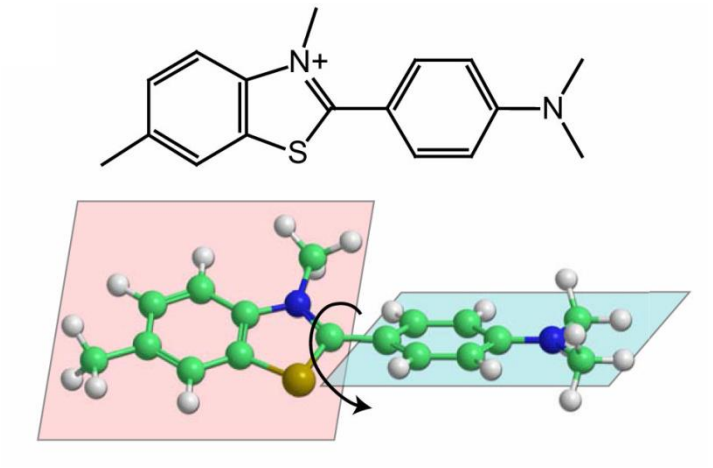

Figure 21. The Structure of Thioflavin-T.[167] Copyright 2010 National Institutes of Health

Thioflavin-T is capable of binding specifically to amyloid fibril structure and gives off fluorescence emission around 480 nm. With the large increase of fluorescence around 480 nm when mixed with Thioflavin-T, the amyloid fibril structures can be determined. The

reason for this fluorescence enhancement after binding has been unveiled by further study.[171-172] It has been suggested that the benzathiole part and the benzylamine rings can rotate freely in solution with a low energy barrier.[172] The excited state of ThT was quickly quenched by the rotation process, results a low fluorescence emission. When binds to amyloid structure, the two parts are sterically "locked" in their places and cannot rotate with ease to quench the fluorescence. Therefore the viewers can observe a prominent increase in the fluorescence spectra.[171, 173]

The mechanism behind the binding process has also been studied and several different models have been proposed,[167, 174] such as channel binding models by Kreb and coworkers[165] and the self-assembly models by Khurana and coworkers.[174-175] Among them, the assembly model based on critical micelle concentration was questioned by some later studies[176] and the channel binding model is widely accepted. In this model, ThT selectively binds to the "cross-strand ladders" side chains of the peptides in protein.[165] These ladders are naturally formed during the self-assembly process and are generally parallel to the long axis of fibrils. In this way, these side-chains can generate the channel-like binding sites for ThT molecules to attach.[177-179]

In general, the ThT binding assay has become a standard protocol to diagnose amyloid fibril type structure in protein or peptides series. We also used this method to examine the structure of our spiropyran self-assembly system.

2.2 Results and Discussion

Design of spiropyran conjugates

The design of Spiropyran (SP) tetrapeptides Fmoc-KK(SP)KF-NH_2 is based on a previous study of 7-(diethylamino)-3-coumarin carboxylic acid (7-DAC) -tetrapeptides conjugates[104-107] which can self-assemble into nanofiber structure. The Fmoc- group and the phenyl group of phenylalanine (Figure 22) can assemble through both hydrophobic force and also π-π stacking. The alternation hydrophilic and hydrophobic amino acids sequence has been discovered to have the tendency to form β-sheets in aqueous solution and they can establish a hydrophilic phase on one side and a hydrophobic phase on the other sides.

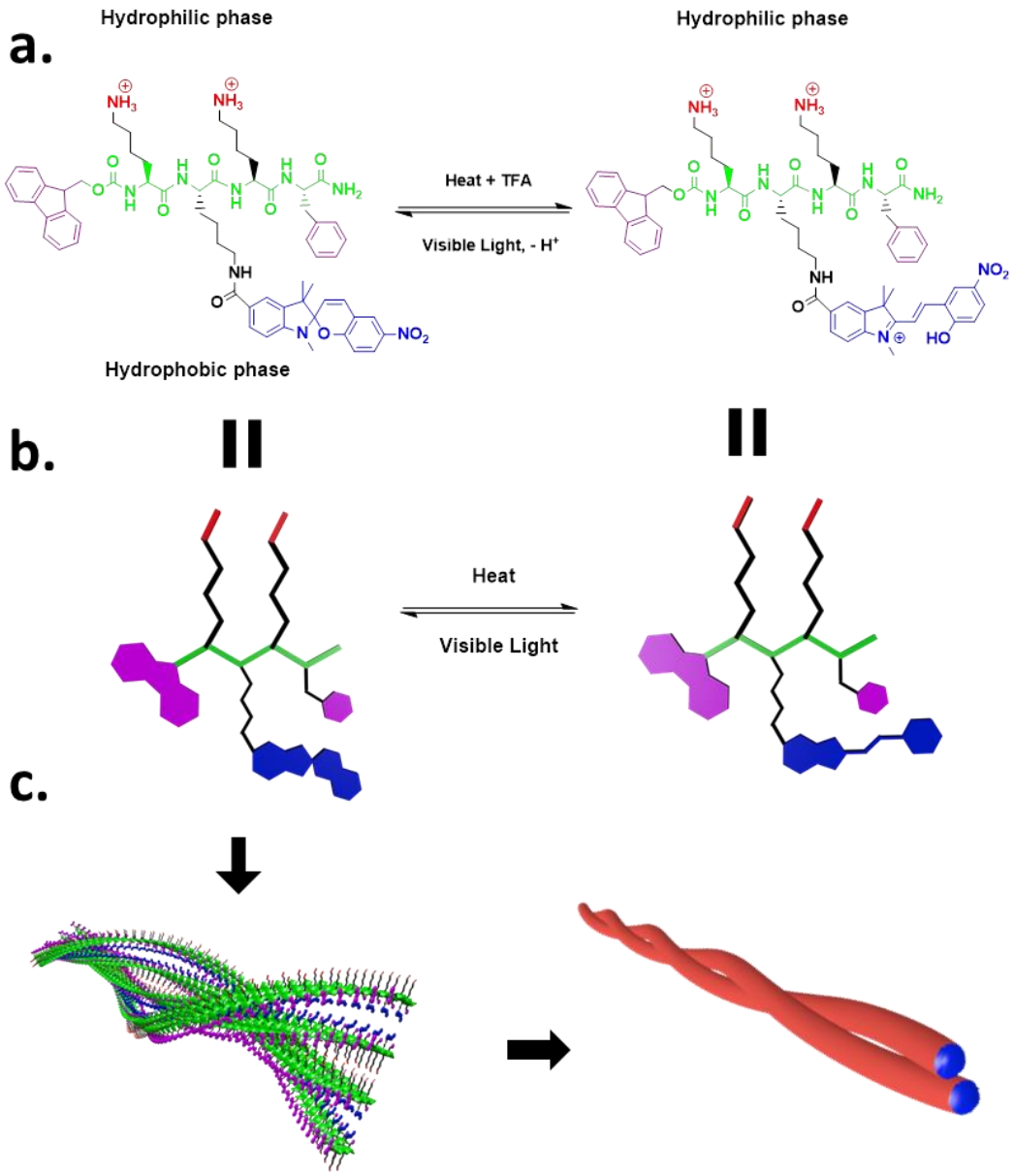

Figure 22. a. The structural and design of SP-tetrapeptide conjugates which undergo structural change into the MEH form with heat in acidic condition. b. Schematic representation of SP and MEH tetrapeptides monomer. c. Proposed self-assembly model of SP tetrapeptides.

In our design, the KKKF amino acid sequence (shown in green, Fig. 2) can provide the β-sheet interactions among molecules. In addition, the spiropyran stay at the hydrophobic side. Under visible light, the closed spiropyran form can provide more hydrophobic forces to further stabilize the self-assembly structure. The protonated free amine group of lysine can provide the repulsive electrostatic interaction for the hydrophilic phase. Under UV=254 nm irradiation or enough heat, the spiropyran will isomerize into the open merocyanine (ME) form with the photo-cleavage of the C-O bond.[147] With this structural change, the protonated merocyanine form structure in acidic condition is much more polar than the original spiropyran form, which may interrupt the entangled fibril structure. This open form is relatively stable under dark conditions without visible light irradiation. With visible light irradiation, the open merocyanine form can be reversibly changed back into the hydrophobic closed form and reform the fibril networks.

Synthesis and property of Fmoc-KK(SP)KF-NH_2 (5)

Compound 1',3',3'-Trimethyl-5'-carboxy-6nitrospiro[2H-benzopyran-2,2'-3H-indole] (**4**) was synthesized via four step reactions from 4-hydrazinobenzoic acid as shown in scheme 1. The 2,3,3-Trimethyl-5-carboxy-3H-indole (**1**) is formed by the condensation reaction of this precursor and isopropylmethylketone. The methylation of 1 with iodomethane gives indolium product 1,2,3,3-Tetramethyl-5-crboxy-3H-indolium iodide (**2**). Then **2** is dissolved in KOH solution to afford 1,3,3-Trimethyl-2-methylene-5-carboxy-3H-indole (SP3). A condensation of **3** and 2-hydroxyl-5-nitrobenzaldehyde yields the **4** (SP-COOH) spiropyran piece. This piece is used as a building block to synthesis the Fmoc-KK(SP)KF-NH_2 tetrapeptides following the standard solid-phase synthesis scheme on rink amide resin.

Fmoc-Phe-OH was coupled to the rink amide resin (loading 0.8 mmol/g) with 1,3 - diisopropylcarbodiimide (DIC), and 1- hydroxybenzotriazole (HOBt) (300% mol each relative to resin) in 1:1 dimethylformamide/dichloromethane (DMF/DCM). Fmoc group was removed under 20 % piperidine in DMF. Fmoc-Phe-OH, Fmoc-Lys(Boc)-NH2 and Fmoc-Lys(Mtt)-OH were coupled to the peptide-resin in sequence under fluorenylmethyloxycarbonyl group (Fmoc-) protected amino acids, HBTU, HOBt and N,N - diisopropylethylamine (DIPEA) in DMF. The methytrityl (Mtt-) protecting group was removed with 1% TFA. The SP4 was then coupled to the free amine group after the Mtt deprotection. The final product was cleaved off the resin under concentrated TFA solution, precipitated from diethyl ether and purified with high performance liquid chromatography (HPLC). The purity of product was assessed by ^{1}H, ^{13}C NMR, ESI and analytical HPLC.

1. Synthesis of SP-COOH (**4**).

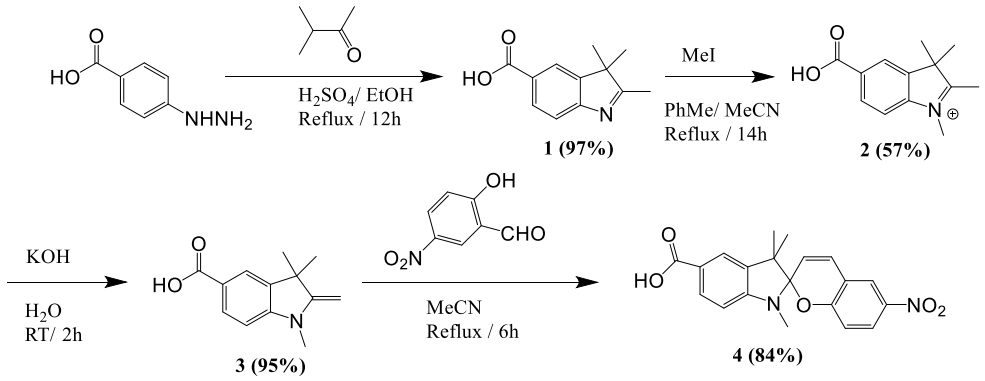

2. Synthesis of Tetrapeptides Fmoc-KK(SP)KF-NH_2(**5**)

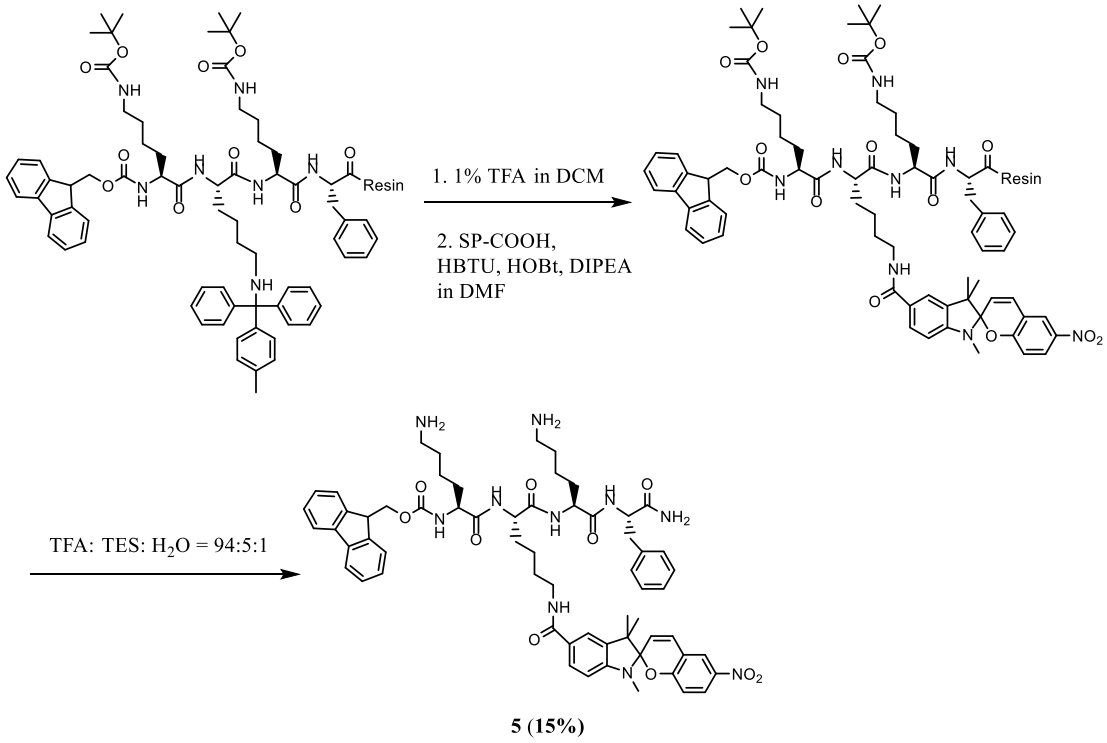

5 (15%)

Scheme 1. Synthesis Scheme of Fmoc-KK(SP)KF-NH_2(**5**).

Photo-responsive gel-solution conversion

To achieve the three different forms: ME, MEH and SP, four different 10 mM stock solutions of compound **5** (Fmoc-KK(SP)KF-NH_2) were prepared in H_2O and 0.75% TFA of H_2O respectively and labeled a~d. All solutions a~d were heated up to 60℃ for 1 h and then cooled down to room temperature in order to open the spiropyran moiety. Solutions a and c were prepared in water, solution a was aged 3 days in dark trying to keep the open ME form. Solution c was aged under visible light (broad LED light spectrum) for 3 days, trying to change back to the SP form under irradiation. Meanwhile, two other solutions, b and d were prepared in 0.75% TFA aqueous solution. Solution b was aged in dark for 3 days to keep the MEH form and solution d were aged under visible light irradiation (broad LED light spectrum) for 3 days to change back into the SP form. In H_2O, Fmoc-KK(SP)KF-NH_2 stays as a solution form under both visible light and in dark (Figure 23). Interestingly, in 0.75% TFA, the tetrapeptide conjugates solution d formed gel after aging(Figure 23,24). When heated up to over 60℃, the hydrogel formed by Fmoc-KK(SP)KF-NH_2 can change into liquid solution states and is rather stable under dark condition (Fig.4). This process is reversible, since Fmoc-KK(SP)KF-NH_2 solution can form hydrogel again under visible light irradiation.

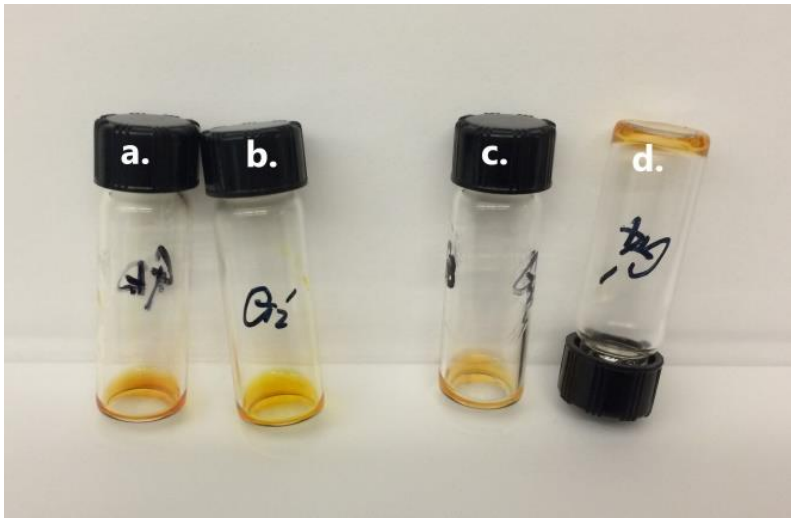

Figure 23. Solution images of 10 mM Fmoc-KK(SP)KF-NH_2: Solution a. 10 mM **5** in H_2O kept in dark for 3 days, b. 10 mM **5** in 0.75% TFA kept in dark for 3 days, c. 10 mM **5** in H_2O and aged under visible light for 3 days, d. 10 mM **5** in 0.75% TFA and aged under visible light for 3 days.

As is shown in Figure 23, in 0.75% TFA, Fmoc-KK(SP)KF-NH_2 stay as the hydrophobic closed spiropyran form under visible light so that a rather fibril network can be established and even gel is formed. When heated to over 60℃, the spiropyran part converts into the protonated merocyanine form (MEH). The protonated merocyanine form (MEH) is much polar than the original closed spiropyran form (SP) so that it interrupted the stability of the hydrophobic phase and further damaged the fibril network. The ratio change of the closed and the open forms under different temperature has been investigated by analytical HPLC (Figure 27~28). Solution b and gel formed by solution d can change into each other's state with light irradiation or heat (Figure 24).

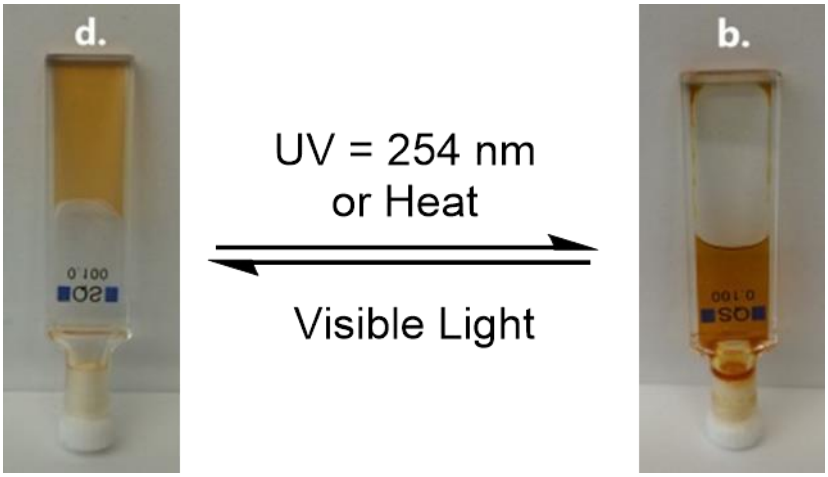

Figure 24. Conversion of 10 mM Fmoc-KK(SP)KF-NH_2 in 0.75% TFA between the gel state (solution d) and the liquid state (solution b).

Ratio study of open and closed forms for photo-switchable gel under visible light irradiation

The structural change of spiropyran can also be investigated by analytical HPLC since different closed and open forms of spiropyran have their distinct retention time. The open form merocyanine is much more polar than the closed spiropyran form and thus have a smaller retention time.

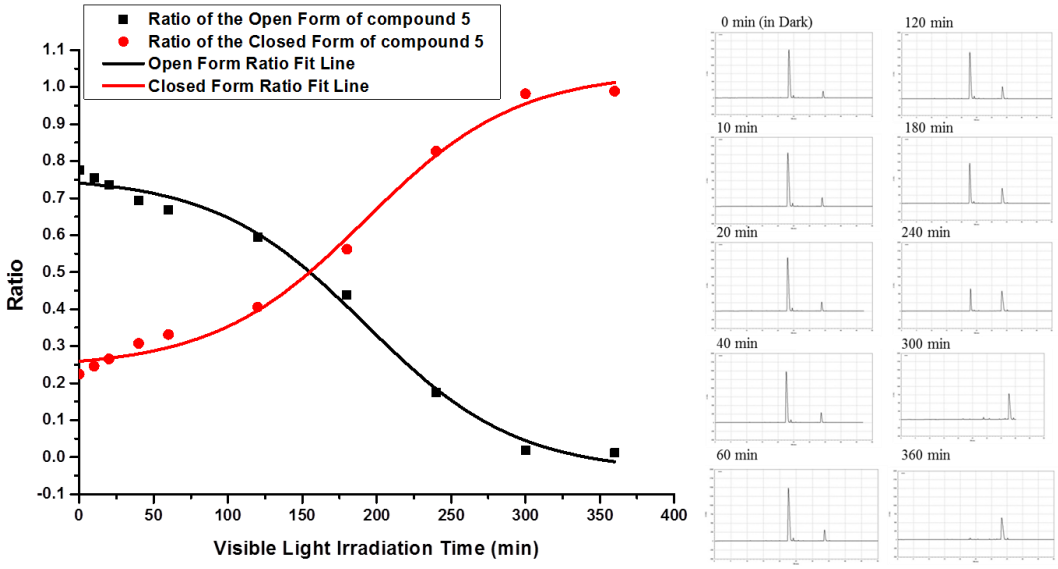

Figure 25. Ratio change of the open and the closed forms of 10 mM spiropyran tetrapeptides solution in 1% TFA under visible light irradiation. Solution b is the starting solution (time = 0).

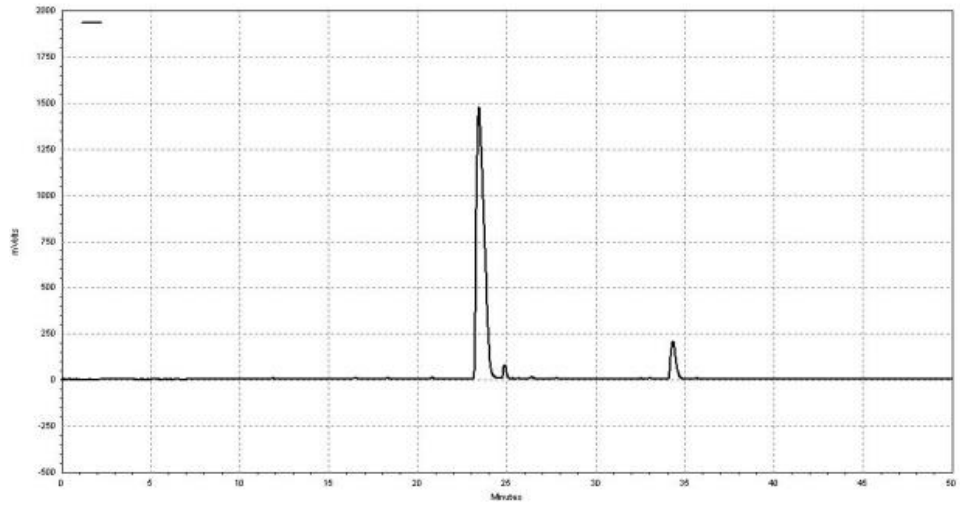

0 min (in Dark)

Continued

Figure 26. Corresponding reverse-phase analytical HPLC graphs of spiropyran tetrapeptides during the irradiation process. All graphs were taken at 370 nm UV absorbance with 0.1% TFA of Acetonitrile/H_2O solution, method: 0~5 min 27% acetonitrile, increase to 75% acetonitrile at 50 min, decrease to 20% at 55 min.

Figure 26 continued

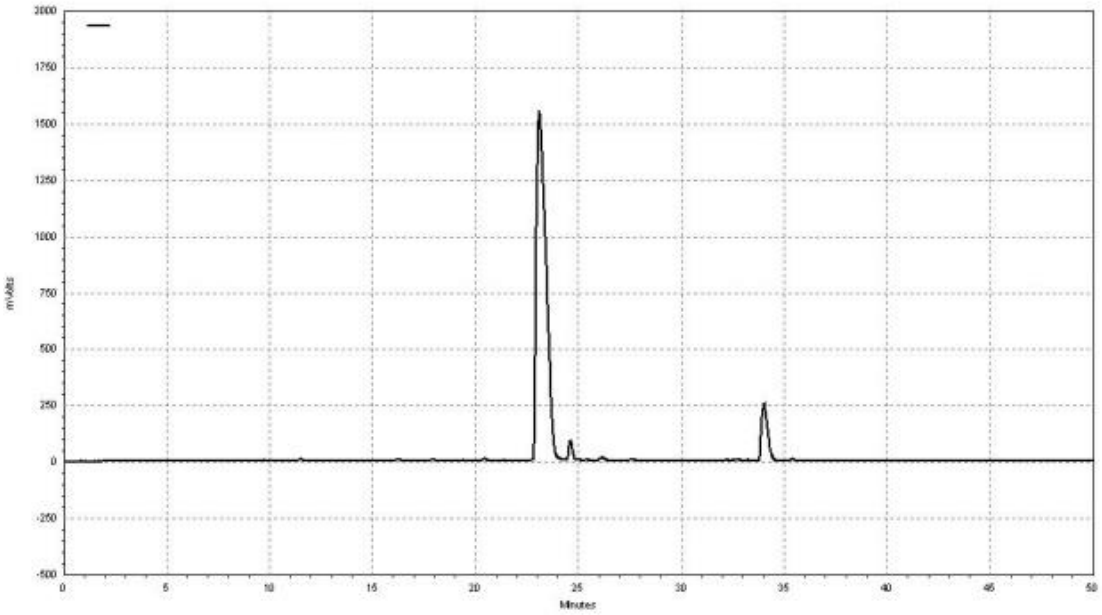

10 min

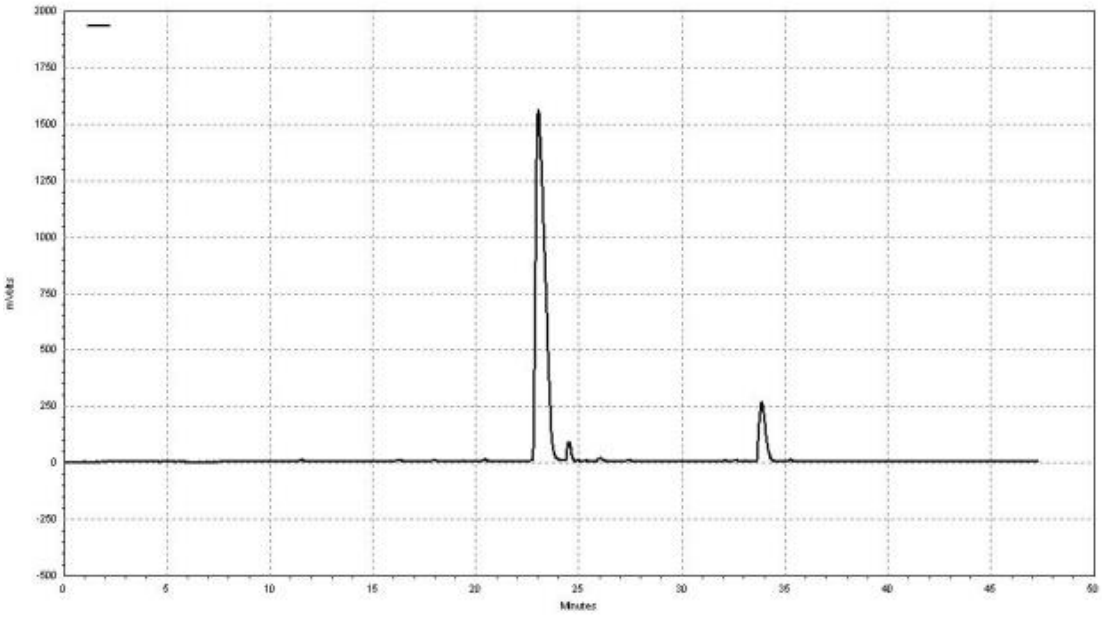

20 min

Continued

Figure 26 continued

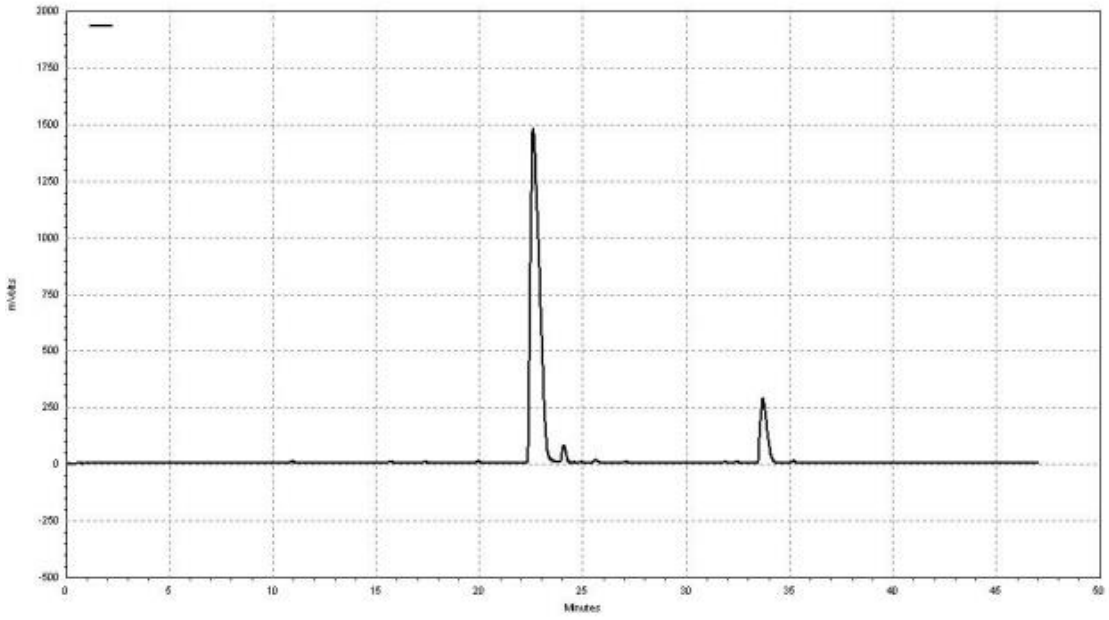

40 min

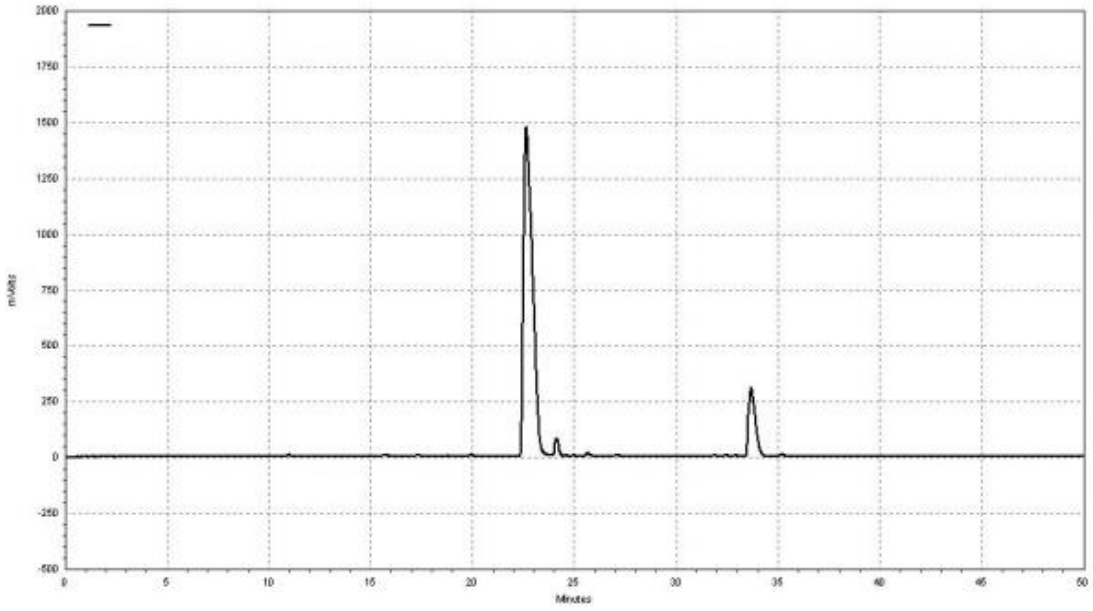

60 min

Continued

Figure 26 continued

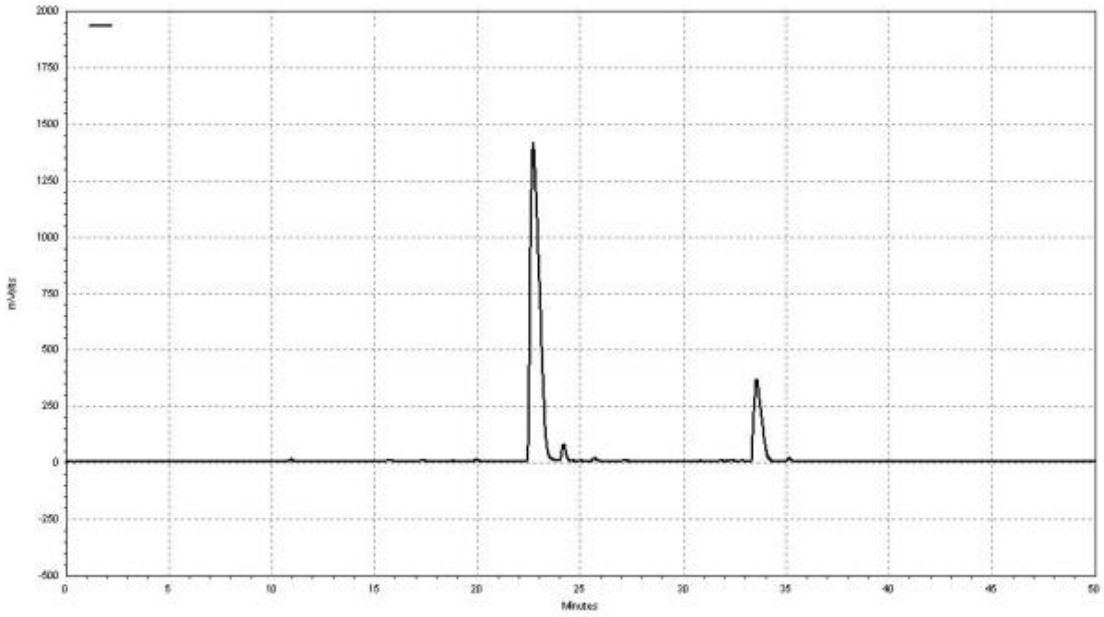

120 min

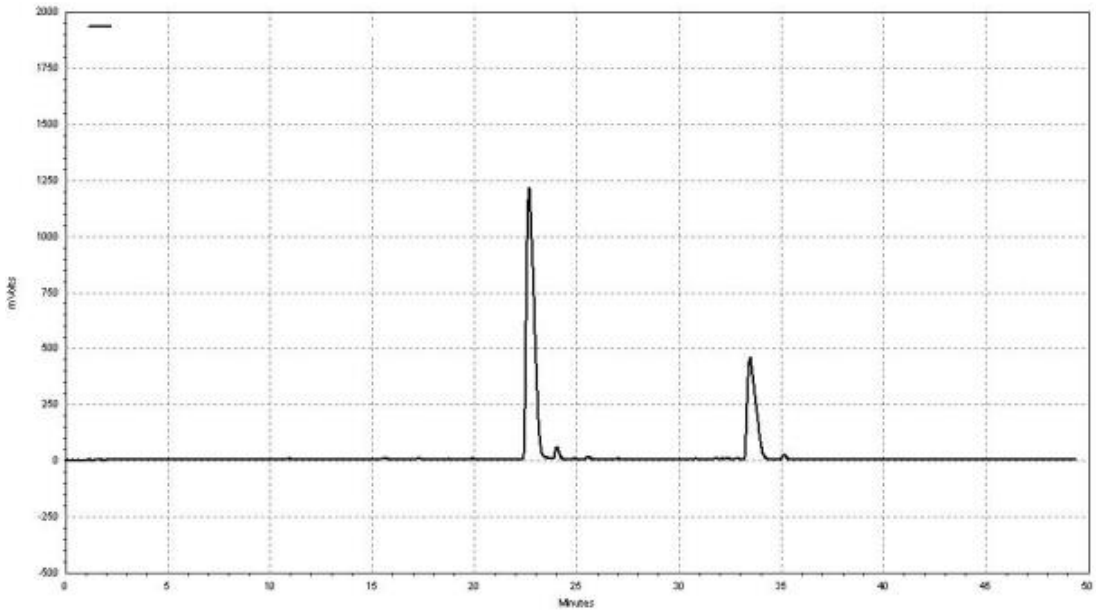

180 min

Continued

Figure 26 continued

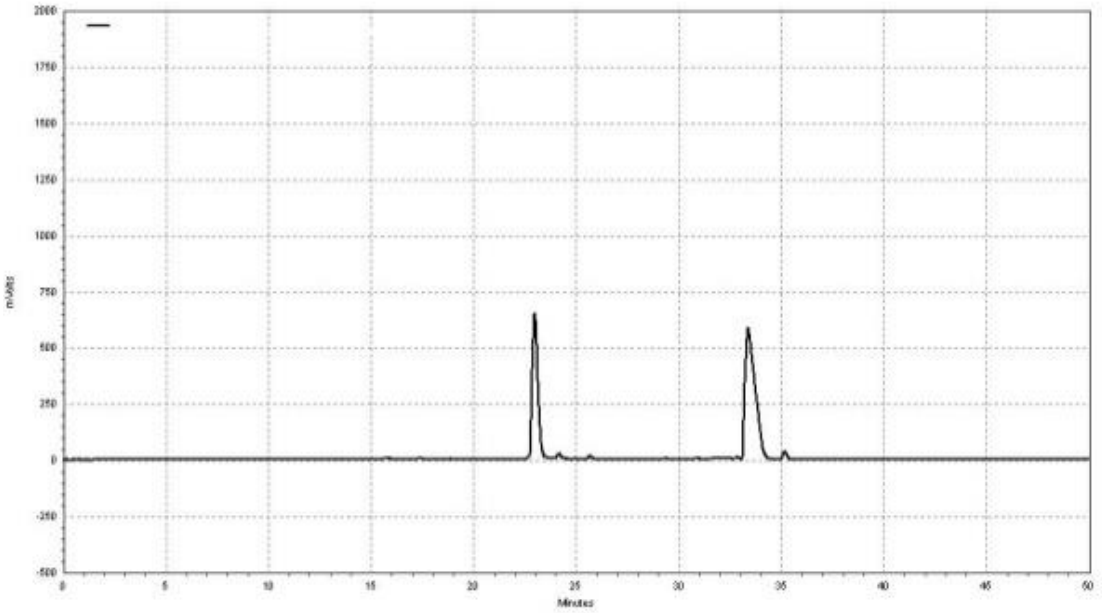

240 min

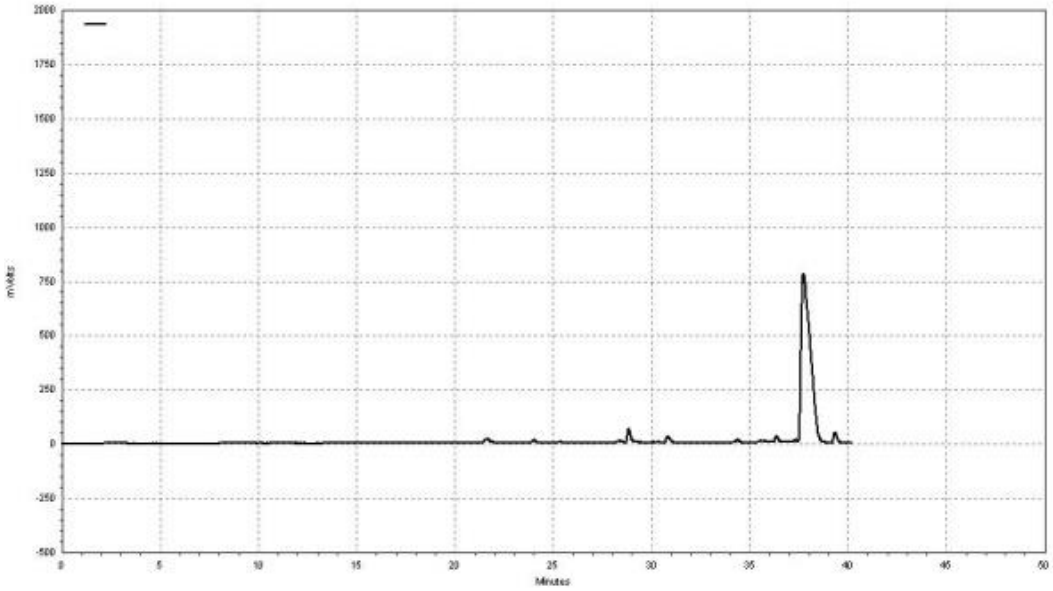

300 min

Continued

Figure 26 continued

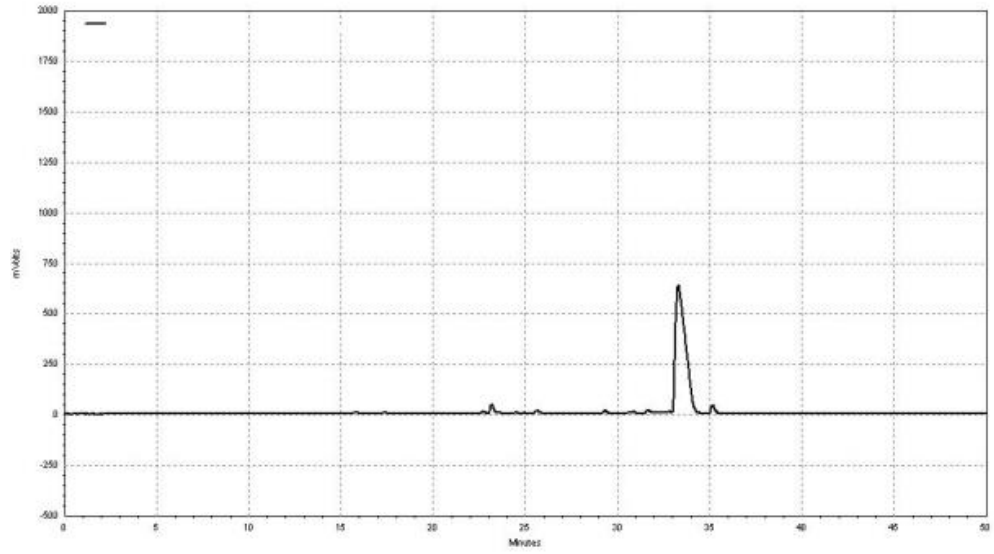

360min

The existence of closed form of spiropyran and the two different open form of spiropyran can be observed by analytical HPLC. From HPLC absorption, at time 0, solution b has 77.6% of open spiropyran form (Figure 25). After visible light irradiation, a new peak with a larger retention time appeared in the HPLC study increased drastically. With longer time irradiation, the open form peaks decreased as the closed form peak increased. After 6 hours' irradiation, the closed form ratio reaches 98.9% and the open form decreased to 1.10%. The change in analytical HPLC study with visible light irradiation further confirmed the structural change from open protonated merocyanine form to the closed spiropyran form. Gelation of the 10 mM solution b also occurred after 3 days irradiation under visible light of LED broad spectrum at 20 ℃.

Thermo-controlled transformations between the closed and the open form of spiropyran tetrapeptides.

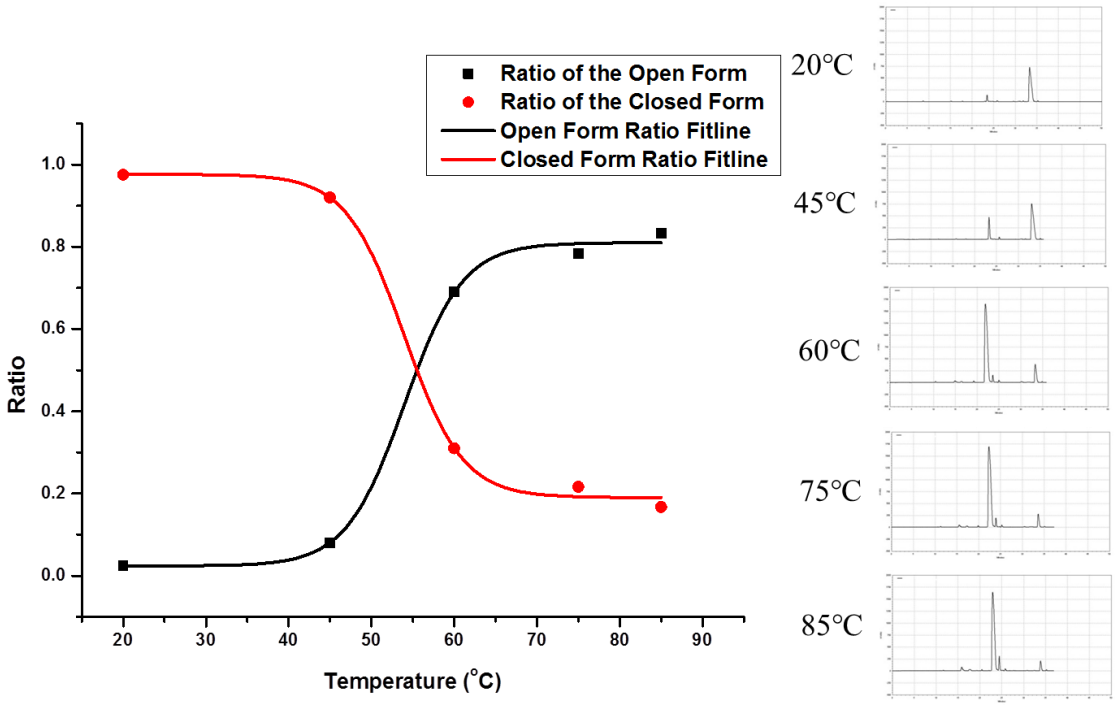

Figure 27. Ratio change of the open and the closed forms of 10 mM spiropyran tetrapeptides **5** solution in 0.75% TFA at different temperature.

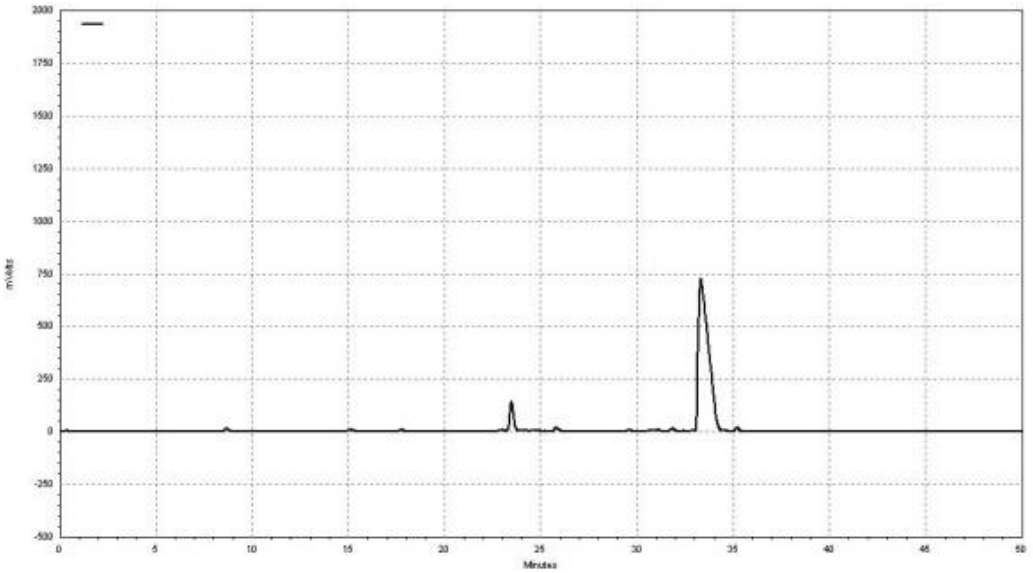

20℃

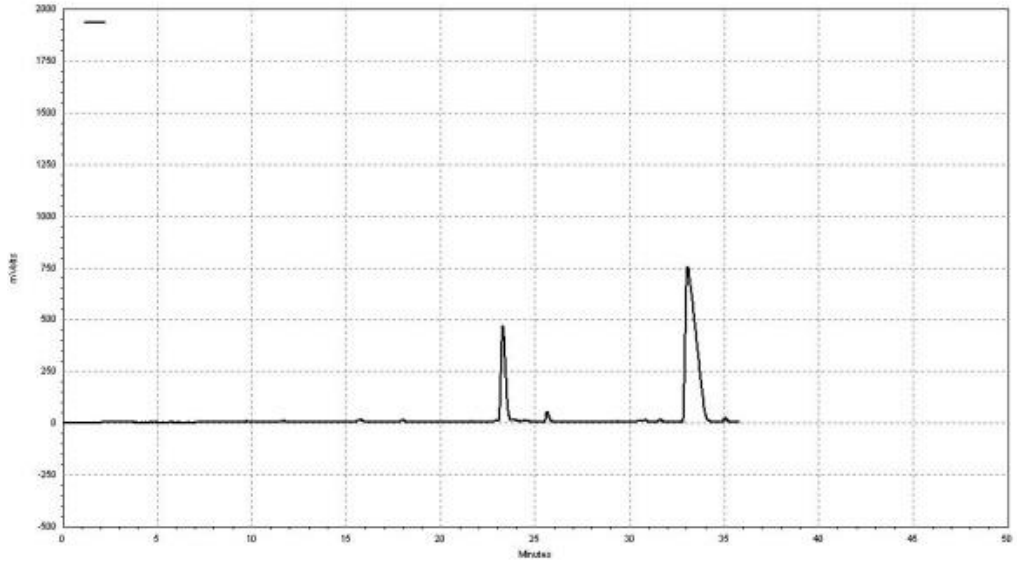

45℃

Continued

Figure 28. Corresponding analytical HPLC peaks of solution under different temperature during the heating process. All graphs were taken at 370 nm UV absorbance with 0.1% TFA of Acetonitrile/H_2O solution, method: 0~5 min 27% acetonitrile, increase to 75% acetonitrile at 50 min, decrease to 20% at 55 min.

Figure 28 continued

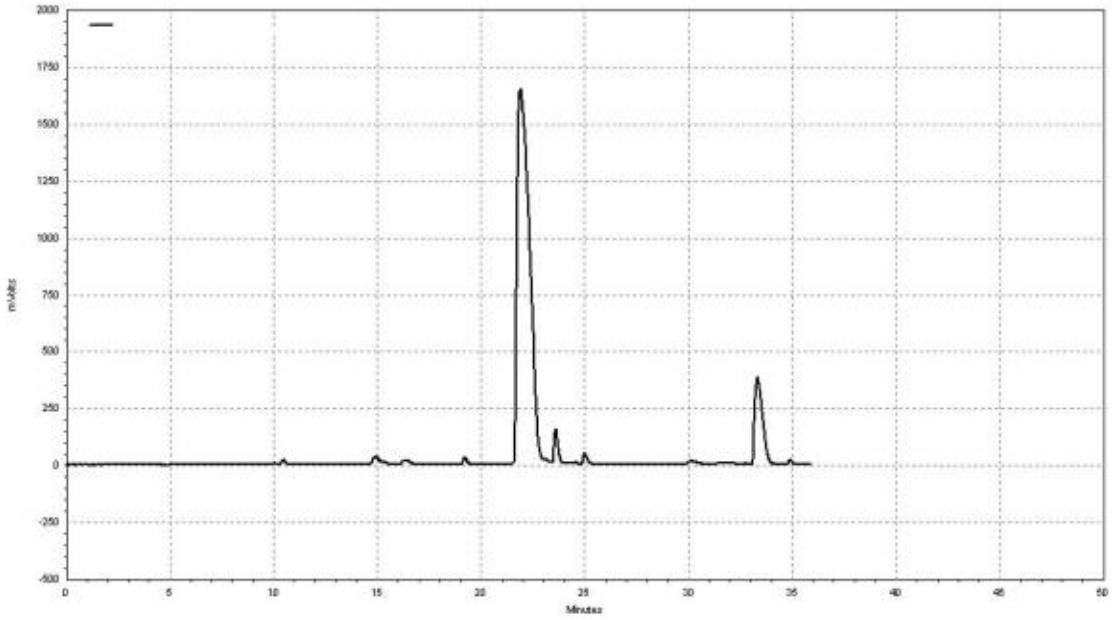

60°C

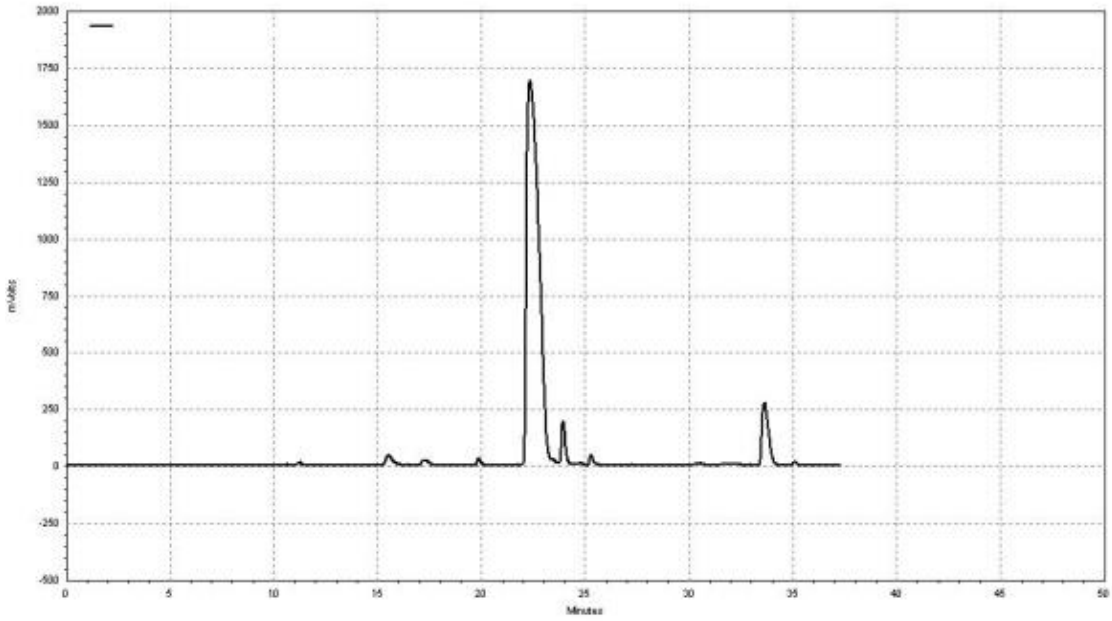

75°C

Continued

Figure 28 continued

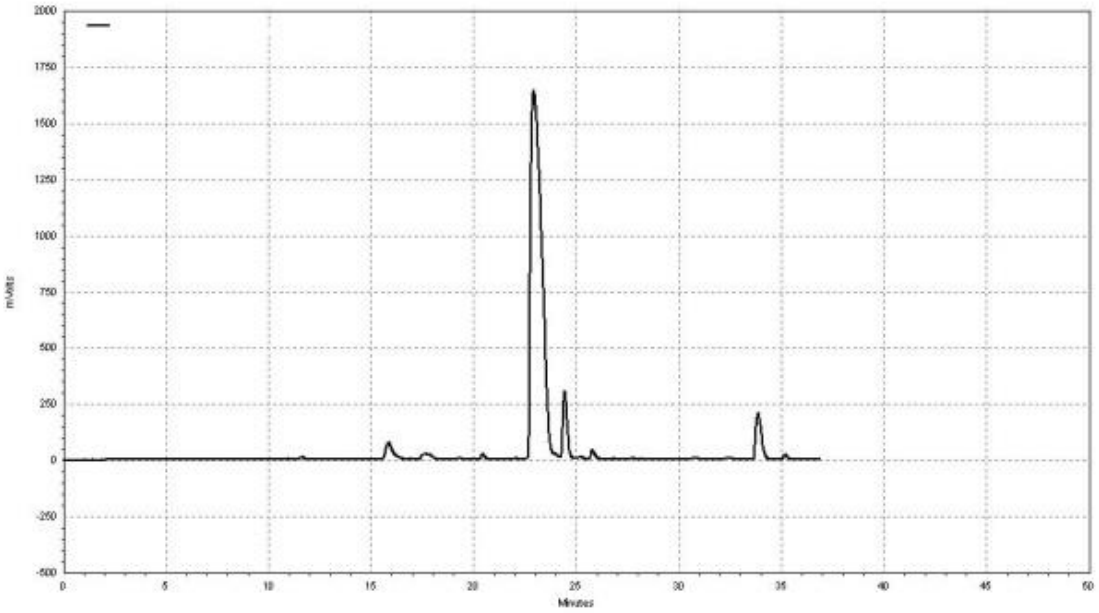

85℃

The opposite process was also investigated by change in temperature as the convert between the closed and the open form of spiropyran is also known as a thermo-controlled process. Fresh 10 mM Fmoc-KK(SP)KF-NH_2 solution in 0.75% TFA was prepared and aged under visible light for 3 days at 20℃ with gelation observed. Then the solution was heated to different temperature by oil bath and stayed for one hour in dark, and then the ratio was studied by analytical HPLC. As temperature increased to 60℃, the gel, formed by 97.6% of closed spyropyran form, changed into solution and the open form ratio increased drastically from 2.4% to 69.0 %. When heated to 85℃, the open form almost reaches 83.3%. The solution formed after heating was cooled down into 20℃ and kept in dark for a week. It stayed as liquid form with no gelation occurred. This also confirmed

that the solution state forms and stays as the compound stays in majorly open form. When opposed under visible light for a week, the solution can changed back into the gel form as the open form convert back into the closed form. Therefore, the reversed closed spyropyran form to the open protonated merocyanine form process was achieved by heating process. This solution-gelation convention can be tested for at least 3 cycles. This shows the reversibility of the interconversion between two states.

Ratio study of gel d heated and stays at 60℃ for different time

The influence of time during heating process has also been studied. The 10 mM Fmoc-KK(SP)KF-NH_2 solution in 0.75% TFA solution gelated in visible light was heated by 60℃ oil bath in dark and the ratio was tested after different time. The ratio of the open form increased immediately from 1.60% to 72.8 % as the temperature increased during the one hour in the 60℃ oil bath and stayed stably over 70% after 3 hours. The solution also formed during the process. This indicates that the ratio of the open and the closed form are rather stable after stay in oil bath for 1 hour. And the thermo-controlled closed to open form conversion is a rather quick process and is almost completed in one hour.

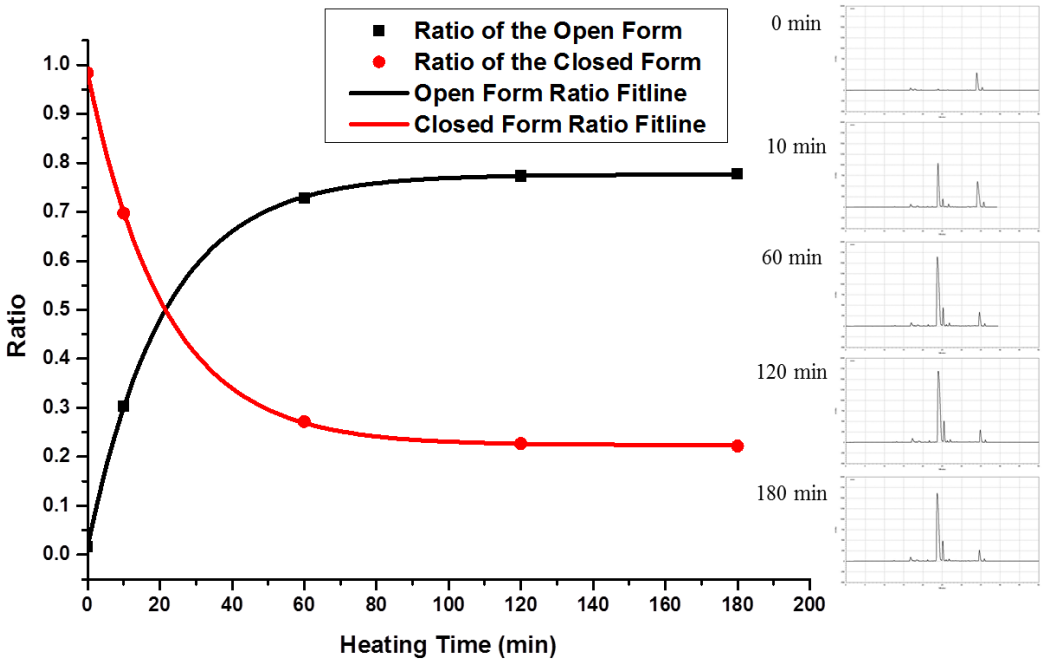

Figure 29. Ratio change of the open and the closed forms of 10 mM spiropyran tetrapeptides solution in 0.75% TFA heated and stays at 60℃ for different time and corresponding analytical HPLC.

Ratio Study of gel d under UV = 254 nm irradiation

The reversed process has also been investigated under UV = 254 nm irradiation after the solution formed gel. And the corresponding ratio change has been studied by HPLC. After 3 days aging under visible light, gelation has been discovered and the ratio of closed and open form has also been tested. The initial gel has 96.0% closed form, 2.05% open form and a small amount of decomposed impurities with an ESI of 1105.5. With 30 min UV = 254 nm irradiation, the gel changed into solution again with the open form increased and stays rather stable around 40%, the closed form also decreased into 47.6%. With longer irradiation, more closed form has decomposed into the impurities. This

suggests that the opposite transformation from closed spiropyran form to the open form is a partially-reversed process.

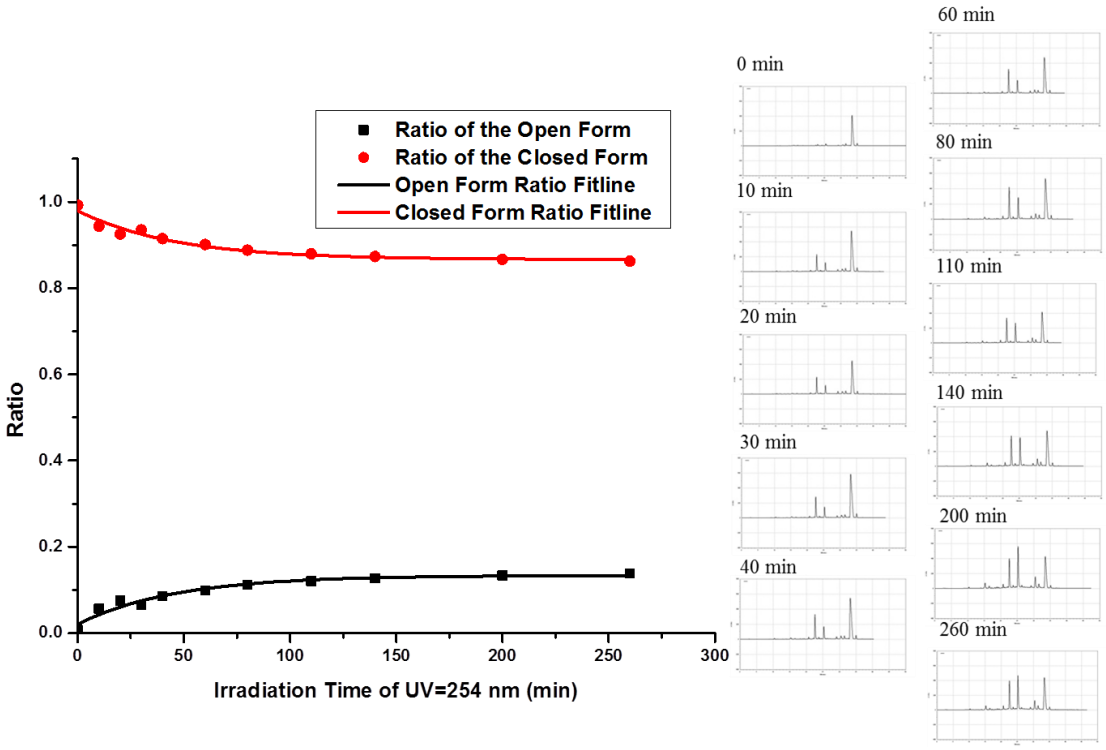

Figure 30. Ratio Study of the open and the closed forms of 10 mM spiropyran tetrapeptides solution in 1% TFA (gel d) under UV = 254 nm irradiation and corresponding analytical HPLC.

Transmission Electron Microscopy (TEM)

The self-assembly behavior of the tetrapeptide solutions (a~d) were investigated by transmission electron microscopy (TEM) after dilution to 1mM. For aqueous solution a and c, SP-tetrapeptide solutions do not have very ordered self-assembly conformation, mostly amorphous aggregates. In 0.75% TFA and aged under visible light, solution d turned into gel and revealed nanofiber structure under TEM. Each fiber was formed by two strands of fibril of 6 ±1nm diameter twisted together. The fibers further entangle into

a network structure and thus form hydrogel. When heated up to 60℃ and aged in dark in the presence of TFA, tetrapeptides majorly stays in the protonated open form with a small amount of protonated closed form, which provides minimal self-assembly of nanofiber structures. The protonated open form failed to assemble into ordered structures since it is too polar and hydrophilic. For the small amount of the protonated closed form, the hydrophobic phases of molecules face each other. Most of nanofibers are separated as monomers rather than entangled together.

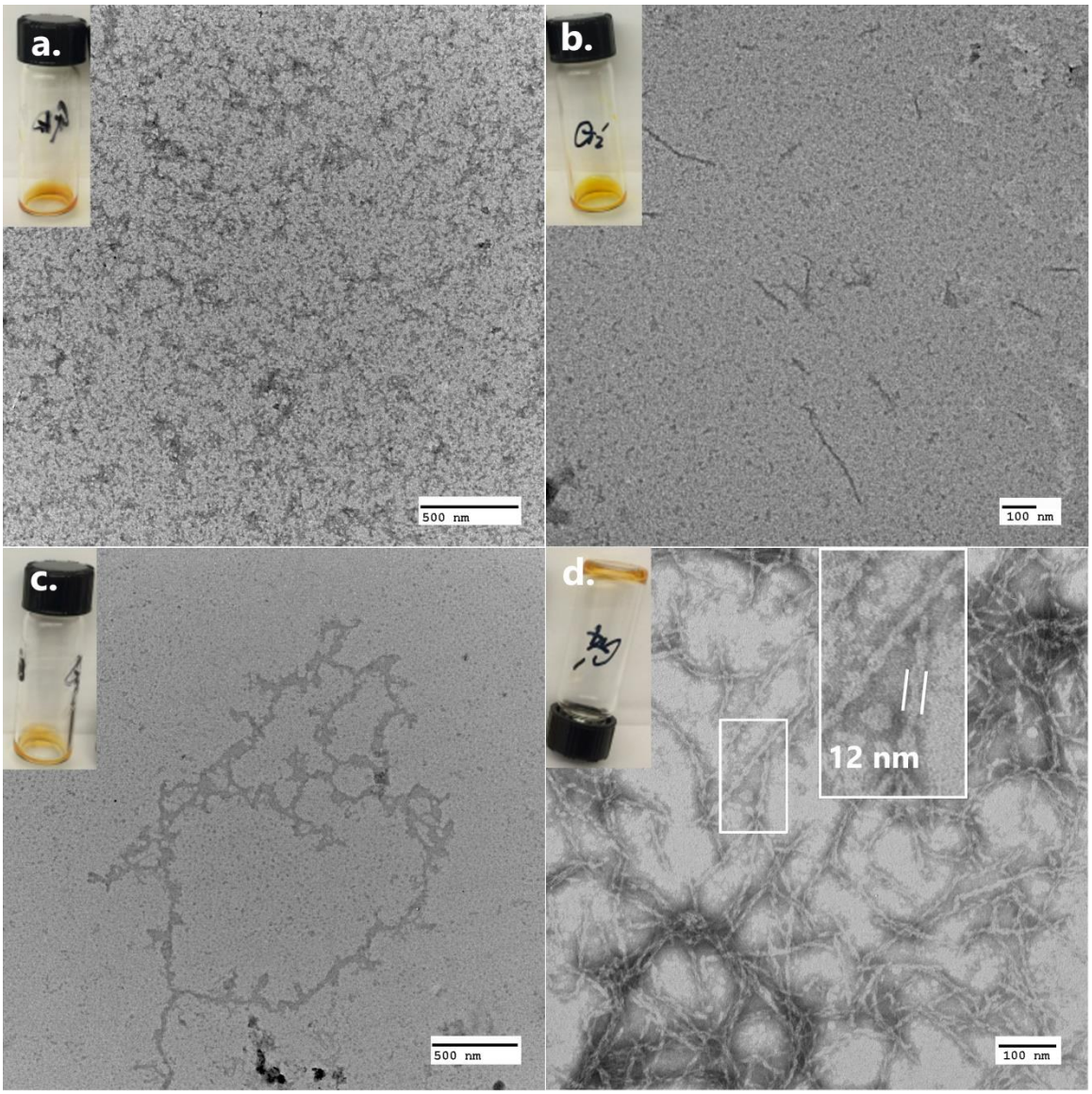

Figure 31. TEM images of solution a, b, c and d. a. Solution a: 1 mM **5** in H_2O kept in dark for 3 days, b. Solution b: 1 mM **5** in 0.75% TFA kept in dark for 3 days, c. Solution c: 1 mM **5** in H_2O and aged under visible light for 3 days, d. Solution d: 1 mM **5** in 0.75% TFA and aged under visible light for 3 days.

Atomic Force Microscopy (AFM)

In the gel formed by solution d, nanofiber structures were observed by atomic force microscopy. In the AFM image, each nanofiber is twisted and a pair of fibers further

entangled into twisted fibrils structure. The thickness of each fibril is around 3 nm, which is smaller than the 5±1nm diameter measurements by TEM images. This difference is most likely due to the compression of the fibril by the AFM tip. These observations are consistent with the amyloid fibrils conformation found in the TEM study.

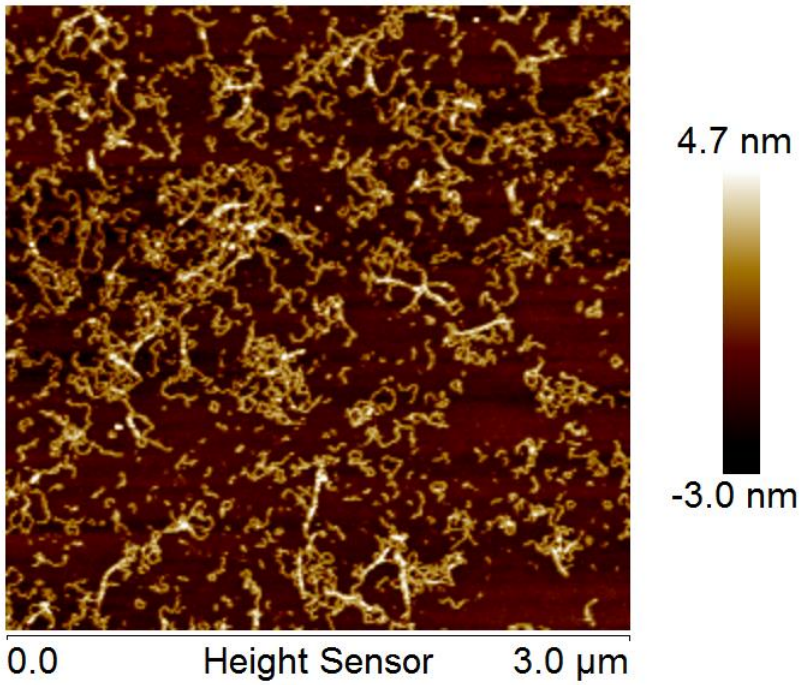

Figure 32. AFM image of nanofibers of gel d (1 mM Fmoc-KK(SP)KF-NH_2 in 0.75% TFA aged under visible light for a week at 20℃).

Thioflavin-T(ThT) binding experiment

The self-assembly nanofiber structures of gel d were investigated by Thioflavin-T (ThT) binding experiment (Figure 33). The ThT binding experiments suggest the conformation of amyloid fibers for the observed fiber structures. Amyloid formation can be detected by ThT as an indicator. Upon binding to amyloid fibrils, the fluorescence emission of ThT will increase strongly when excited at 450 nm. As shown in Figure 33,

without gel d (Fmoc-KK(SP)KF-NH_2) addition, ThT experiences weak fluorescence. However, when 5 μL gel d were added to 0.5 mL 0.05 mM ThT working solution, a drastic increase of fluorescence intensity of emission at 482 nm was observed. With another 5 μL gel d added to the system, fluorescence intensity further enhanced significantly as more gel d bond to ThT. These results suggest the successful binding of ThT with gel d, which indicates the self-assembly nanofibers formed by gel d adopt the β-sheet amyloid fibril structure as we expected.

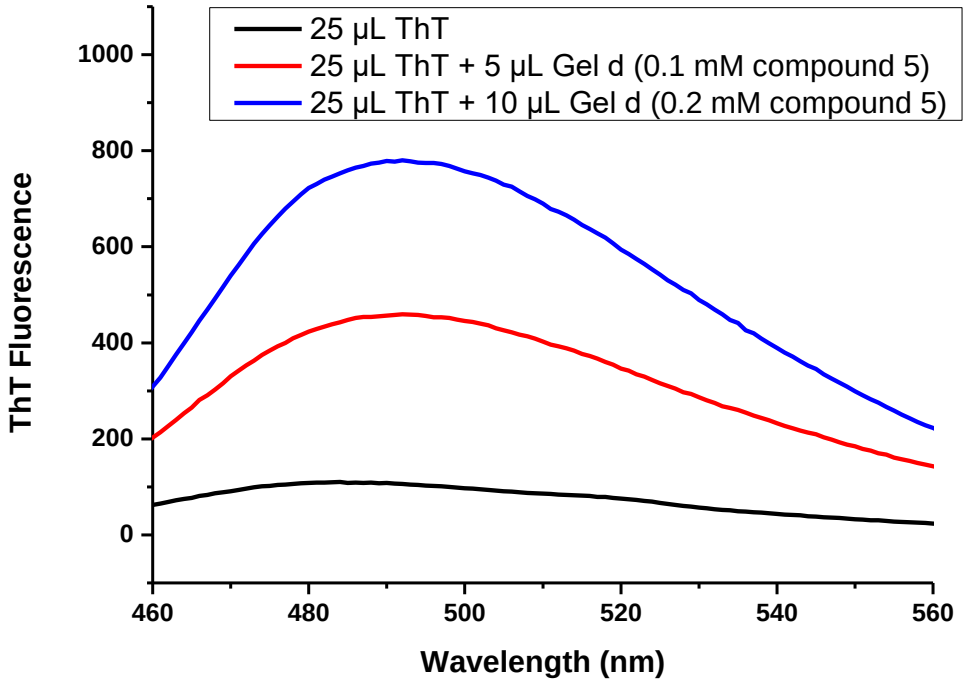

Figure 33. Fluorescence emission spectra of 25 μL ThT with varying gel d concentrations. Black line: 25 μL ThT without gel d binding. Red line: 25 μL ThT with 5 μL gel d addition (0.1 mM Fmoc-KK(SP)KF-NH_2). Blue line: 25 μL ThT with 10 μL gel d addition (0.2 mM Fmoc-KK(SP)KF-NH_2).

Ultraviolet-visible (UV-Vis) Spectroscopy

The conversion between closed spiropyran form (SP) and the open merocyanine form (ME) can be observed by Ultraviolet-visible (UV-Vis) microscopy and analytical HPLC. In H_2O, when heated up to 60℃ and kept in dark (solution a) Fmoc-KK(SP)KF-NH_2 has a small peak at 500~550 nm, which originates from the merocyanine (ME) π-π* electronic transition and indicates the presence of the deprotonated open form of merocyanine (ME)[148], (Figure 34 black line). The weak intensity of this peak demonstrates that, SP-tetrapeptides majorly stays as the closed spiropyran form (SP)(80.8%), which is confirmed with analytical HPLC (Figure 35a). In HPLC, the tetrapeptides with the protonated merocyanine form showed as a different peak from the closed spiropyran form with higher polarity. With visible light irradiation, this small peak disappeared, indicating that Fmoc-KK(SP)KF-NH_2 the almost complete change into closed spiropyran form (Figure 34 blue line), which is 99.4% based on the HPLC study (Figure 35c). For solution in 0.75% TFA, after UV irradiation and kept in dark, there is a distinct peak around 415 nm (Figure 34, red line), which is the absorption band of the protonated merocyanine form[156]. In this condition, a large portion of SP-tetrapeptides changes into the protonated open merocyanine form (85.6% in Figure 35b). With visible light irradiation, the decreased intensity of the peak around 415 nm reveals that the tetrapeptides covert back into the closed spiropyran form (Figure 34, pink line) with a 99.5% ratio (Figure 35d). The intense absorption band around 270 nm is related to the electronic transitions of the aromatic benzene ring. The band around 340 nm indicates the internal charge-transfer transition in the spiropyran system[156]. Although it is not distinct

,but both solutions in 0.75% TFA have slight blue shifts compared with the aqueous solutions, indicate that an H-type π-π interaction contributes to the self-assembly behavior.

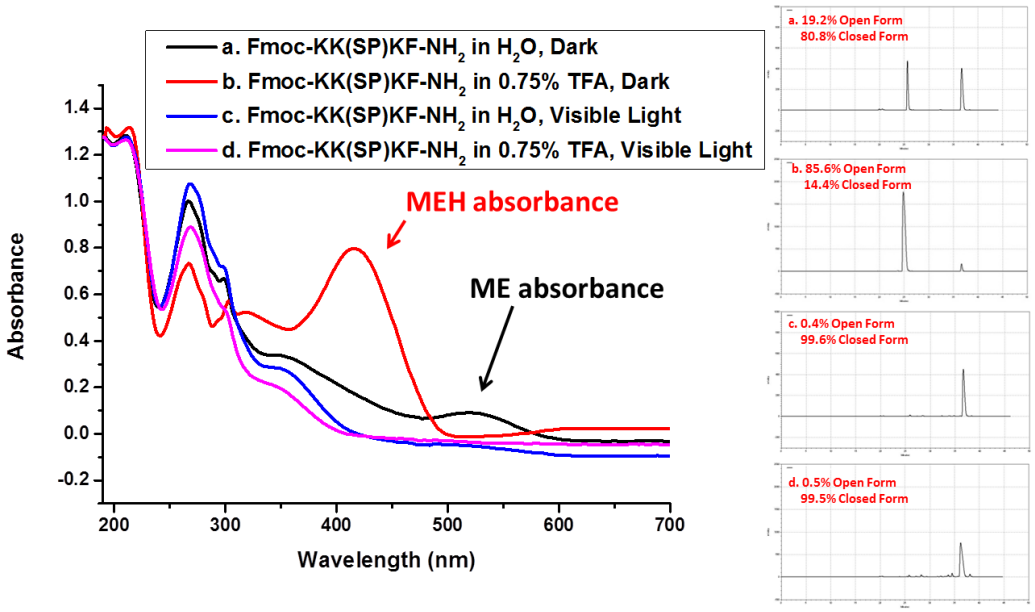

Figure 34. The UV-vis absorption of tetrapeptides Fmoc-KK(SP)KF-NH_2 solution a~d.(0.5 mM) a. in H_2O kept in dark, b. in 0.75% TFA kept in dark, c. in H_2O and aged under visible light, d. in 0.75% TFA and aged under visible light.

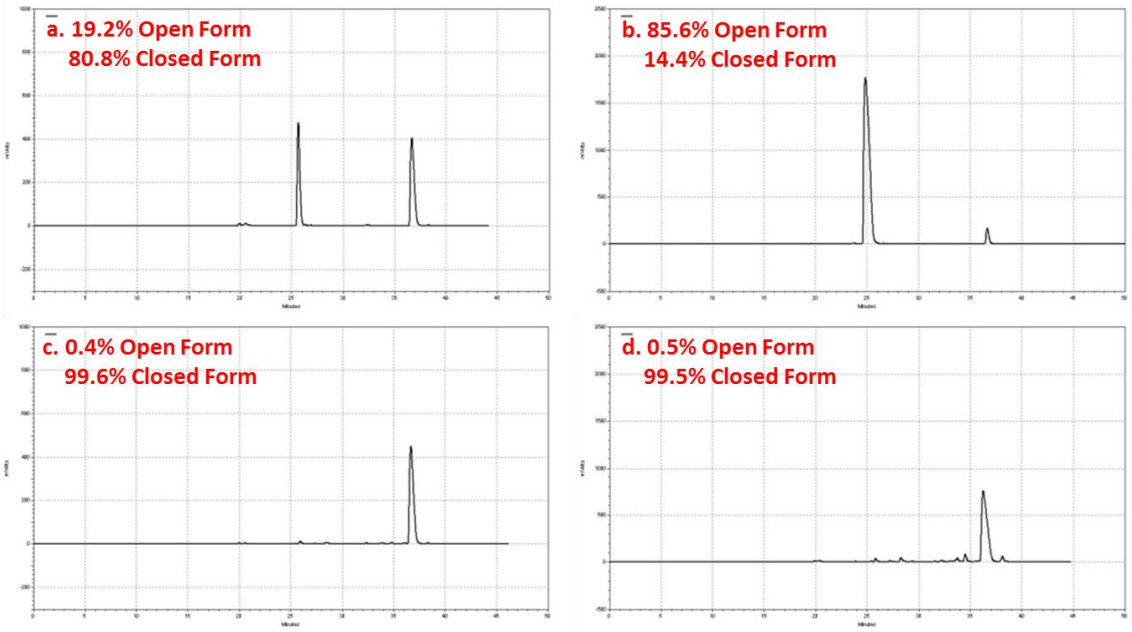

Figure 35. The corresponding analytical HPLC ratio of Fmoc-KK(SP)KF-NH2 for UV and CD study: a. in H_2O in dark (19.2% Open from, 80.8% Closed form), b. in 0.75% TFA in dark (85.6% Open form, 14.4% Closed form), c. in H_2O under visible light (0.4% Open form, 99.6% Closed form), d. in 0.75% TFA under visible light (0.5% Open form, 99.5% Closed form).

Circular Dichroism (CD) Study

To investigate the relative spatial arrangement of Fmoc-KK(SP)KF-NH_2 molecules in the assembly, the corresponding CD spectra of a~d four solutions have also been measured. For both aqueous solution (a,c), there is no distinct CD signal for self-assembly, which corresponds to the amorphous aggregates in TEM measurements. For the Fmoc-KK(SP)KF-NH_2 solution in 0.75% TFA in dark(b), there is no distinct CD signals either, corresponding to the minimal assemblies in TEM (Figure 36b).For the sample in 0.75% of TFA under visible light (solution d), the CD spectra have two distinct negative absorbance bands, around 230 nm and around 275 nm. The broad negative band

exhibited near 220 nm is also the signature absorbance of β-sheet type secondary structure[180]. Thus the nanofibers formed by Fmoc-KK(SP)KF-NH_2 solution in 0.75% TFA is formed by the protonated closed forms with a β-sheet type secondary structure. The excitonic couplets centered at 267 nm correspond to the UV absorption peak at 269 nm, which is for the electronic π-π* transition band from the indoleline part of spiropyran[181]. This transition, responsible for the first absorption band, is parallel to long axis of indoleline part of spiropyran moiety as reported.[182] The negative exciton couplets indicate an M-type helical structure for assembly.

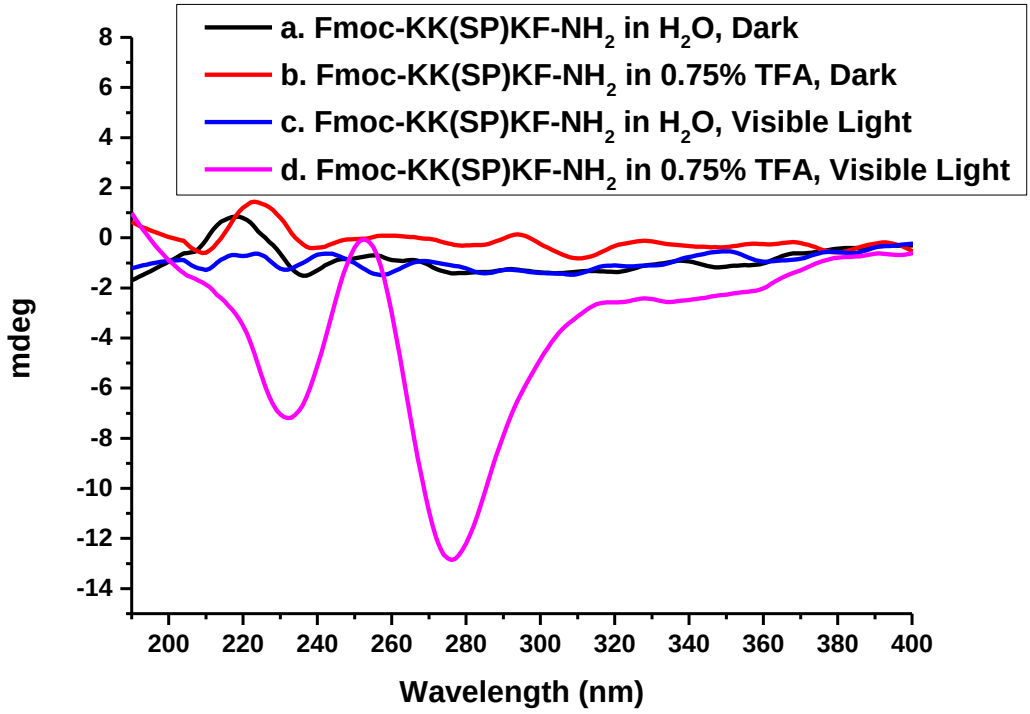

Figure 36. CD spectra (0.5 mM) of tetrapeptides Fmoc-KK(SP)KF-NH_2 solution a~d.

Fourier-transforminfrared (FT-IR) spectrum study

Fourier-transform infrared (FT-IR) studies were conducted to investigate the secondary structure of spiropyran tetrapeptide conjugates in self-assembly. For both sample b and d, H_2O and TFA solvents were removed by lyophilization, and were re-dissolved in D_2O to get the FTIR spectra a and b respectively (Figure 37). In both spectra, the major peaks appeared at 1674 cm^{-1} are referred to the C=O stretch absorption band of the amide group of spiropyran. The place of the amide I band vibrations arising from C=O stretch of amide group is a signature for different secondary structures in poly-peptides and proteins. For the gel solution under visible light formed by the closed spiropyran forms, a distinct peak at 1630 cm^{-1} indicates a β-sheet secondary structure, typically 1620 -1640 cm^{-1} amide I band. After deconvolution, a small peak around 1648 cm^{-1}, which is among the 1640 -1650 cm^{-1} non-ordered structure absorption band, showed a small portion of Fmoc-KK(SP)KF-NH_2 with non-ordered secondary structure with 12%. However, the major secondary structure for the closed spiropyran form assembly is β-sheet with a much stronger absorption band that takes up 88%. Therefore, the tetrapeptides backbone majorly adopts a β-sheet secondary structure in the assembly, which is consistent to the CD spectra in Figure 36. For solution in dark formed by the open merocyanine form, a non-ordered structure band around 1644 cm^{-1} is much stronger and no significant β-sheet band was observed, consistent with the CD spectra, indicating a dominate random coil secondary structure.

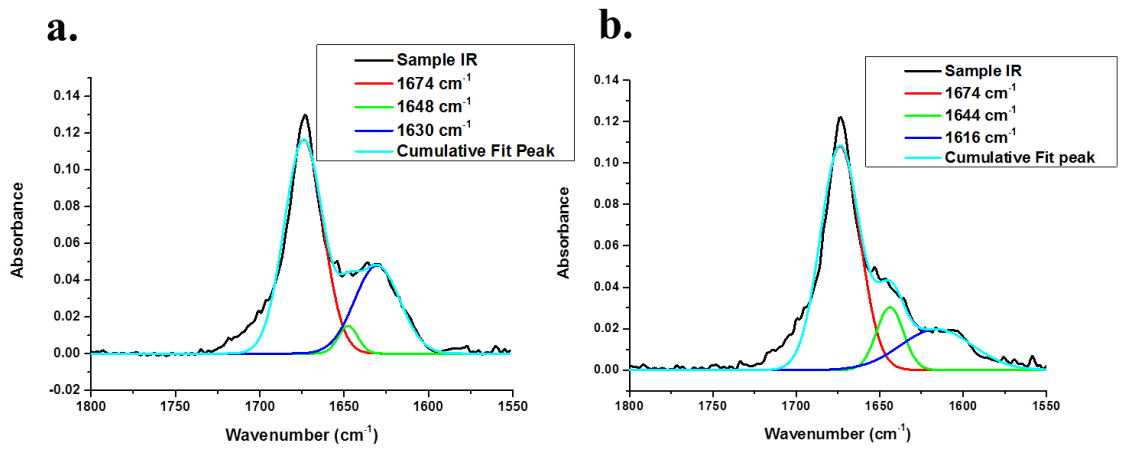

Figure 37. FT-IR spectra of the tetrapeptides sample b and d re-dissolved in D_2O to prepare 20 mM solution after lyophilization. a. Gel d under visible light (20 mM), b. solution b in dark (20 mM).

Rheology Study

The physical property of gel after annealing process has been tested under the mode of dynamic sweep at sweep rate of 6.28 rad/s. Solution d was aged for a week to form gel sample after first heating cycle. Then the gel has been heated to 60°C for an hour and it turns into dark liquid solution as a large part of spiropyran opens. Then the solution was cooled down and aged for another week to form gel for the second cycle. The rheology of the second cycle gel was tested after one week of the heating up process. In Figure 38, both the first and the second cycle exhibit higher storage modulus (G') than lost modulus (G"), which reveals the viscoelastic property of the gel. The storage moduli of both samples exceed the corresponding lost moduli by a factor of 5. The second cycle gel was even more viscoelastic than the first cycle gel, with a significantly higher storage modulus of 260 Pa, the lost modulus has also increased to around 50 Pa. This increased

viscoelasticity showed a rather good recovery of physical properties of gel and indicates that the changing process is reversible. The reason for this change remains unclear. One hypothesis is that the heating process did not break down the gel fibers completely; short fibers still remain in the solution. So after cooling down and aging, a further branched gel fiber network was formed with an even firmer gel. The mechanical property of gel is concentration-dependent.

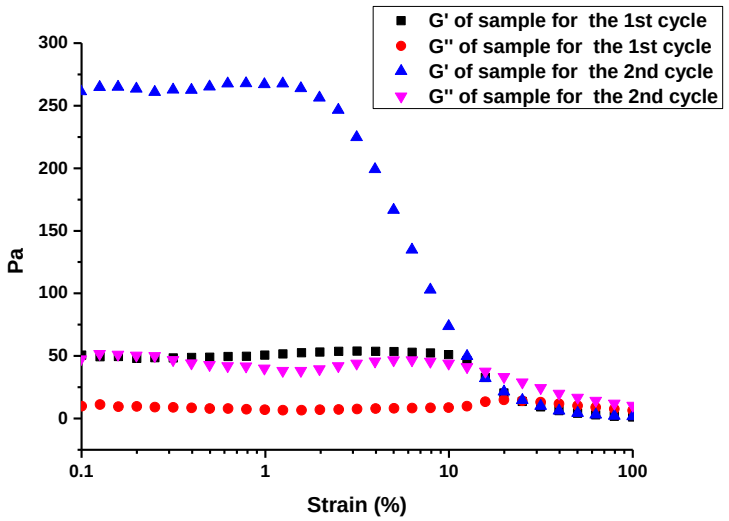

Figure 38. Rheology of 10 mM Fmoc-KK(SP)KF-NH_2 sample gel in 0.75% TFA for 1st and 2nd heating cycle.

The 20 mM sample showed a much stronger viscoelasticity with a storage modulus of around 380 Pa and a similar tolerance of % strain (Figure 39). It also takes much longer to form a gel since is more concentrated, which takes longer to be converted by visible light and forms a stronger gel with more fiber networks under higher concentration.

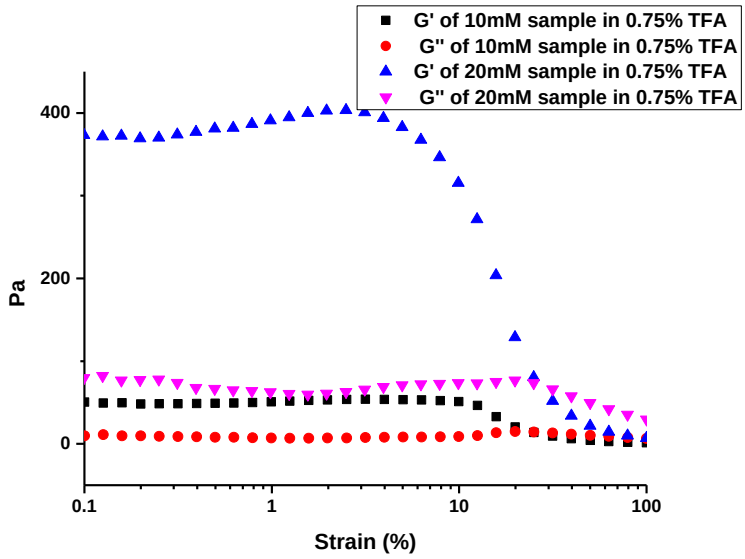

Figure 39. Rheology of 10 mM and 20 mM Fmoc-KK(SP)KF-NH_2 sample gel in 0.75% TFA.

The influence of TFA concentration has also been studied, three 10mM Fmoc-KK(SP)KF-NH_2 under 0.75%, 1.0% and 1.5% TFA concentration solutions were prepared. The sample under 1.5% TFA precipitated out and failed to form gel. Sample in 1.0% and 0.75% TFA formed gel successfully after two days' aging. The rheology properties of them have been tested after 1 week aging (Figure 40). The sample in 1% TFA shows a better viscoelasticity than the sample in 0.75% TFA with a storage modulus of 110 Pa, but less tolerant to the external force as it started to break down under a much smaller strain of 2% strain.

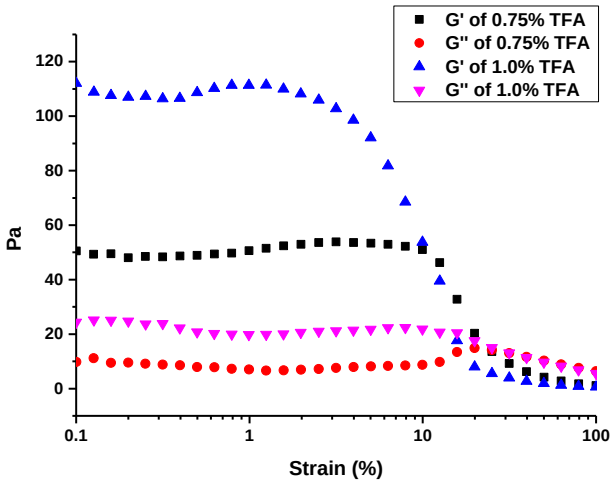

Figure 40. Rheology of gel samples formed by 10 mM Fmoc-KK(SP)KF-NH_2 in 0.75% TFA and 1.0% TFA.

2.3 Conclusions

We have designed and synthesized a spiropyran tetrapeptides conjugate Fmoc-KK(SP)KF-NH_2 following the solid-phase synthesis route. This compound can dissolve in 0.75% TFA aqueous solution and self-assemble into amyloid β-sheet nano-fibrils structure and further form gel on macroscale. When heated up to over 60 ℃， spiropyran opens and formed the polar protonated MEH form. This process disrupts the nano-fibril assembly and turns gel into solution form. The assembly and disassembly were confirmed by CD study. With visible light irradiation, protonated merocyanine form releases the proton and converts back into the closed spiropyran form, restoring nano-fiber assembly structure and gel property, rendering the entire process reversible. The transision between different states of SP, MEH can be monitored by UV-Vis spectrum and also analytical HPLC. Both CD and Infrared spectrums revealed that Fmoc-

KK(SP)KF-NH_2 tetrapeptides adopt β-sheet secondary structure. The gel properties was tested and confirmed by rheometer.

Herein, we report a novel type of photo-and thermos-responsive assembly material that switches its rheology properties in macroscale based on the reversible chemical structural change of a small organic molecule. This type of material is very rare so far. Our molecule can provide valuable insights to future materials design and may further be applied to optical memory devices, wettability and even drug-delivery systems.

2.4 Experimental Section

Materials and General Method

The Fmoc-amino acids, and 1- hydroxybenzotriazole (HOBt), 2-(1H-benzotriazol-1-yl)-1,1,3,3-tetramethyluronium hexafluorophosphate (HBTU) were purchased from Chem-Impex Int'l Inc. The rink amide resin was obtained from ChemPep. 4-hadrazinobenzoic acid, propylmethylketone, iodomethane and 2-hydroxyl-5-nitrobenzaldehyde were purchased from Sigma-Aldrich. All the solvents were obtained from Fisher Scientific and All NMR solvents were from Cambridge Isotope Labs. Reversed-phase HPLC was conducted on C18 columns with use of water/acetonitrile/TFA gradients between 68:32:0.1 and 25:75:0.1. NMR spectra were obtained on Bruker AMX 400 pectrometers. All SP1~SP4 are known compounds, their NMRs are adopted from previous literature[183].

2,3,3-Trimethyl-5-carboxy-3H-indole (1)

4-hadrazinobenzoic acid (6.1 g, 40 mmol), propylmethylketone (4.8 mL, 44 mmol) and concentrated H_2SO_4 (1.0 mL) was added to EtOH (120 mL) solution and heated under reflux for 12 h and then cooled to room temperature and filtered. Then a saturated aqueous solution of $NaHCO_3$ (60 mL) was added to the filtrate and EtOH was removed under pressure. The left solution was washed with dicloromethane (DCM) (3 ×40 mL). Then the pH of aqueous phase was adjusted to 4 with 1M HCl solution and then washed with DCM (4 ×40 mL). The combined organic phase DCM was dried over $MgSO_4$ and distilled under reduced pressure to obtain 2,3,3-Trimethyl-5-carboxy-3H-indole (7.88 g, 97%) as a brownish solid: mp = 192℃; FABMS m/z = 204 $[M + H]^+$; ^{1}H NMR (400 MHz, $CDCl_3$) δ = 1.35 (6H, s), 2.40 (3H, s), 7.69 (1H, d, 8 Hz), 8.07 (1H, d, 1Hz), 8.15 (1H, dd, 1 and 8 Hz), 10.64 (1H, bs); ^{13}C NMR (100MHz, $CDCl_3$) δ = 15.6, 23.0, 54.1, 119.7, 123.4, 128.4, 130.9, 145.5, 156.7, 171.0, 192.9[183] .

1,2,3,3-Tetramethyl-5-crboxy-3H-indolium iodide (2)

A solution of **1** (7.78 g 38 mmol) and MeI (2.8 mL, 44 mmol) in toluene/MeCN (2/1, v/v) 90mL was heated under reflux under argon for 14 h. The mixture was cooled to 0 ℃ and the resulting precipitate was filtered washed with EtOH (5mL) and hexane (40 mL) to obtain 1,2,3,3-Tetramethyl-5-crboxy-3H-indolium iodide (7.60 g, 57%) as an orange color solid: FABMS *m*/*z* = 219 $[M + H]^+$; ^{1}HNMR [400 MHz, CD3CN/CD3OD (5:1, v/v)] δ = 2.93 (6H, s), 4.07 (3H, s), 5.32 (3H, s), 9.18 (1H, d, 8 Hz), 9.63 (1H, dd, 1 and 8 Hz), 9.68 (1H, d, 1 Hz); ^{13}C NMR = 75 MHz, CD_3CN/CD_3OD (5:1, v/v)] δ = 22.4, 36.0, 56.0, 116.4, 125.5, 132.2, 133.5, 143.2, 167.5[183].

1,3,3-Trimethyl-2-methylene-5-carboxy-3H-indole (3)

A solution of the **2** in aqueous sodium hydroxide (0.32 M, 100 mL) was stirred at room temperature for 2 h. The pH of the solution was adjusted to 7 with aqueous HCl (1 M) and the solution was washed with isopropanol/DCM(1/1, v/v) 6 × 30 mL. The organic phase was dried over $MgSO_4$ and filtered, the solvent was removed under reduced pressure to yield 1,3,3-Trimethyl-2-methylene-5-carboxy-3H-indole (4.57 g 95%) as pink solid: FABMS *m*/*z*) = 218 $[M + H]^+$; ^{1}H NMR (400 MHz, $CDCl_3$) δ =1.37 (6H, s), 3.11 (3H, s), 4.00-4.02 (2H, m), 6.56 (1H, d, 8 Hz), 7.79 (1H, d, 2 Hz), 7.98 (1H, dd, 2 and 8 Hz); ^{13}C-NMR (100 MHz, $CDCl_3$) δ = 29.1, 30.0, 43.8, 104.5, 119.1, 123.9, 132.2, 137.9, 151.2, 162.3, 171.6[183].

1',3',3'-Trimethyl-5'-carboxy-6nitrospiro[2H-benzopyran-2,2'-3H-indole] (SP-COOH) (4)

(4.56 g 21 mmol) and 2-hydroxyl-5-nitrobenzaldehyde (4.22g, 25 mmol) was dissolved in 250 mL MeCN and heated under reflux under argon for 14 h. The solution mixture was cooled to 0 ℃ and the resulting precipitate was filtered and washed with hexane (50 mL) to afford 1',3',3'-Trimethyl-5'-carboxy-6nitrospiro[2H-benzopyran-2,2'-3H-indole] (SP-COOH) as a pinkish solid (6.47g, 84%). FABMS *m*/*z* = 367 $[M + H]^+$; ^{1}H NMR [400 MHz, $(CD_3)_2SO$] δ =1.13 (3H, s), 1.24 (3H, s), 2.76 (3H, s), 6.02 (1H, d, 10Hz), 6.70 (1H, d, 8 Hz), 6.92 (1H, d, 9 Hz), 7.26 (1H, d, 10 Hz),7.69 (1H, d, 8 Hz), 7.81 (1H, dd, 2 and 8 Hz), 8.02 (1H, dd, 3 and 9 Hz), 8.24 (1H, d, 3 Hz), 12.39 (1H, s); ^{13}C NMR (100 MHz, CDCl3) δ =19.5, 25.5, 28.4, 51.5, 105.9, 106.2, 115.4, 118.8, 120.9, 121.6, 122.8, 122.9, 125.8, 128.5, 130.8, 135.9, 140.7, 151.2, 158.9, 167.3[183].

Fmoc-KK(SP)KF-NH_2

The protected amino acid, tetrapeptides Fmoc-K(Boc)K(Mtt)K(Boc)F-NH_2 were manually synthesized through standard solid-phase peptides synthesis scheme on rink amide resin (loading 0.8 mmol/g) by using Fmoc-Phe-OH, Fmoc-Lys(Boc)-NH2 and Fmoc-Lys(Mtt)-OH. Fmoc-Phe-OH were coupled to the rink amide resin swelled in DCM for 1 h, with standard techniques: 1,3 - diisopropylcarbodiimide (DIC), and 1-hydroxybenzotriazole (HOBt) (300% mol each relative to resin) in 1:1 DMF/DCM for 1.5 h. The general amino acids coupling steps were completed with adding 2.0 equivalents of targeted fluorenylmethyloxycarbonyl group (Fmoc-) protected amino acids, HBTU, HOBt and 4.0 equivalents of N,N - diisopropylethylamine (DIPEA) and reacted for 1.5 h. A solution of 20 % piperidine in DMF was used to deprotect the Fmoc group and the removal of methytrityl (Mtt-) protecting group was accomplished with adding 1% trifluoroacetic acid (TFA) in DCM for 8 × 5min, then the deprotected free amine was coupled with 1.5 equivalencts of **4** with HBTU, HOBt and DIPEA in DMF. The SP-peptide conjugates were cleaved from the resin by the TFA/triethylsilane/water (94 / 5 / 1) at room temperature for 2 h. The crude tetrapeptides were precipitated with cold diethylether and purified by reversed-phased HPLC on preparative Varian Dynamax C18 column and stored as lyophilized powers at 0 ℃. Peptide purity was assessed by analytical reverse-phase HPLC and identity confirmed using ESI-TOF mass spectrometry and NMR. FABMS m/z = 1119.5662 $[M + H]^+$ Detailed ^1H NMR [400 MHz, $(CD_3)_2SO$] and ^{13}C NMR [400 MHz, $(CD_3)_2SO$] are reported in Appendix A. Detailed HPLC and FABMS are reported in Appendix B.

Preparation of Spiropyran Tetrapeptides Solution

The freeze-dried tetrapeptides Fmoc-KK(SP)KF-NH_2 was added to water and 0.75% TFA in water solution to prepare 10 mM stock solution. Each solution was divided by half; half of the solution was irradiated by UV = 254 nm for 3 h and aged at room temperature in dark condition for 3 days and the other half was moved under visible light of table lamp and aged for 3 days at room temperature. And name each solution a, b, c and d.

Transmission Electron Microscopy (TEM) Measurement – Negative Stain TEM

Fmoc-KK(SP)KF-NH_2 sample solution in H_2O and 0.75% TFA (10 mM) were prepared and aged in dark for 3 days before the measuments. The solutions were freshly diluted to 1 mM and sonicated until completely dissolved. 10 μL drops of each SP-tetrapeptide solution was applied to carbon coated copper grid (Ted Pella, Inc.) for 3 min. The excess solution was removed with filter paper and dried, and then the grid was floated on 10 μL drops of 2 % wt uranyl acetate solution for negative stain for 1 min.

Atomic Force Microscopy (AFM)

AFM images were collected on Bruker AXS Dimension Icon Atomic Force Microscope under a nitrogen atmosphere in tapping mode using silicon tips (NSC14/AIBS, μMasch). Diluted sample solutions were dropped on freshly cleaved mica and allowed to dry for 30 min before imaging. The scanning speed was at a line frequency of 0.5 Hz, and the original images were sampled at a resolution of 512 × 512 pixels.

Ultraviolet-visible (UV-Vis) Spectroscopy Measurement

The UV-Vis spectroscopy studies were conducted using a 1 mm path length quartz cuvette over the range of 200-700 nm at room temperatue. Sample solutions (0.5 mM) were prepared by freshly dilute the 10 mM peptides solution in water and 0.75 % TFA.

Spiropyran Closed and Open Form Measurement and UV Calibration

The ratio of the closed and the open form of spiropyran tetrapeptides were measured by analytical reverse-phase HPLC. 10 mM Fmoc-KK(MC)KF-NH_2 stock solution in 0.75% TFA (solution b) were prepared and stored in dark without visible light irradiation. The sample's analytical HPLC graph was taken at 370 nm (0 min visible light irradiation). Simultaneously, corresponding UV spectrum was taken on the same sample immediately diluted to 0.5 mM. Irradiate the rest of stock solution under visible light for 6 hours, and the UV spectra of sample under 120 min, 240 min and 360 min light irradiation were taken immediately after dilution. Corresponding analytical HPLC graphs were taken (Figure 41). The retention areas of HPLC peak were integrated and corresponding UV absorbance were recorded. The ϵ_1 of Fmoc-KK(MC)KF-NH_2 and ϵ_2 of Fmoc-KK(SP)KF-NH_2 at 370 nm were calculated by using Beer-Lambert law: $A=\epsilon cl$. ϵ_1 = 885.7 $M^{-1}cm^{-1}$ and ϵ_2 = 290.1 $M^{-1}cm^{-1}$. The ratio of the open and the closed forms were then calibrated.

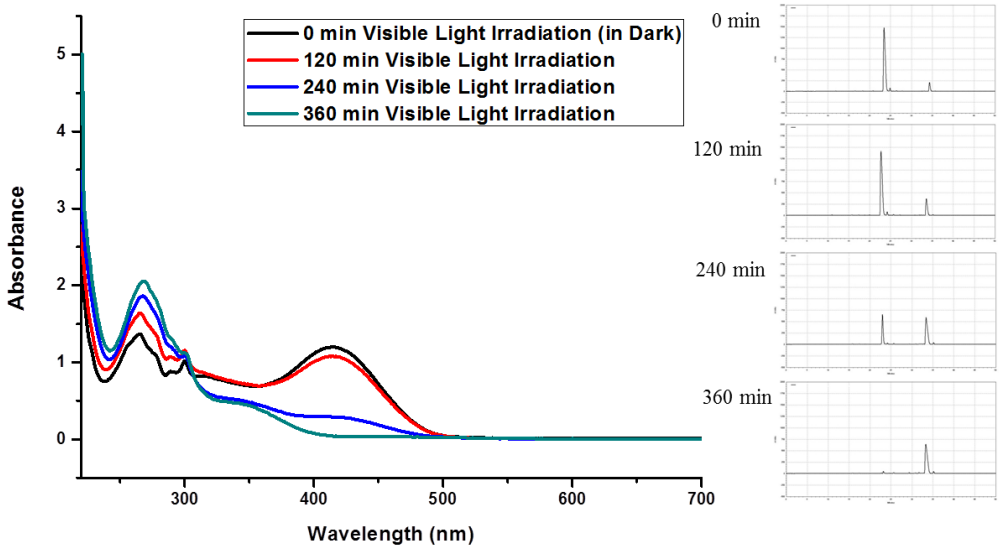

Figure 41. UV of 0.5 mM Fmoc-KK(SP)KF-NH_2 in 0.75% TFA under visible light irradiation and corresponding analytical HPLC.

Circular Dichroism (CD) Spectroscopy Measurement

CD spectra were recored on a Jasco CD spectrometer under a nitrogen atmosphere. Experiments were performed in a quartz cell with a 1 mm path length over the range of 200-700 nm. Samples were prepared from the H2O and 0.75% TFA (10mM) solution aged for 3 days at room temperature and freshly diluted to 0.5 mM before measurements.

Fourier-transforminfrared (FT-IR) spectrum

Fourier-transform infrared (FT-IR) studies were conducted by Shimadzu IRAffinity-1 FTIR spectrophotometer. Two solutions were prepared in 0.75% TFA aqueous solution (10 mM) and aged for a week under visible light to form gel and kept in dark respectively, lyophilized into solid states and dissolve in H_2O and lyophilized

immediately to remove solvent. After repeating this process three times, TFA and solvent was removed. Then the solid was dissolved in D_2O to prevent the overlap of strong around bending vibrational band of H_2O around 1600-1700 cm^{-1} region. Another solution was prepared by dissolve the spiropyran tetrapeptides in TFE.

Thioflavin-T(ThT) binding experiment

2.5 mM ThT stock solution was prepared by adding 8 mg ThT to 10 mL PBS and filter through 0.3 μm syringe filter and then kept in dark in 4℃ fridge. Dilute the stock solution to 0.05 mM with PBS solution immediately before the analysis. The fluorescence intensity of 0.5mL diluted ThT solution was measured with excitation at 440 nm (slitwidth 5 nm) and emission at 482 nm (slitwidth 10 nm). Then 5μL gel d (10 mM Fmoc-KK(SP)KF-NH_2 aged for a week) was added to the diluted ThT solution and stirred for 1 min. The corresponding fluorescence was measured and recorded. Another 5μL gel d was added subsequently and stirred for 1 min and the fluorescence emission spectrum was measured.

Rheology

The physical properties of gel formed by Fmoc-KK(SP)KF-NH_2 has been tested by the Advanced rheometric expansion system (ARES) rheometer using dynamic sweep mode at sweep of 6.28 rad/s.

Chapter 3: Self-assembly of Photo-responsive Spiropyran Monopeptide and Dipeptides

3.1 Introduction

Photochromism by definition is the reversible conversion of a chemical species between two isomer states with diverse absorption spectra under photoirradiation in one or both directions.[132, 144, 184-187] Among the known photo-switch chromophores, spiropyran and spirooxazine derivatives have become a well-known thermally reversible family accompanied with reversible color change. Upon UV irradiation or heat, the closed spiropyran form can transform into the open merocyanine form on the right side, which is also thermally unstable (Figure 42).[188]

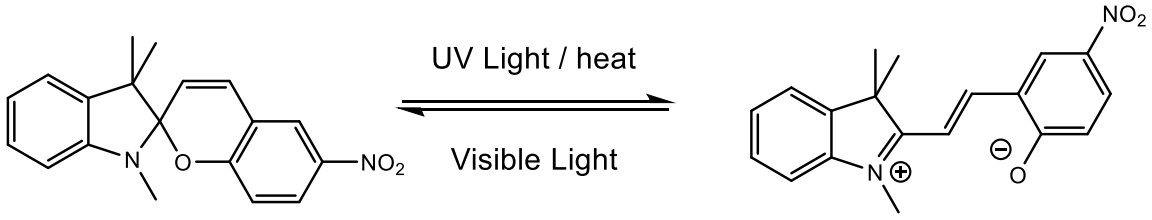

Figure 42. The transformation between nitro spiropyran and merocyanine

The interconversion between two states is based on pericyclic reaction of 1.6-electrocyclization by the photochemical or thermal cleavage of C-O bond[147]. The lone pair electron on N of the left part partially donates to a vacant antibonding σ*- orbital of the spiro C-O bond which cause the extension of the spiro C-O bond. On the contrary, the

$n_O \rightarrow \sigma^*_{CN}$ orbital interaction is much weaker due to the weaker donation of oxygen whose electronegativity is stronger.[147] This longer spiro C-O bond facilitates the photochemical or thermal cleavage process.

The thermal equilibrium of spiropyran in solution has been reported (Figure 43). When X = CH, the spiropyran 20 cleaves the C-O bonds and forms intermediate 21, which quickly change into planar isomers 22. The configurations of the C-C double bond, X-C double bond and the partially double bond C-X are labled cis (C) and trans (T). The most stable isomer was reported to be the TTC isomer.[189-193] It has also been confirmed that polar solvent and electron withdrawing group, such as nitro group, on the right chromene moiety at para position to O can assist stabilizing the ring-opened merocyanine form since it stabilize the negative charge of the zwitterionic form. This zwitterionic form is also much polar than the closed spiropyran form.

As previously mentioned, the three forms of spiropyran, SP, ME and MEH possess different physical and chemical properties and moreover, display different absorbance band in UV spectrum which can be easily detected[156-163].

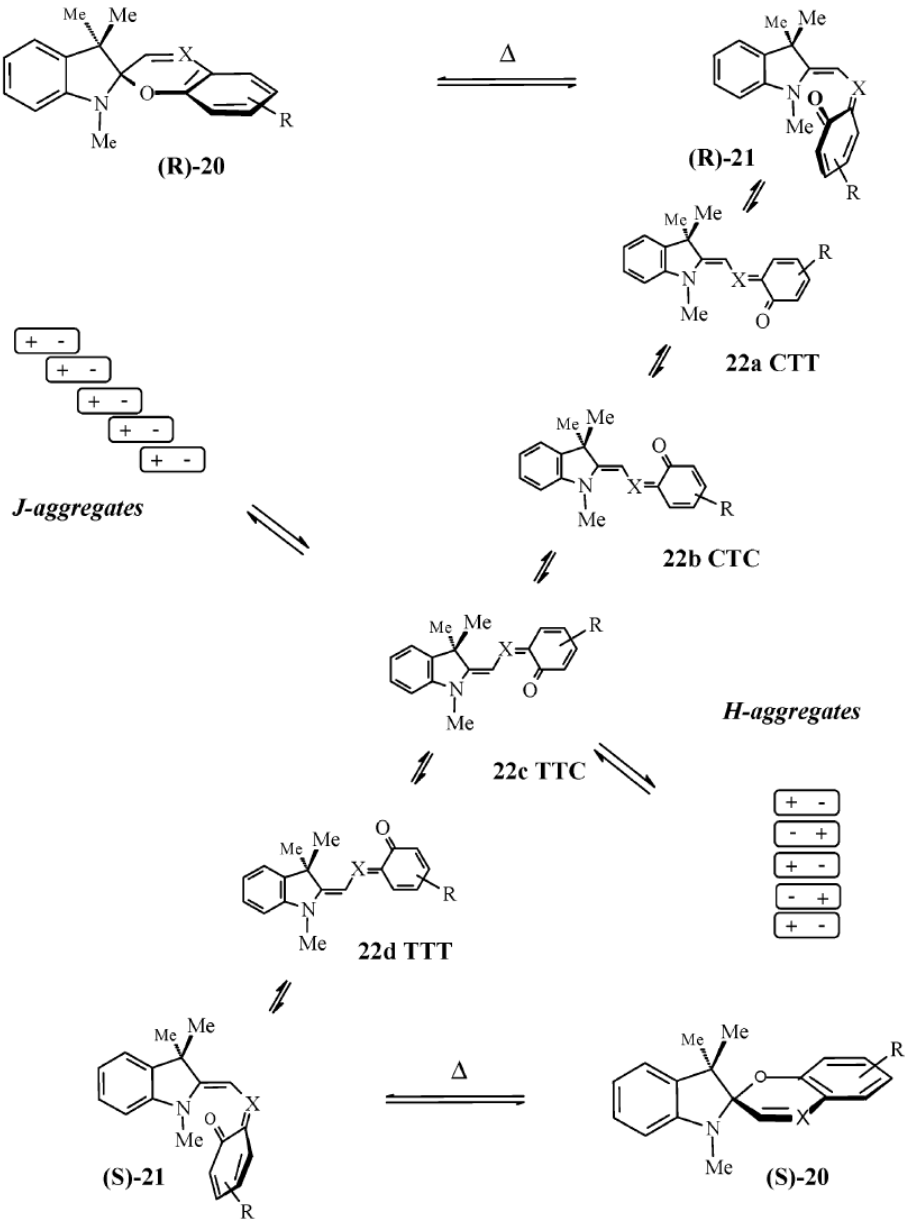

Figure 43. Thermal equilibrium of spiropyran in solution (X = CH). Copyright 2004 American Chemistry Society.[147]

Several self-assembly systems have been designed incorporated with the photo-switch chromophore, spiropyran. In 2014, a photo-controlled hyperbranched

polyglycerol[194] with spiropyran self-assembly material was developed by Son and coworkers.[195] They have designed a structure connecting polyglycerols with spiropyran (Figure 44). Having plethora of hydroxyl groups, the polyglycerols serve as a hydrophilic moiety whereas the closed spiropyran serve as the hydrophobic moiety. Upon UV irradiation, the spiropyran convert into the much polar merocyanine form that causes the disassembly. This assembly and disassembly process can be achieved by light irradiation at different wavelengths. This design may be applied as a smart drug-delivery system.

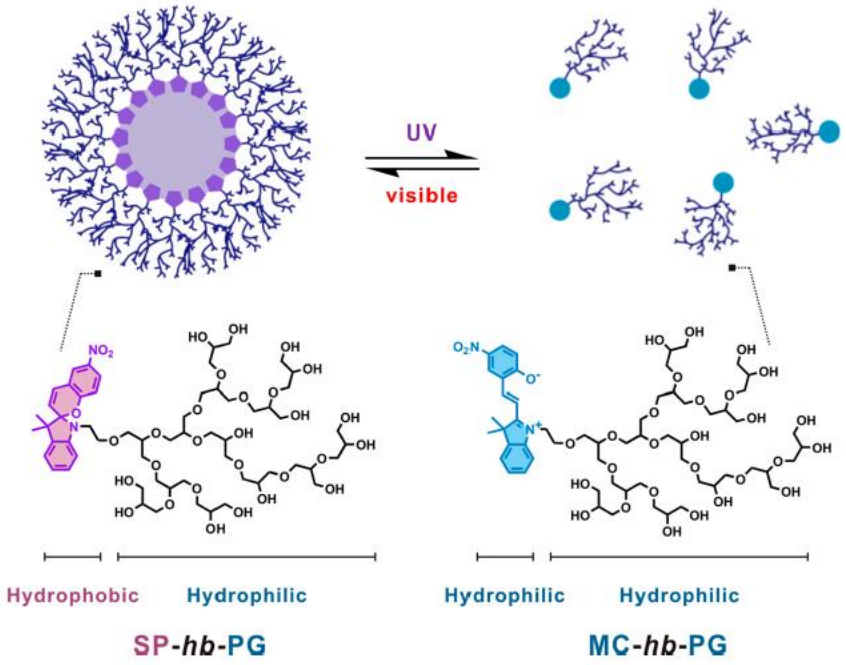

Figure 44. Photo-responsive micelle assembly and disassembly of spiropyran-hyperbranched polyglycerol.[195] Copyright 2014 American Chemical Society.

In their design, the spiropyran (SP) piece and a hydrophobic alkyl chain (C16) was associated with the polyoxometalate (POM) platforms with covalent bond. The POMs are

known as molecular oxides with charges and well-defined sizes[196]. The POM used in the design is a hydrophilic Anderson-type POM with tetrabutylammonium (TBA) complex, $(TBA)_3[MnMo_6O_{18}\{(OCH_2)_3CNHC_{21}H_{19}N_2O_4\}\{(OCH_2)_3CNH_2\}]$.The monomer can be represented as SP-POM-C16.

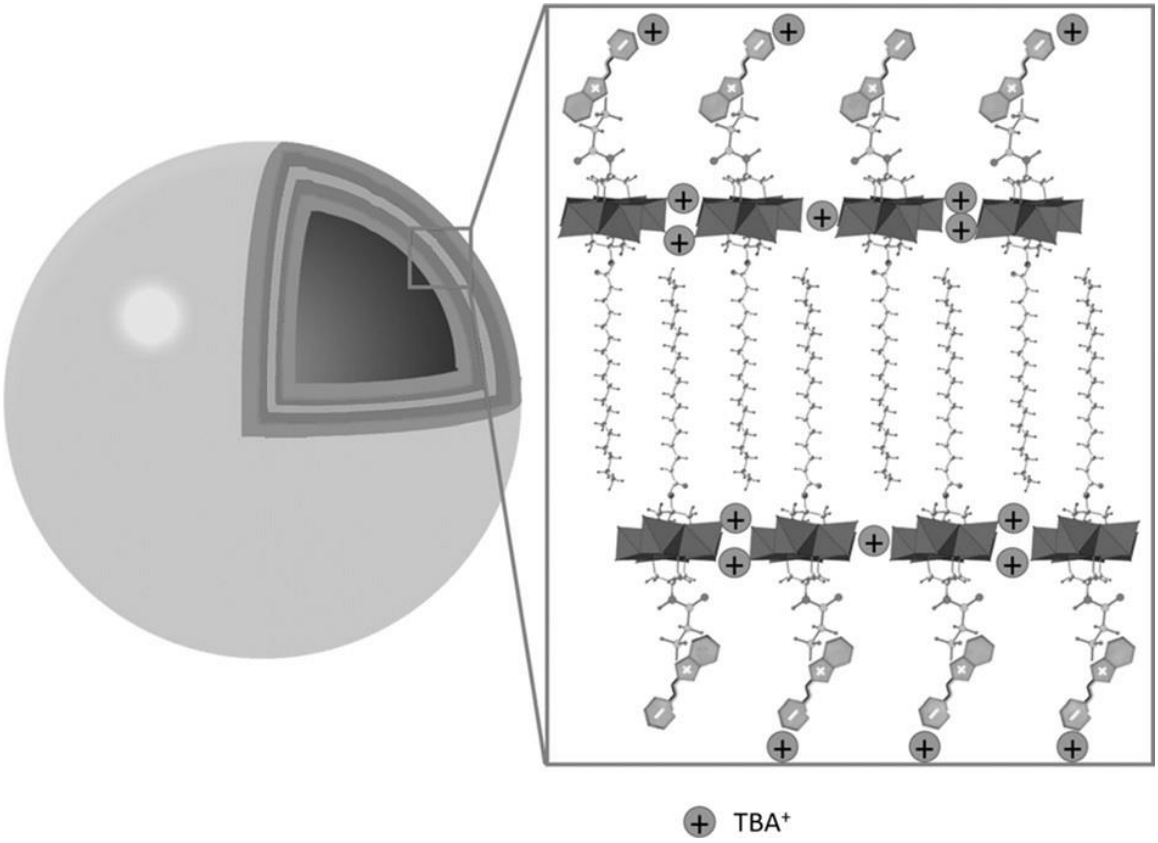

Figure 45. Illustration of self-assembly model of the hybrid SP-POM-C16 in polar solvent.[197] Copyright 2016 Wiley-VCH Verlag GmbH & Co. KGaA, Weinheim

This hybrid molecule SP-POM-C16 is discovered to be insoluble in water or toluene with too much hydrophobic interaction. However, the self-assembly process was triggered upon UV irradiation at 365 nm that changed the SP into merocyanine (ME) isomer. During this process, a hydrophilic head containing the charged ME piece and

POM piece was formed. The molecule changed into the surfactant-like structure that possesses a hydrophobic tail and a hydrophilic head. As a result, vesicles have been discovered in polar solvent (acetonitrile solutions containing 2.0 or 2.5 v/v% H_2O). Interestingly, in nonpolar solvent, the reverse vesicles with better stability were also discovered. The vesicles can be reversibly assembled and disassembled with corresponding light control.

In 2015, Wang and coworkers have done a fantastic job on spiropyran smart material development.[18] They have fabricated a poly(ethylene oxide)-*b*-PSPA (PEO-*b*-PSPA) diblock copolymer that can assemble into polymersomes that can change its permeability on and off upon light irradiation. The SPA stands for the spiropyran (SP) piece containing a unique carbamate linkage (Figure 46). In their design, the PEO-*b*-PSPA molecules are capable of self-assemble into vesicle structures with the preorganization of SP moieties into bilayer membrane structure caused by the carbamate-incurred hydrogen bonding. When irradiated with light (λ_1 < 420 nm), the SP moiety changes into the zwitterionic merocyanine (MC) moiety, the vesicle structures will remain due to the enhanced cooperative MC-MC interactions. Albeit the same conformation in assembly structures, the permeability of the vesicle changes as hydrophilic small molecules can enter the membrane with the hydrophilic MC moiety. With λ_2 > 450 nm irradiation, the permeability is turned off as MC changed back into hydrophobic spiropyran moiety.

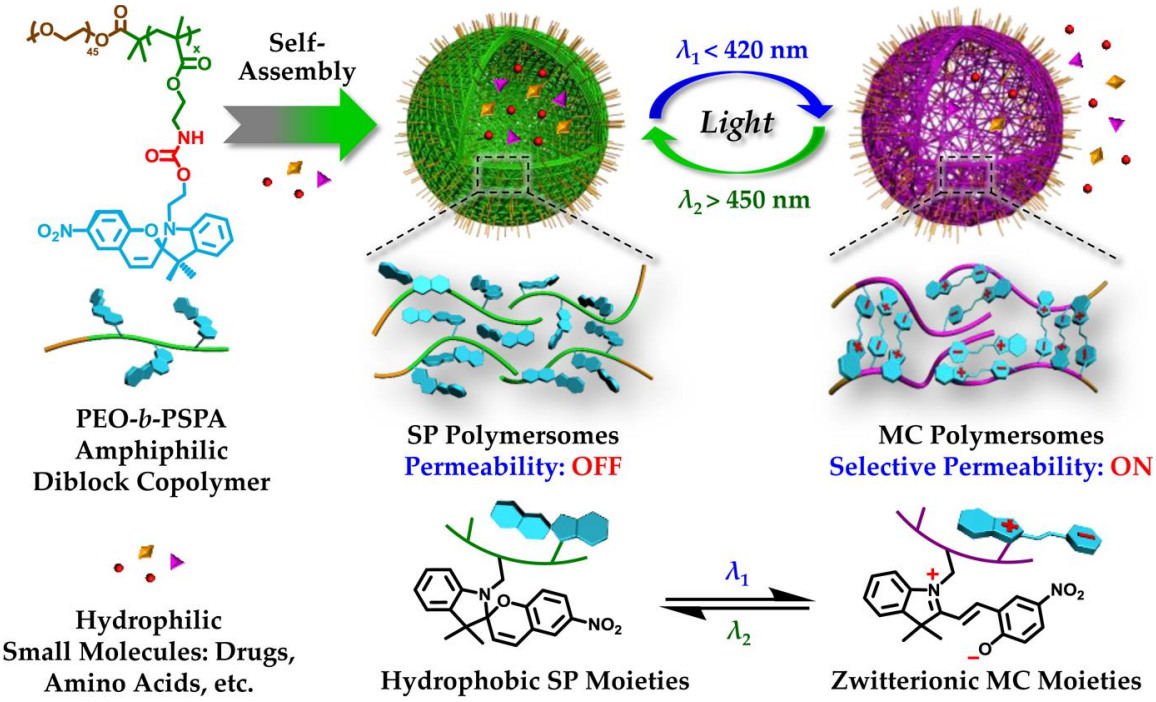

Figure 46. Model of assembled polymersomes of amphiphilic PEO-*b*-PSPA diblock copolymers and its photo-responsive permeability.[18] Copyright 2015 American Chemistry Society.

The SP and MC conversion is confirmed by both UV study and cryo-TEM when the vesicles doped with cysteine-stabilized Au NPs (AuNP-Cys). The PEO-*b*-PSPA with zwitterionic MC moiety can attract the AuNP-Cys on the membrane surface with electrostatic attractions whereas the SP moiety will not. As a result, the gold nanoparticles are observed attaching on membranes of MC moieties only. Moreover, the permeability ON and OFF process is confirmed by confocal laser scanning microscopy study and the cumulative photo-control-release of anticancer drug, 2′-deoxy-5-fluorouridine (5-dFu).

Most of self-assembly designs based on spiropyran moiety are rather large molecules that are inconvenient and complicated in synthesis. Herein, we report a series of small and simple molecules incorporating the spiropyran moiety and their and photo-controlled self-assembly behaviors.

3.2 Results and Discussion

Design of spiropyran-monopeptide and spiropyran-dipeptides

A series spiropyran-monopeptide: NH_2-K(SP)-OH, NH_2-K(SP)-NH_2, Ac-K(SP)-NH_2, spiropyran-dipeptides: NH_2-KK(SP)-OH, Ac-KK(SP)-OH, Fmoc-KK(SP)-OH Fmoc-KK(SP)-NH_2 hybrids have been designed and synthesized following standard solid-phase peptides synthesis strategy with the spiropyran carboxylic acid piece **SP-COOH**. Detailed synthesis are listed in the 3.4 experimental section.

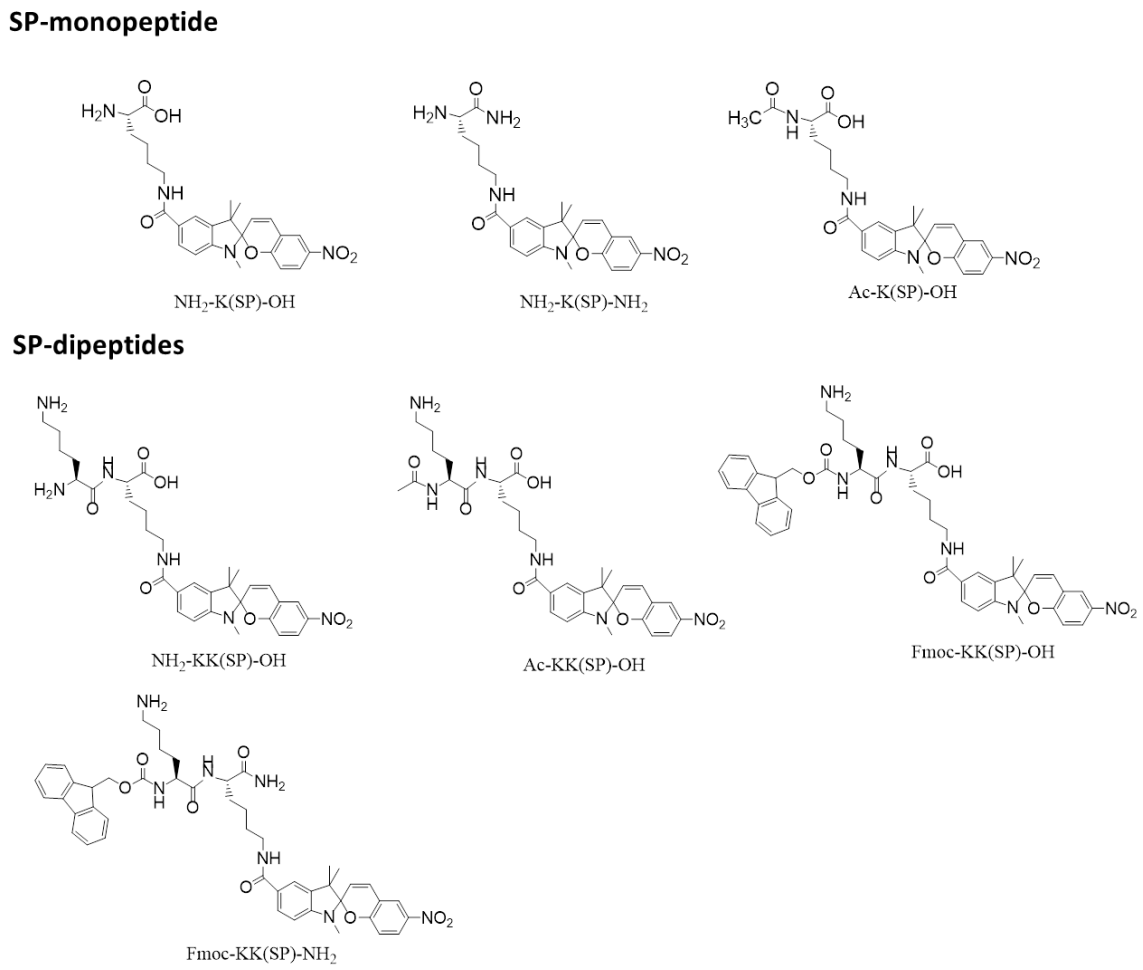

Figure 47. Chemical structures of spiropyran-peptide(s) hybrids.

Ultraviolet-visible (UV-Vis) Spectroscopy

UV-Vis spectra were taken to confirm the merocyanine, protonated merocyanine and spiropyran forms transformations. Solution A, B and C after annealing were diluted to 0.5 mM and corresponding UV-Vis spectra were taken before and after 3 days visible light irradiation.

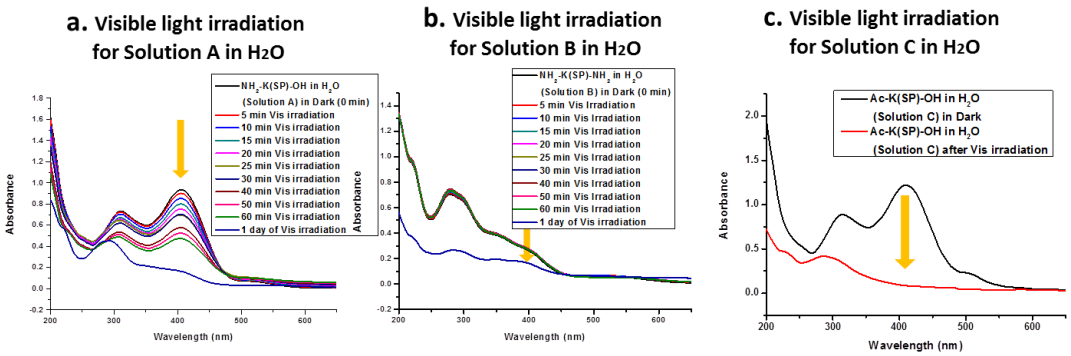

Figure 48. UV-Vis spectra of 1 mM solution A, B and C after LED broad spectrum visible light irradiation. a. Solution A, b. Solution B, c. Solution C.

As indicated in Figure 52, solution A after annealing in dark shows a strong peak at 405 nm before visible light irradiation, which is near the reported signature absorbance for protonated merocyanine (MEH) form. This indicates a large portion of NH_2-K(SP)-OH undergoes ring-opening and protonation process after heated up to 75℃ and cooled down and stays as the NH_2-K(MEH)-OH form. Besides, a very small peak at 520 nm, which is the absorbance area of merocyanine form, reveals a existence of small portion of the open form without protonation NH_2-K(ME)-OH. Inevitably there is also a portion of NH_2-K(SP)-OH exist due to the incomplete transformation. This solution has both ribbon and sheets structures on nano scale. After visible light irradiation, both peaks at 405 nm and 510 nm decrease and disappear, showing the complete transformation into the closed spiropyran form that forms only sheets nano-structures. Similarly, solution C before visible light irradiation has a strong peak at 410 nm and a small peak at 510 nm, corresponds to a large portion of Ac-K(MEH)-OH form and a small portion of Ac-K(ME)-OH that overall forms nanobelt assembly structure. After visible light irradiation,

the disappearance of both peaks indicates the conversion into closed SP form. Consequently, large non-ordered sheets are formed during the irradiation process. Different from solution A and C, solution B after annealing in dark condition only has very weak absorbance at 404 nm that corresponds a very small portion of the protonated open form. The majority of is still the closed spiropyran form. The small peak also vanishes after visible light irradiation. This explains the similar short nanotube assembly structures of solution B before and after irradiation as the compound majorly stays in the NH_2-K(SP)-NH_2 form.

The reverse process of UV=254 nm irradiation was not very effective for A, B and C water solutions.

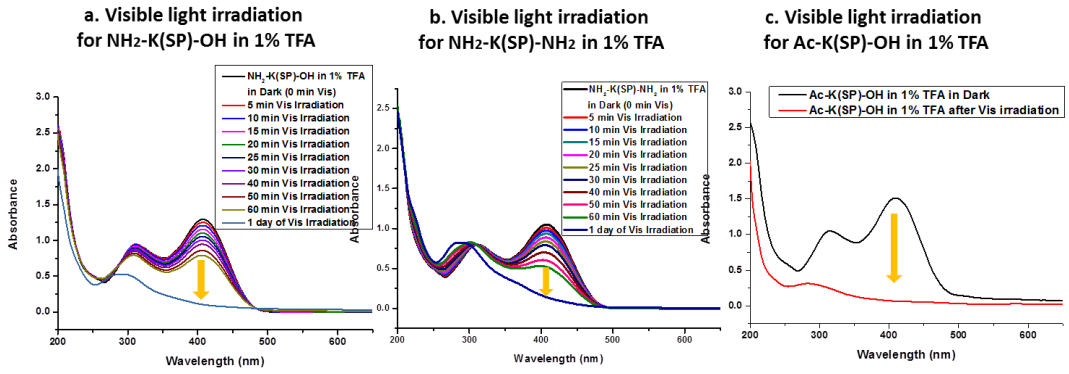

Figure 49. UV-Vis Absorbance of 1 mM 1% TFA sample solutions before and after visible light irradiation: a. NH_2-K(SP)-OH in 1% TFA , b. NH_2-K(SP)-NH_2 in 1% TFA, c. Ac-K(SP)-OH in 1% TFA.

For the three compounds in 1% TFA aqueous solutions, we can see there are no absorbance bands around 510 nm for graphs of both before and after visible light irradiation, showing no ME forms in the strong acidic solutions as expected. A large

portion of compounds stay in the protonated open MEH form after annealing in dark, as the strong absorbance around 410 nm, after visible light irradiation, the peak disappears as all MEH changed into SP forms. All solutions in 1% TFA fail to form ordered assembly structures due to the strong repulsion under this strong acidic condition.

The photo-controlled reverse ring-opening process was tested under UV=254 nm irradiation for **N**H_2-K(SP)-OH and NH_2-K(SP)-NH_2 in H_2O. Unfortunately, after 1 hour irradiation, there is no significant change in the UV spectra, indicating the reversing ring-opening process was not efficient in H_2O solution for both compounds.

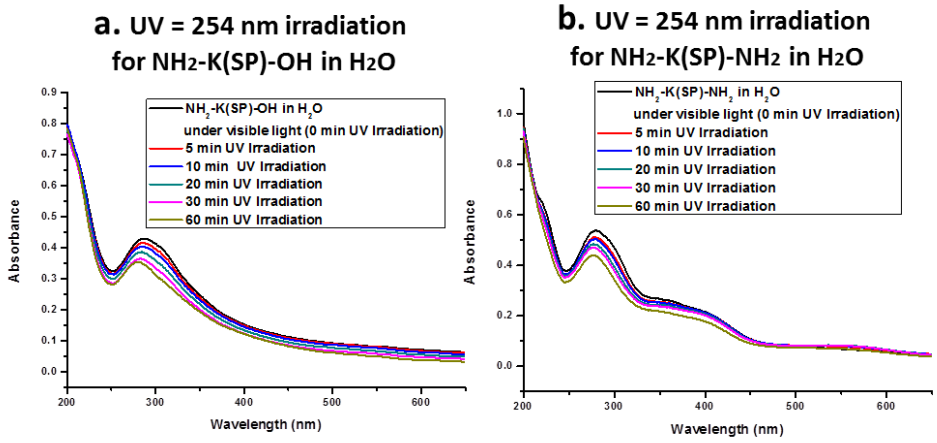

Figure 50. UV-Vis spectra of 1 mM compounds under UV=254 nm irradiation of the closed form NH_2-K(SP)-OH and NH_2-K(SP)-NH_2 in H_2O.

The solution colors also changed during the visible light irradiation process (Figure 55), for **N**H_2-K(SP)-OH and NH_2-K(SP)-NH_2 in H_2O solution, after annealing , they showed bright orange and red color that indicates the existence of open form ME and protonated open form MEH. For **N**H_2-K(SP)-OH and NH_2-K(SP)-NH_2 in 1% TFA, both

solutions showed yellow color due to the protonated open MEH form, corresponds to the UV-Vis absorbance around 410 nm on the spectra. After visible light irradiation, all of the solutions turned into the colorless, revealing the formation of the colorless spiropyran form. This colorless result also was shown in the UV-Vis spectra as no significant absorbance bands were presenting in the visible light region (400 nm~800 nm).

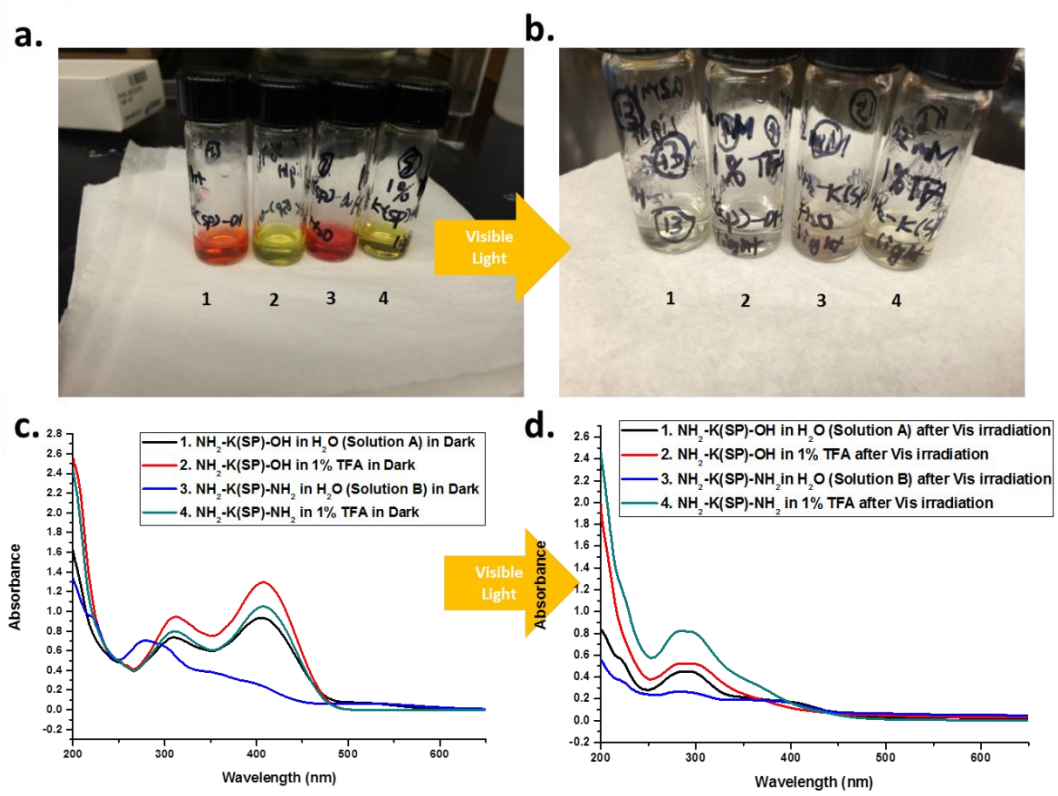

Figure 51. a. Photos of 1 mM solutions 1~4 after annealing in dark: 1. NH_2-K(SP)-OH in H_2O, 2. NH_2-K(SP)-OH in 1% TFA 3. NH_2-K(SP)-NH_2 in H_2O, 4. NH_2-K(SP)-NH_2 in 1% TFA, b. Photos of 1 mM solutions 1~4 after visible light irradiation, c. corresponding UV-Vis absorbance for a, d. corresponding UV-Vis absorbance for b.

For dipeptides NH_2-KK(SP)-OH and Ac-KK(SP)-OH in H_2O after annealing (solution D and E), the UV-Vis absorbance spectra were also taken. NH_2-KK(SP)-OH showed a rather strong peak around 405 nm, relating to the absorbance of the protonated open MEH form, NH_2-KK(MEH)-OH. The weak peak around 510 nm indicates a very small portion of ME form, NH_2-KK(ME)-OH. Overall, solution majorly stays in the protonated open form NH_2-KK(MEH)-OH that did not assemble. After visible light irradiation, solution D changed to the complete closed spiropyran form, NH_2-KK(SP)-OH that assemble into large sheets structure as the bands at 405 nm and 510 disappears. Diversely, solution E showed majorly stays in the closed SP form both after annealing in dark and after visible light irradiation since the ring-opening process is less favored in the equilibrium. Consequently, solution E has sheets and nanobelt assembly structure both before and after visible light irradiation.

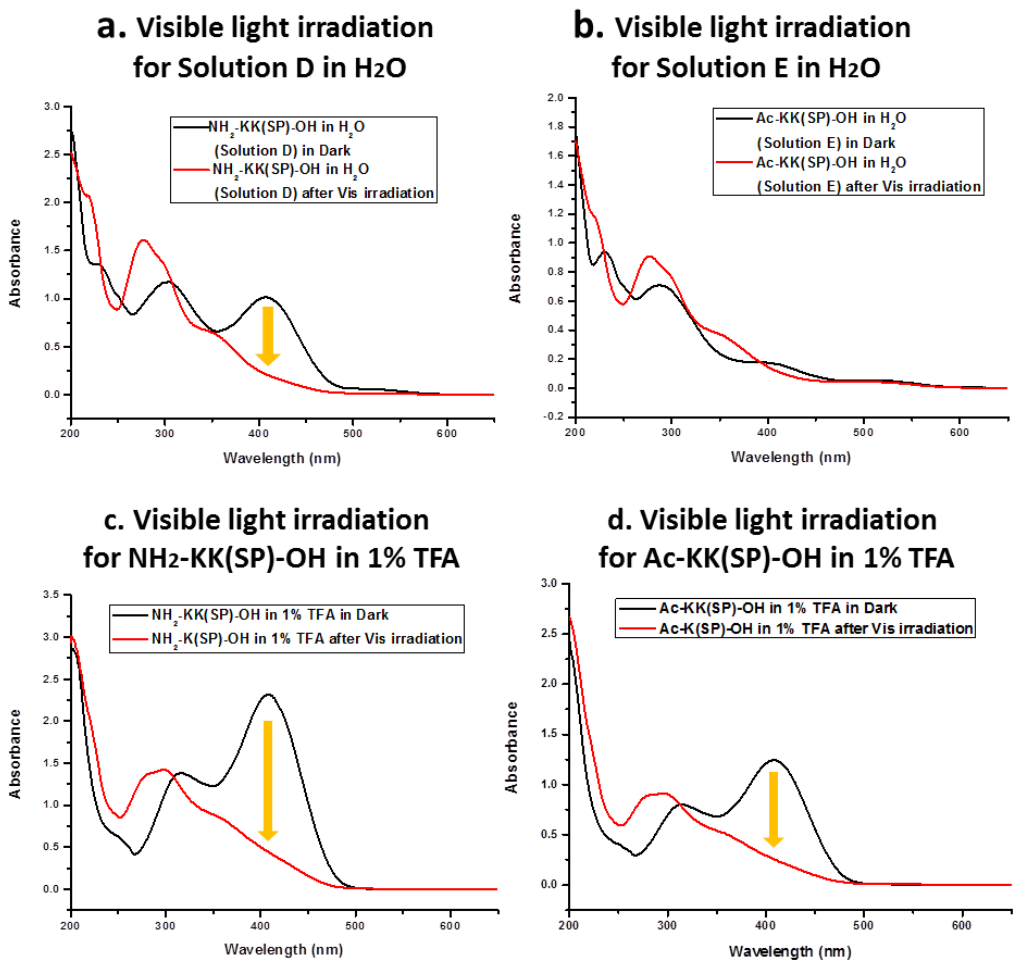

Figure 52. UV-Vis Absorbance of 1 mM sample solutions before and after visible light irradiation in H_2O and 1% TFA: a. NH_2-KK(SP)-OH in H_2O (solution D) , b. Ac-KK(SP)-OH in H_2O (solution E), c. NH_2-KK(SP)-OH in 1% TFA, d. Ac-KK(SP)-OH in 1% TFA.

From the spectra of the 1% TFA dipeptides solution NH_2-KK(SP)-OH, Ac-KK(SP)-OH, a higher ratio of protonated MEH form was observed with a stronger peak around 405 nm as acid assists the ring-opening process. No ME forms existed as no peaks around 510 nm were shown at this strong acidic condition.

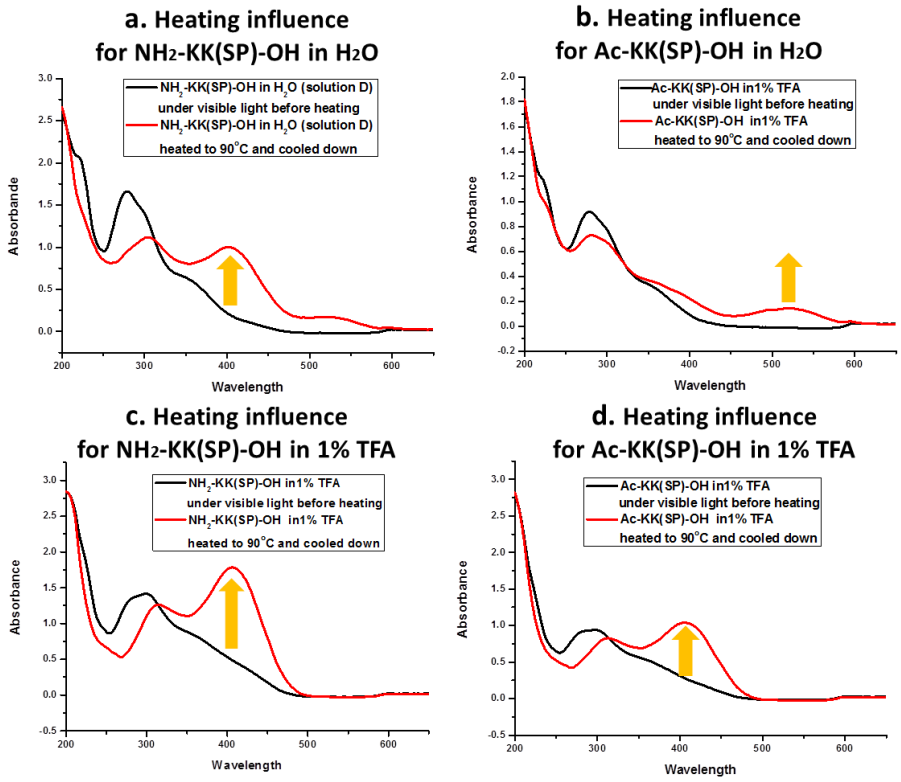

Figure 53. Heat the 1 mM solutions to 90℃ and cool down to room temperature, the UV-Vis spectra of solutions before and after the heating process: a. NH_2-KK(SP)-OH in H_2O, b. Ac-KK(SP)-OH in H_2O, c. NH_2-KK(SP)-OH in 1% TFA, d. Ac-KK(SP)-OH in 1% TFA.

The reverse ring-opening heating process was also investigated. The NH_2-KK(SP)-OH and Ac-KK(SP)-OH solutions were heated to 90℃ and corresponding UV-Vis absorbance were tested. Generally heating process can open the spiropyran ring, TFA

addition will enhance the ring-opening ratio. As shown in Figure 57, NH_2-KK(SP)-OH in H_2O showed a large portion of MEH form with the absorbance increased at 405 nm and a small portion of ME form at 510 nm after the heating process. Ac-KK(SP)-OH showed two small ME and MEH peaks after heating as a small portion of the SP rings are opened. For both compounds in 1% TFA, the ring-opening process was more effective with strong peaks around 405 nm corresponding to the MEH absorbance.

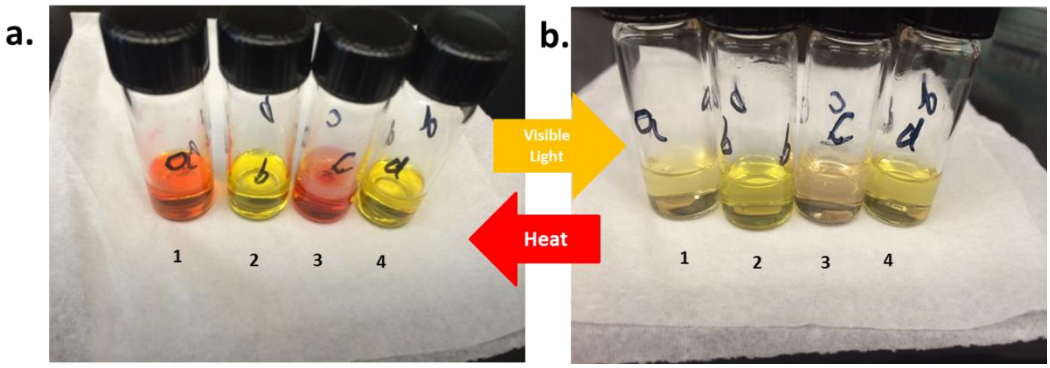

Figure 54. a. Photos of 1 mM solutions 1~4 after annealing in dark: 1. NH_2-KK(SP)-OH in H_2O, 2. NH_2-KK(SP)-OH in 1% TFA 3. Ac-KK(SP)-OH in H_2O, 4. Ac-KK(SP)-OH in 1% TFA, b. Photos of solutions 1~4 after visible light irradiation.

Color changes for the dipeptides solutions can also be observed during the ring closing/opening process. The aqueous solutions after annealing process in dark have shown orange color, which is the mixture color for both ME and MEH forms. With 1% TFA addition, solution color turned yellow for MEH forms. After visible light irradiation, all solution colors fade as the colorless spiropyran form increases. The reversing coloring process can be achieved by heating the solution to 90℃.

For Fmoc dipeptides Fmoc-KK(SP)-OH and Fmoc-KK(SP)-NH_2, UV-Vis absorbance were also studied.

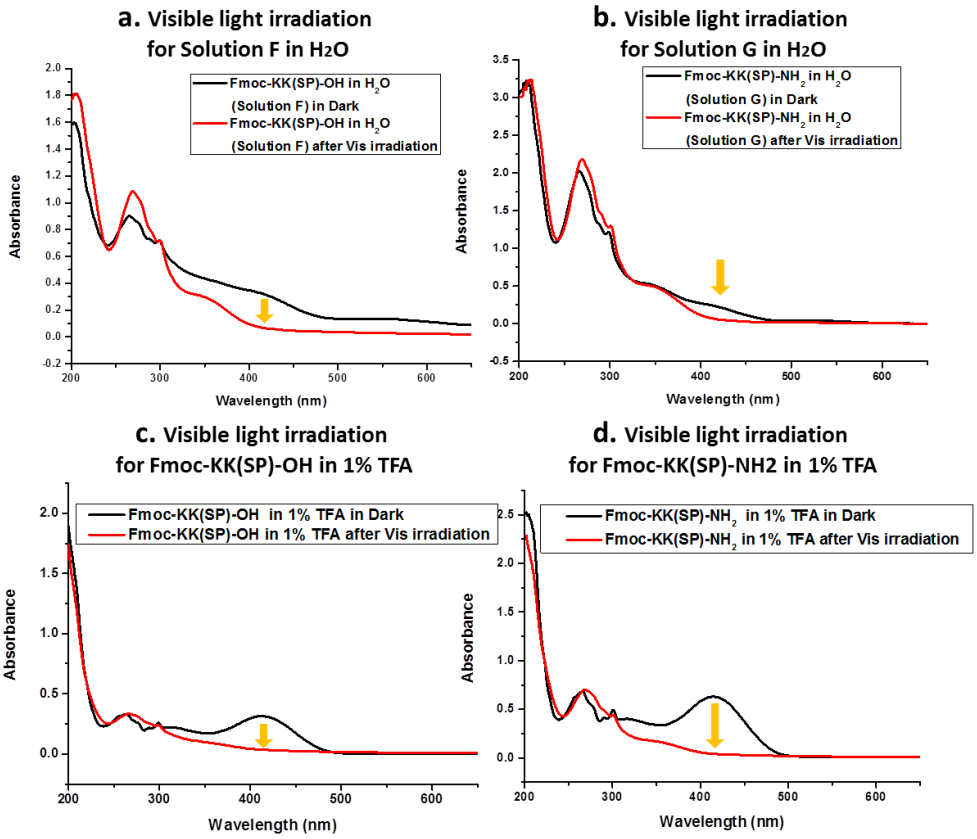

Figure 55. UV-Vis Absorbance of 1 mM sample solutions before and after visible light irradiation in H_2O and 1% TFA: a. Fmoc-KK(SP)-OH in H_2O (solution F) , b. Fmoc-KK(SP)-NH_2 in H_2O (solution G), c. Fmoc-KK(SP)-OH in 1% TFA, d. Fmoc-KK(SP)-NH_2 in 1% TFA.

Fmoc-KK(SP)-OH H_2O solution after annealing displayed a mixture of MEH, ME and SP forms as both peaks around 405 nm and 510 nm present but not strong, indicating possibly considerable amount of SP forms. In TEM study, some sheets-like structure were observed due to the presence of closed SP form, but not prominent as the other

forms did not form ordered assemblies. Fmoc-KK(SP)-NH_2 H_2O solution after annealing showed mostly SP form and a small portion of MEH form with the weak absorbance peak. Visible light irradiation changed MEH to SP form and the SP form conjugate self-assembles into the belt-like sheet structures. Both Fmoc dipeptides in 1%TFA showed a higher portion of MEH forms in 1% TFA with the rather strong peaks around 405 nm. Visible light can also change the solutions into the closed SP forms. But both before and after visible light irradiation, no ordered assembly structures were observed in 1% TFA solutions.

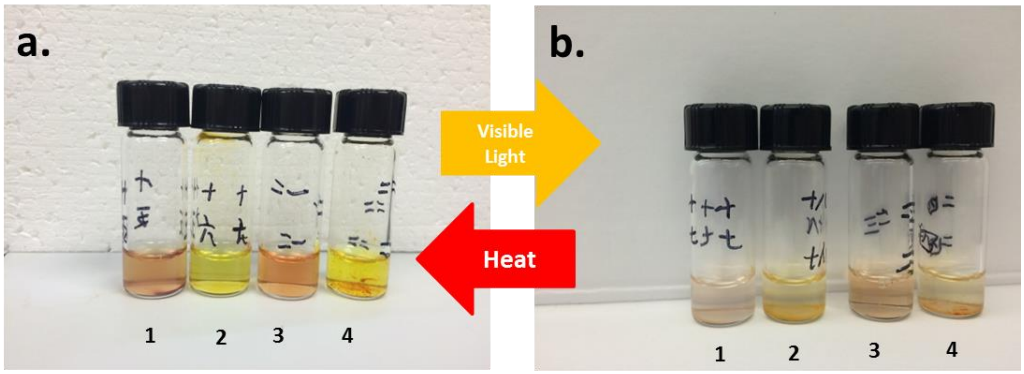

Figure 56. a. Photos of 1 mM solutions 1~4 after annealing in dark: 1. Fmoc-KK(SP)-OH in H_2O, 2. Fmoc-KK(SP)-OH in 1% TFA 3. Fmoc-KK(SP)-NH_2 in H_2O, 4. Fmoc-KK(SP)- NH_2 in 1% TFA, b. Photos of solutions 1~4 after visible light irradiation.

Similarly, the solutions after annealing showed darker color via ring-opening reactions. However, the colors are generally lighter than other SP-peptides solutions after anealing as less ME/MEH forms were produced, which was also shown as weaker absorbance bands in the UV-Vis graphs. Addition of 1% TFA change the orange color into yellow as the ME changed into MEH forms. All colors for the four solutions faded

after visible light irradiation as ring close reaction changed the open forms into the colorless spiropyran form. Heating process can also bring the color back via ring-opening process.

Transmission Electron Microscopy (TEM)

Three 10 mM solutions were prepared and labeled A: NH_2-K(SP)-OH, B: NH_2-K(SP)-NH_2 and C: Ac-K(SP)-OH in H_2O. The solutions were heated to 75℃ and cooled down in dark condition to get the majorly open merocyanine (ME) forms. The pH values of solutions were tested to be around 3 to 4, which means the compounds majorly stay as the protonated merocyanine (MEH) forms. NH_2-K(MEH)-OH, NH_2-K(MEH)-NH_2 and Ac-K(ME)-OH. The solutions were aged without light irradiation for another 3 days; corresponding TEM images were taken after solutions diluted to 1mM to investigate the assembly behaviors. Then the solutions were moved to visible light and irradiated for

another 3 days and turned almost colorless. The self-assembly behaviors were examined.

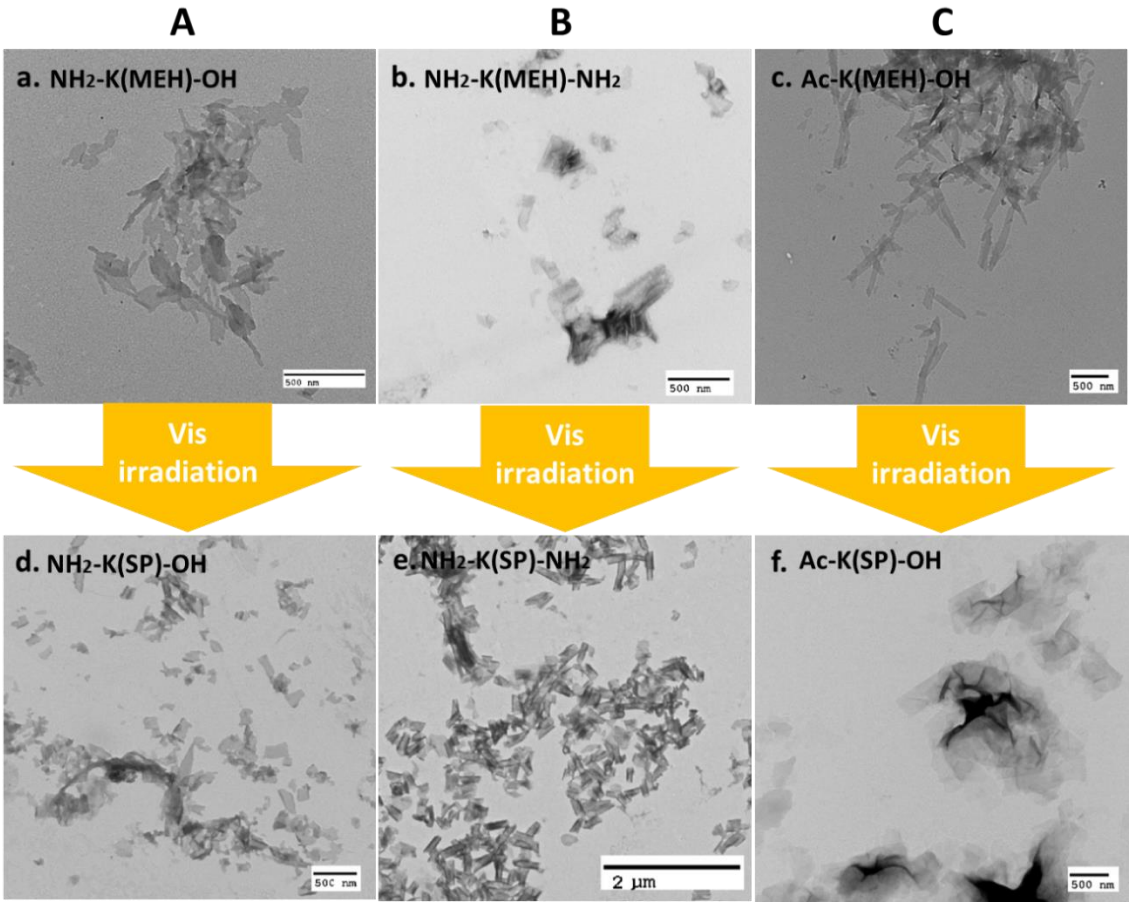

Figure 57. TEM images of 1mM solution A, B and C before and after visible light irradiation for 3 days. Before: a. NH_2-K(MEH)-OH, b. NH_2-K(MEH)-NH_2 c. Ac-K(MEH)-OH. After Vis irradiation: d. NH_2-K(SP)-OH, e. NH_2-K(SP)-NH_2 f. Ac-K(SP)-OH.

Solution A adopts a mixed ribbon and sheets-like assembly structure after heating and cooling process and aged without light irradiation, which means it majorly stays in the NH_2-K(MEH)-OH form. We hypothesis that the ribbon-like structure was formed by the open merocyanine NH_2-K(MEH)-OH forms, since with visible light irradiation, nearly all assembly structure changed to flat sheets conformations with almost no ribbons

found. It is known that the conversion from the open ME or MEH form to the closed SP form under visible light is a rather complete process as spiropyran form is thermodynamically more stable.[146] The ribbon like structure can be formed as each NH_2-K(MEH)-OH monomer carries overall one positive charge as the cations were partially mediated by the carboxylate group. For solution B in dark after heating, generally no ordered aggregates were discovered except few tube-like fragments. This may results from the open form NH_2-K(MEH)-NH_2 is too polar and hydrophilic. Each molecule carries two positive charges under this slight acidic condition that are too repulsive to form effective assembly structures. The few tube-like fragments were assembled from the closed form structure NH_2-K(SP)-NH_2. After visible light irradiation, the closed spiropyran form can provide hydrophobic interaction that triggers the assembly, with the electrostatic interaction offered by the cation on lysine residue. Consequently, the NH_2-K(SP)-NH_2 self-assembles into short tube structures with a diameter of 90 ± 1 nm. The short tubes formed are 200-400 nm long. Solution C before irradiation adopts a flat belt like conformation with a width of 104 ± 1 nm and over 500 nm lengths. This may due to the packing of the zwitterionic open merocyanine moieties.

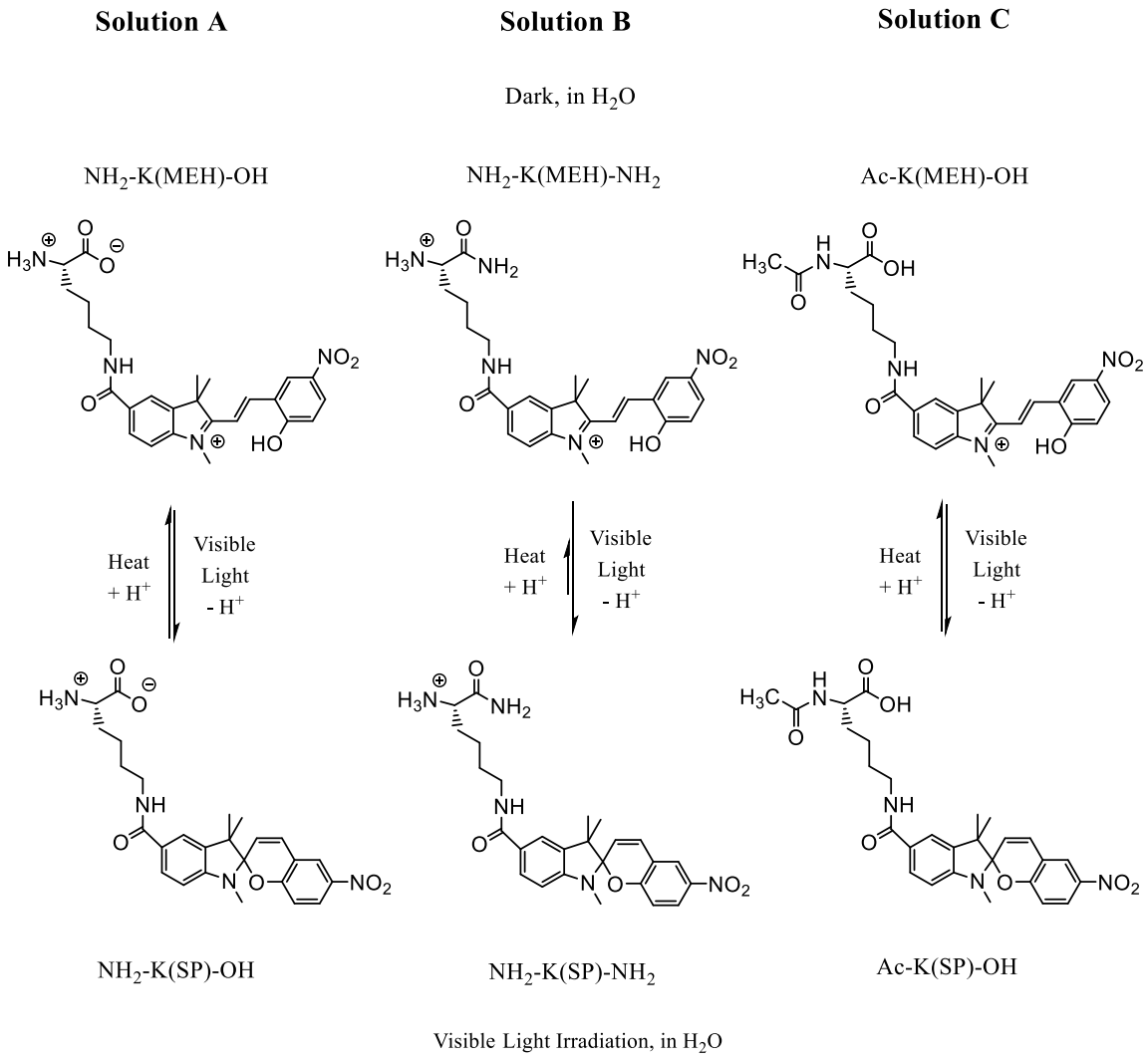

Figure 58. Proposed conversion between the protonated open merocyanine forms and the closed spiropyran forms for solution A, B and C.

The monomer Ac-K(MEH)-OH overall carries one positive charge. The open MEH form is planar due to the large conjugation, which is different from the spiropyran moiety in which the indole and benzopyran part are not in the same plane. This planar structure enhances the π-π stacking interaction that helps assembly. After visible light irradiation,

the closed spiropyran was formed and the Ac-K(SP)-OH amphiphile can self-assemble into large non-ordered sheets-like aggregates with the hydrophobic spiropyran moiety.

When the pH of aqueous solutions A, B and C were adjusted to 7 with $NaHCO_3$, the aggregates precipitated out at this neutral condition with this high salt concentration. As is known that TFA addition assists the ring-open process, NH_2-K(SP)-OH, NH_2-K(SP)-NH_2 and Ac-K(SP)-OH in 1% TFA aqueous solution were also prepared to examine the self-assembly behaviors under strong acidic addition[156]. The protonated open MEH form was also achieved by heating and cooling process in dark condition and aged for 3 days. The closed SP forms were obtained after 3 days irradiation under visible light. For both MEH and SP forms, no ordered aggregates were observed under this strong acidic condition for NH_2-K(SP)-OH, NH_2-K(SP)-NH_2 and Ac-K(SP)-OH in 1% TFA with only large non-ordered sheets-like structure presented.

For SP-dipeptides series, 10 mM solutions in H_2O for NH_2-KK(SP)-OH, Ac-KK(SP)-OH were also prepared and labeled as solution D and E respectively. The open forms and closed forms solutions were obtained by annealing in dark condition or irradiation under visible light. The compounds dissolved well in both solutions. After aging for over three days and diluted to 1mM, the TEM images were taken to investigate the assembly conformations. For all D and E solutions, no ordered assembly forms were observed in TEM for both without and with irradiation. This may result from the high ratio of hydrophilic components with dilysine structures. The molecules overall are too hydrophilic to assembly in aqueous solution. The closed spiropyran piece fail to provide enough hydrophobic forces to assemble as the hydrophilic peptides portion is too high.

Although the transformation between the open and the closed forms were successful based on ultraviolet (UV) study, the molecules did not form effective self-assembly conformations. No assembly behaviors were discovered for NH_2-KK(SP)-OH and Ac-KK(SP)-OH in 1% TFA aqueous solutions for both the open and the closed forms.

To achieve assembly structures for dipeptides, we increase the hydrophobic component portion by incorporating Fmoc group into the dilysine structure and designed the Fmoc-KK(SP)-OH Fmoc-KK(SP)-NH_2 sequences. The corresponding 10 mM stock solutions were prepared. The solutions were annealed in dark to achieve the open forms and labeled solution F and G, and then aged for 3 days. From TEM study, Solution F did not form ordered assembly structures without visible light irradiation when it majorly stays as the protonated open form, Fmoc-KK(MEH)-OH. After visible light irradiation, it converted into the closed spiropyran form Fmoc-KK(SP)-OH that self-assembled into large sheets-like structures. This is due to the hydrophilic to hydrophobic transformation from MEH to SP moiety. The protonated open form Fmoc-KK(MEH)-OH, is too hydrophilic to form assembly structures whereas the closed Fmoc-KK(SP)-OH have both Fmoc- and SP components that can provide enough hydrophobic interaction and π-π association forces for assembly process.

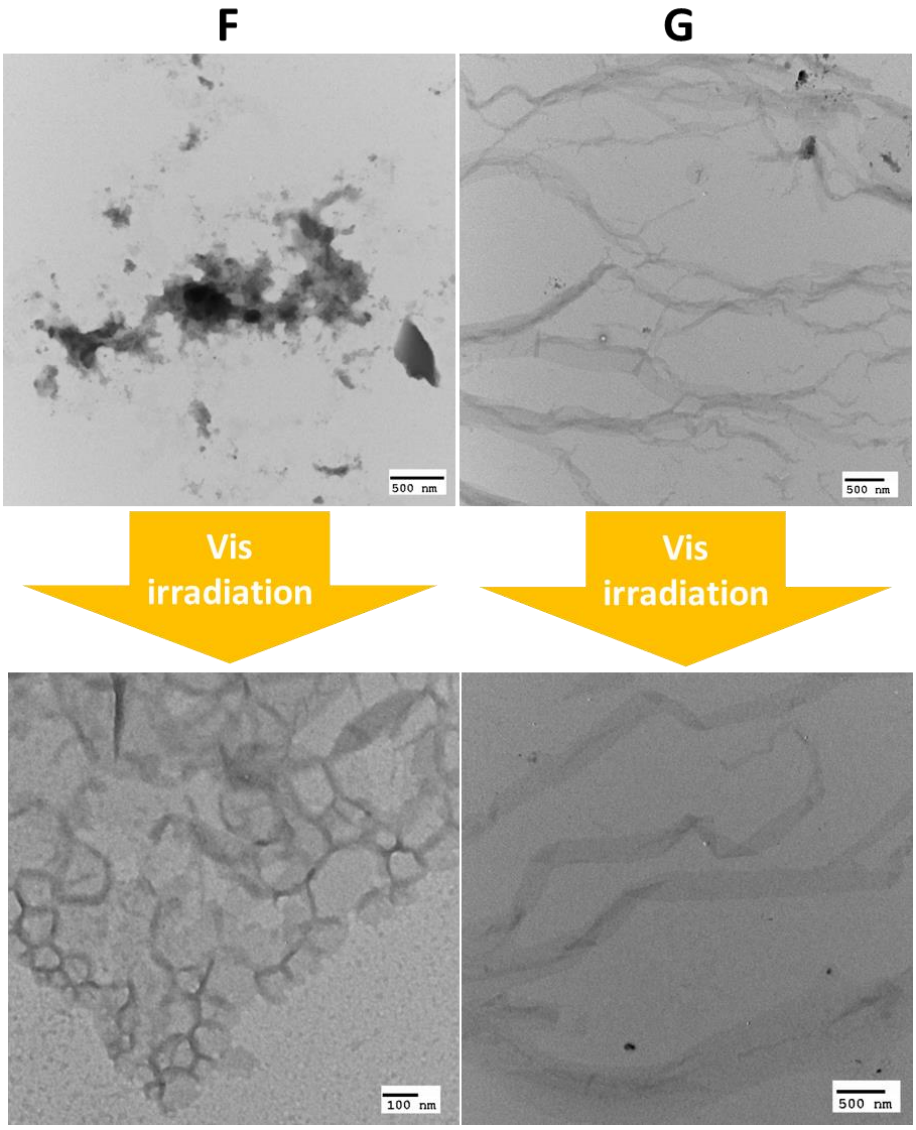

Figure 59. TEM images of 1mM solution F and G before and after visible light irradiation for 3 days.

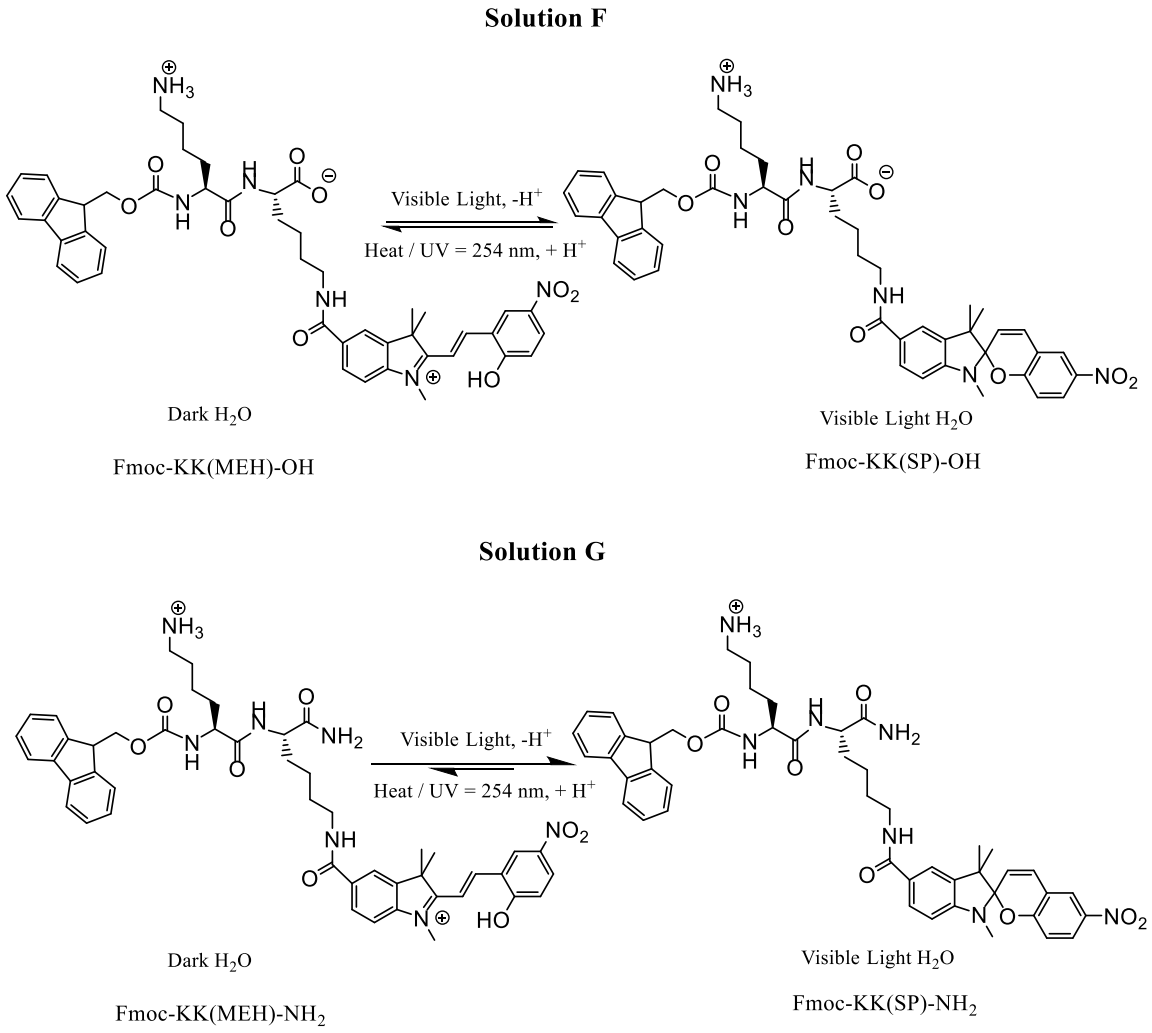

Figure 60. Proposed conversion between the protonated open merocyanine forms and the closed spiropyran forms for solution F and G.

Similarly, from TEM study, solution G without visible light irradiation reveals mostly amorphous with some sheets-like structure. The formation of those few sheets-like structures are possibly from some leftover closed Fmoc-KK(SP)-OH forms due to the incomplete open process (Figure 51). More belt-like sheet structures were observed after visible light irradiation due to the MEH to SP hydrophilic to hydrophobic

transformation. After 1% TFA were added to the Fmoc-KK(SP)-OH Fmoc-KK(SP)-NH_2 aqueous solutions, no ordered assembly structures were observed due to the strong acidic condition that increases the electrostatic repulsion among monomers.

Circular Dichroism (CD) Study

Circular dichroism graphs were taken to study the packing behavior of assembly structures. In the three monolysine-spiropyran hybrids, solution A (NH_2-K(SP)-OH) displayed a positive peak around 275 nm and a negative peak around 310 nm, corresponds to the ribbon and sheet self-assembly of open forms. The negative cotton effect for the exciton couplets centered at 296 nm indicates an M-type aggregates for the ribbons. The couplets corresponds to the electronic π-π* transition band from the indole part of spiropyran[181]. This transition, responsible for the first absorption band, is parallel to long axis of indole part of spiropyran moiety as reported.[182] We can observe the direction change, from negative to positive and from positive to negative in CD spectra after visible light irradiation since the open forms converted into the closed SP forms. The change of exciton couplets can be observed, showing the assembly changed from M-type to P-type helical structures. Similarly, NH_2-K(SP)-OH in 1% TFA also showed peaks at the same region with same directions, also corresponds to the aggregates formed by SP forms. However, the aggregates in 1% TFA are some large irregular sheet-like structures. the For both NH_2-K(SP)-OH and NH_2-K(SP)-NH_2 in 1% TFA after annealing, no absorbance bands were shown in CD graph, indicating no assemblies for the MEH protonated open forms (red lines in Figure 61 a and b). The

peaks for the two CD signals under visible light of all three mono-lysine spiropyran hybrids are quite similar as all assemblies were from the same SP forms (the green and the blue line). The intense negative absorption at 275 nm and the negative absorption at 220 nm are the signature absorbance bands of β-sheet type secondary structure[180]. The positive exciton couplets centered at 290 nm also indicates a P-type helical chirality for the sheets and short tubes formed by SP aggregates. The signal for Ac-K(SP)-NH_2 is much stronger due to the large sheets structure formation. For CD of Ac-K(SP)-NH_2 in H_2O in dark, the negative absorbance at 220 nm also reveals the β-sheet type secondary structure. After visible light irradiation, the assembly structures formed by SP moieties displayed positive exciton couplets centered at 290 nm, indicating P-type helical structure. Before visible light irradiation in H_2O, Ac-K(SP)-NH_2 showed another positive exciton couplets that centered at 505 nm, which corresponds to the electronic transition dipole moment along the long axis of open merocyanine form as reported.[182] This indicates the P-helical assembly structure formed by the open form Ac-K(ME)-NH_2. The signal displayed a strong negative peak around 450 nm and a strong positive peak around 520 nm, with corresponding to the UV absorbance of ME form and MEH forms. This reveals that the ME and MEH forms contributes to the nanobelt assembly structures in H_2O after annealing in dark.

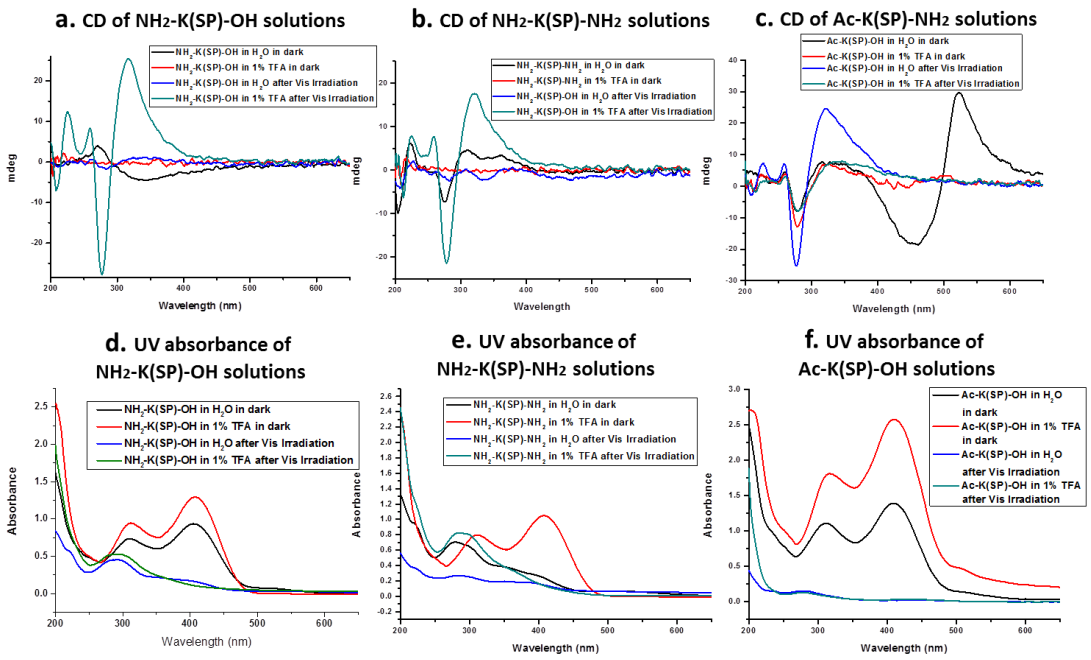

Figure 61. CD of 1mM solutions: a. NH_2-K(SP)-OH, b. NH_2-K(SP)-NH_2, c. Ac-K(SP)-OH Corresponding UV absorbance of 1mM solutions: d. NH_2-K(SP)-OH, e. NH_2-K(SP)-NH_2, f. Ac-K(SP)-OH.

The CD for dipeptides NH_2-KK(SP)-OH and Ac-KK(SP)-OH were also tested. Only amorphous aggregates were observed for the two conjugates solutions based on the TEM study. In accordance with the TEM findings, the CD signals are almost flat for both solutions in H_2O and 1% TFA both before and after visible light irradiation. This confirmed the no assembly results for these two dipeptides as they are too hydrophilic in aqueous solution.

Ratio study of Ac-K(SP)-OH during visible light irradiation

The ratio of the open and the closed form was studied by analytical HPLC during the visible light irradiation for solution G. The protonated open (MEH) forms and closed

(SP) forms have different retention time in HPLC due to polarity change. In 0.1% TFA of acetonitrile and H_2O solution, almost all open forms exist as the MEH forms, which are much polar than the closed SP form and have a smaller retention time.

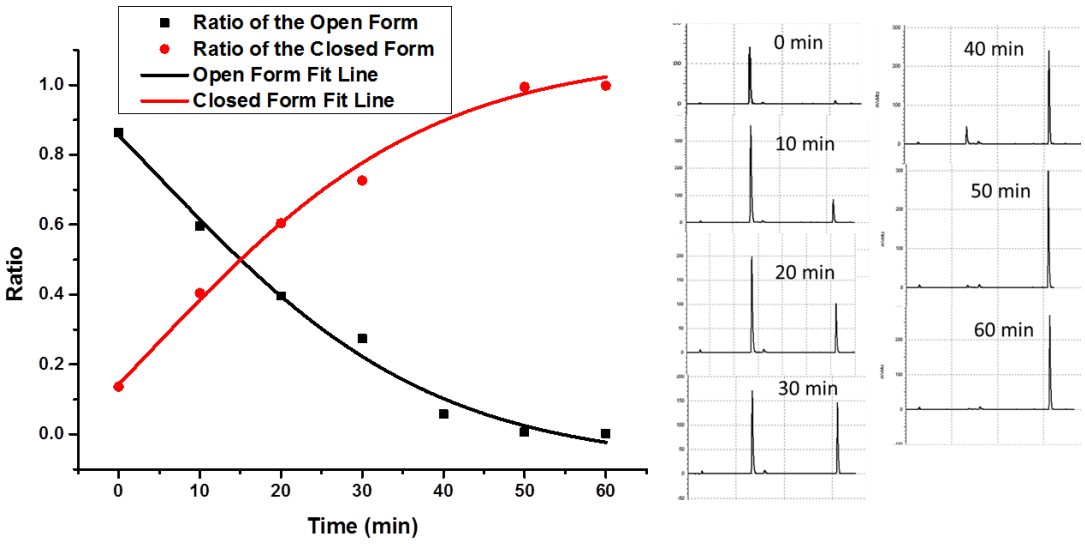

Figure 62. Ratio change and corresponding analytical HPLC of the open and the closed forms of 10 mM Ac-K(SP)-OH in H_2O after annealing under visible light irradiation. Solution G is the starting solution (time = 0).

Solution G originally has 86.4% of MEH forms before visible light irradiation. This water solution can self-assemble into nano-belt structure with the high portion of MEH and ME forms. During the visible light irradiation, the ratio of the closed form increased as the ration of the MEH form decreased. After 50 minutes irradiation, over 99.5% of molecules changed into the closed SP form, revealing the relative complete transformation of the equilibrium. The resulting SP solution can self-assemble into large

irregular sheet structures. This ratio study is consistent with the UV-Vis absorbance result.

Ratio study of Ac-K(SP)-OH in 1% TFA during Heat and UV irradiation.

The reverse ring-opening process for Ac-K(SP)-OH in 1% TFA was also studied as TFA addition helps the ring-opening reaction.

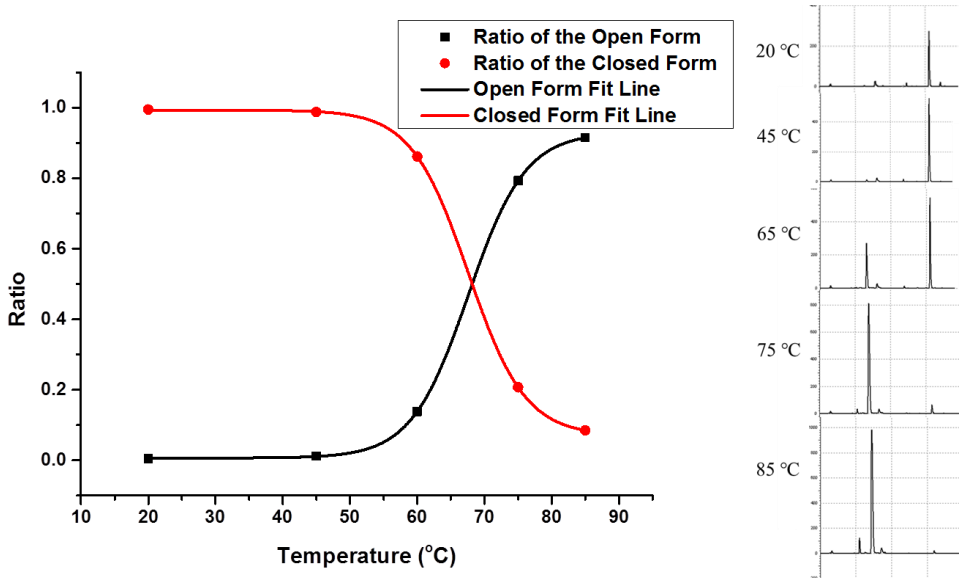

Figure 63. Ratio change and corresponding analytical HPLC of the open and the closed forms of 10 mM Ac-K(SP)-OH in H_2O at different temperature during heating process.

The starting solution is solution G after visible light irradiation which has 99.6% of closed SP form. The solution was heated in dark and the ratio was analyzed by HPLC. After heated to 75℃, the ratio of the open form increased drastically. The ratio of the protonated open form MEH reached 91.5% after heated to 90℃ and the ratio of the closed form dropped. The ratio change during the heating process has displayed great reversibility for the change from SP to MEH forms in acidic condition.

Nevertheless, the influence of UV = 254 nm irradiation was also tested on the same solution closed form SP solution. The results showed very limited change in open form MEH ratio during 1 h irradiation. This result indicates the reversing ring-opening process is not effective under photo-control even in acidic condition for Ac-K(SP)-OH.

3.3 Conclusion

We have designed a series of spiropyran-lysine monopeptide and dipeptides series based on solid-phase peptides synthesis strategy and studied their assembly behaviors. The mono-peptide compound NH_2-K(SP)-OH and Ac-K(SP)-OH adopt different assembly structures from ring closing/opening process. The ring-closing process is achieved via visible light irradiation whereas the ring-opening process can be achieved by the annealing process in dark. NH_2-K(SP)-NH_2, Fmoc-K(SP)-OH and Fmoc-K(SP)-NH_2 can only form aggregates from the closed spiropyran forms. Besides, the ring-opening was hard and incomplete for NH_2-K(SP)-NH_2 and Fmoc-K(SP)-NH_2 aqueous solution. The change among the three states can be observed from change UV-Vis absorbance and also CD signals. The detailed ratio change among SP and MEH form can also be monitored by analytical HPLC. The assembly structures formed by SP bear β-sheet secondary structure and P-type helical structure from CD study. The assembly structures formed by open form possess different CD signals. The two dipeptides compounds NH_2-KK(SP)-OH and Ac-KK(SP)-OH fail to self-assemble due to high hydrophilic part ratio. The ring-opening process is favored in 1% TFA solution under heat, but the compounds cannot self-assemble into ordered nanostructures under this high acidic condition.

In conclusion, we report a series of spiropyran mono-peptide or dipeptide hybrids that have photo- and thermo- responsive self-assemblies by the ring closing/opening conversion of the spiropyran moiety. Although the transformation of the ring-opening process was not ideal and the concrete ratio of the ME and MEH forms remains unclear, this type of compounds is simple and convenient to synthesis, can shed light to future photo-controlled smart material study.

3.4 Experimental Section

Materials and General Method

The Fmoc-amino acids, and 1- hydroxybenzotriazole (HOBt), 2-(1H-benzotriazol-1-yl)-1,1,3,3-tetramethyluronium hexafluorophosphate (HBTU) were purchased from Chem-Impex Int'l Inc. The rink amide resin was obtained from ChemPep. 4-hadrazinobenzoic acid, propylmethylketone, iodomethane and 2-hydroxyl-5-nitrobenzaldehyde were purchased from Sigma-Aldrich. All the solvents were obtained from Fisher Scientific and All NMR solvents were from Cambridge Isotope Labs. Reversed-phase HPLC was conducted on C18 columns with use of water/acetonitrile/TFA gradients between 68:32:0.1 and 25:75:0.1. NMR spectra were obtained on Bruker AMX 400 pectrometers. All SP1~SP4 (SP-COOH) are known compounds, their yields are listed in section 2.4, the NMRs are adopted from previous literature.[183]

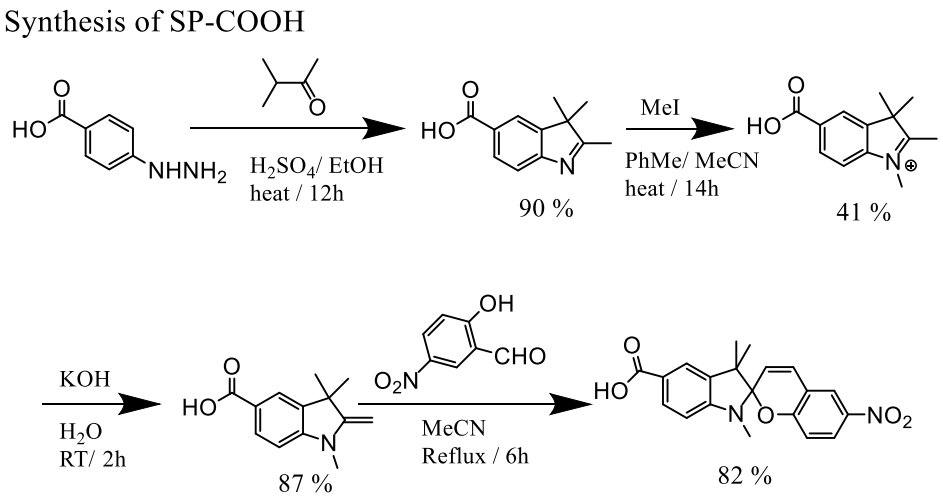

Scheme 2. Synthesis scheme for **4** (SP-COOH).

General preparation of spiropyran-peptide(s).

NH_2-K(SP)-OH

Fmoc-K(Mtt)-Wang Resin was synthesized following standard solid phase peptides synthesis method on Wang resin (loading 1.2 mmol/g) by using Fmoc-Lys(Mtt)-OH. Fmoc-Lys(Mtt)-OH was coupled to the Wang resin after swelled in DCM for 1 h, with DIC, HOBt (300% mol each relative to resin) and 4-dimethylaminopyridine (DMAP) (10% mol each relative to resin)in DCM for overnight. The coupling completion was tested by Kaiser's test. Methytrityl (Mtt-) protecting group was removed by 1% trifluoroacetic acid (TFA) in DCM solution for 8 × 5min, then the deprotected free amine was coupled with 1.5 equivalencts of SP-COOH with HBTU (4.0 equivalents), HOBt (4.0 equivalents), and DIPEA (2.0 equivalents) in DMF for overnight. Fmoc group was deprotected under a solution of 20 % piperidine in DMF. The NH_2-K(SP)-OH were cleaved from the Wang resin by the TFA : TES : H_2O : DCM = 60 : 2.5 : 2.5 : 35 solution

at room temperature for 1.5 h. The crude product precipitated with cold diethylether and purified by reversed-phased HPLC on preparative Varian Dynamax C18 column and stored as lyophilized orange powers (88.4 mg 35%).^{1}H NMR (400 MHz; DMSO-d_6) δ =1.14 (3H, s), 1.25 (3H, s), 1.35-1.41 (2H, m), 1.45-1.51 (2H, m), 1.70-1.76 (2H, m) 2.75 (3H, s), 3.25 (2H, dd, 6 and 9 Hz), 3.31(1H, dd, 6 and 7 Hz), 6.02 (1H, d, 10Hz), 6.67 (1H, d, 8 Hz), 6.89 (1H, d, 9 Hz), 7.26 (1H, d, 10 Hz), 7.64 (1H, d, 2 Hz), 8.09 (1H, dd, 2 and 8 Hz), 8.06 (1H, dd, 3 and 9 Hz), 8.21-8.28 (3H, m), 8.70 (1H, t, 5 Hz), 9.08 (1H, d, 3 Hz). ESI-MS for $C_{26}H_{31}N_4O_6$ $[M+H]^+$ calculated 495.22; found.

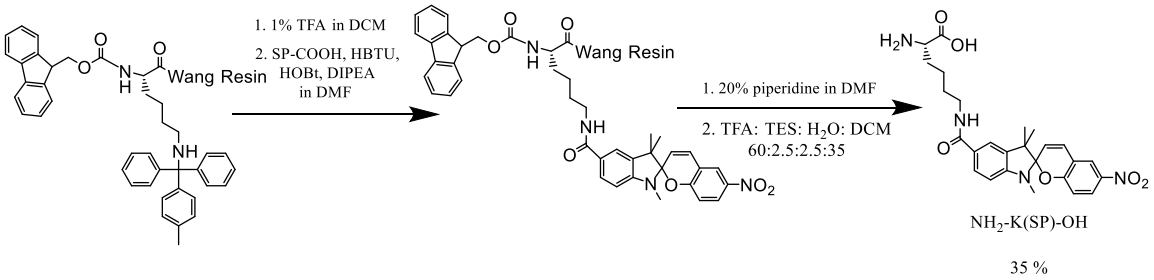

Scheme 3. Synthesis route for NH_2-K(SP)-OH.

NH_2-K(SP)-NH_2

Fmoc-K(Mtt)-Resin was prepared following standard solid phase peptides synthesis method on rink amide resin (loading 0.8 mmol/g). After swelled for 1 h, Fmoc-Lys(Mtt)-OH was couple to the rink amide resin with DIC and HOBt (300% mol each relative to resin) in 1:1 DMF/DCM for 1.5 h. After deprotection of Mtt group and coupling of SP-COOH, Fmoc group was removed by 20 % piperidine in DMF. The spiropyran-peptide was cleaved off the resin in TFA/triethylsilane/water (94 / 5 / 1) solution at room

temperature for 2 h and precipitated out in diethyl ether. The product was and purified by reversed-phased HPLC and lyophilized as orange powders (31 mg 15%). ^{1}H NMR (400 MHz; DMSO-d_6) δ =1.14 (3H, s), 1.25 (3H, s), 1.35-1.41 (2H, m), 1.51-1.57 (2H, m), 1.71-1.76 (2H, m) 2.73 (3H, s), 3.24 (2H, dd, 6 and 9 Hz), 3.69 (1H, dd, 6 and 7 Hz), 6.02 (1H, d, 10Hz), 6.67 (1H, d, 8 Hz), 6.88 (1H, d, 9 Hz), 7.25 (1H, d, 10 Hz), 7.63 (1H, d, 2 Hz), 7.71 (1H, dd, 2 and 8 Hz),7.55(1H, s), 7.82 (1H, s), 8.00-8.08 (4H, m), 8.19 (1H, t, 5 Hz), 8.25 (1H, d, 3 Hz). ESI-MS for $C_{26}H_{32}N_5O_5$ $[M+H]^+$ calculated 494.24; found 494.26.

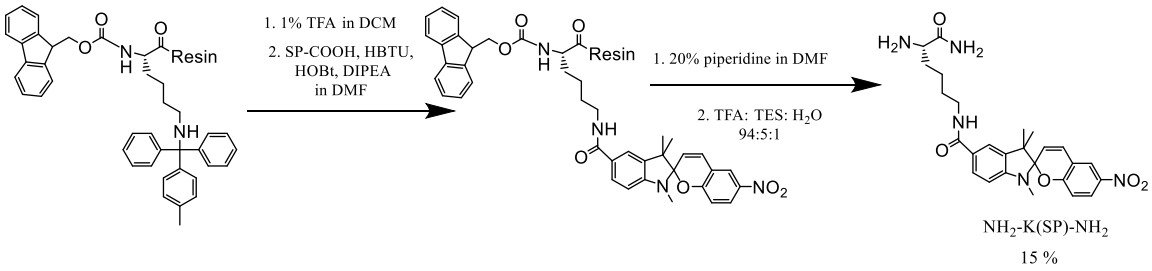

Scheme 4. Synthesis route for NH_2-K(SP)-NH_2.

Ac-K(SP)-OH

Fmoc-K(SP)-Wang resin was prepared on Wang resin (loading 1.2 mmol/g). Fmoc group was removed by 20 % piperidine in DMF and then washed. A solution of acetic anhydride/DIPEA/DMF = 1:1:8 (v : v : v) was prepared and added. After reacted for 1 h, Ac-K(SP)-Wang resin was cleaved off the resin by the TFA : TES : H_2O : DCM = 60 : 2.5 : 2.5 : 35 solution. The crude product precipitated with cold diethylether and purified

by reversed-phased HPLC. The product was obtained as dark orange solid (60 mg 23%). ESI-MS for $C_{28}H_{33}N_4O_7$ $[M+H]^+$ calculated 537.23; found 537.23.

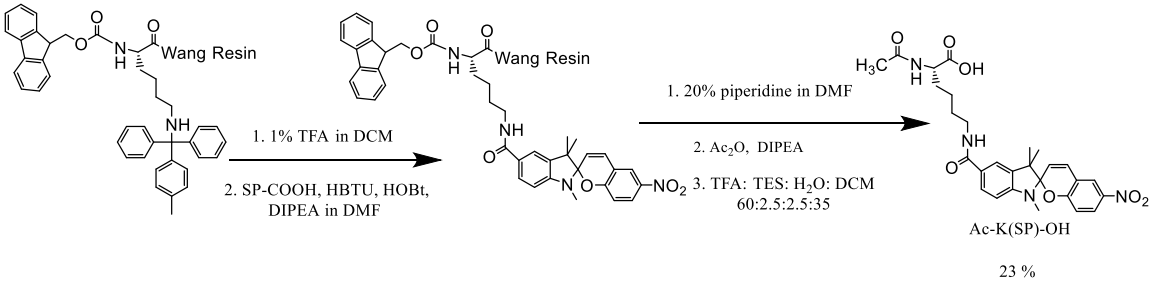

Scheme 5. Synthesis route for Ac-K(SP)-OH.

Spiropyran dipeptide hybrids Synthesis

A series of spiropyran dipeptide conjugates, NH_2-KK(SP)-OH, Ac-KK(SP)-OH, Fmoc-KK(SP)-OH and Fmoc-KK(SP)-NH_2 were designed and synthesized based on standard solid-phase peptides synthesis strategy with following schemes. The product were purified by reversed-phased HPLC on preparative Varian Dynamax C18 column and yields 169 mg (55%), 53 mg (16%), 57 mg (14%) and 87 mg (21%) respectively. The detailed ^{1}H NMR [400 MHz, $(CD_3)_2SO$] and ^{13}C NMR [400 MHz, $(CD_3)_2SO$] are reported in Appendix A.

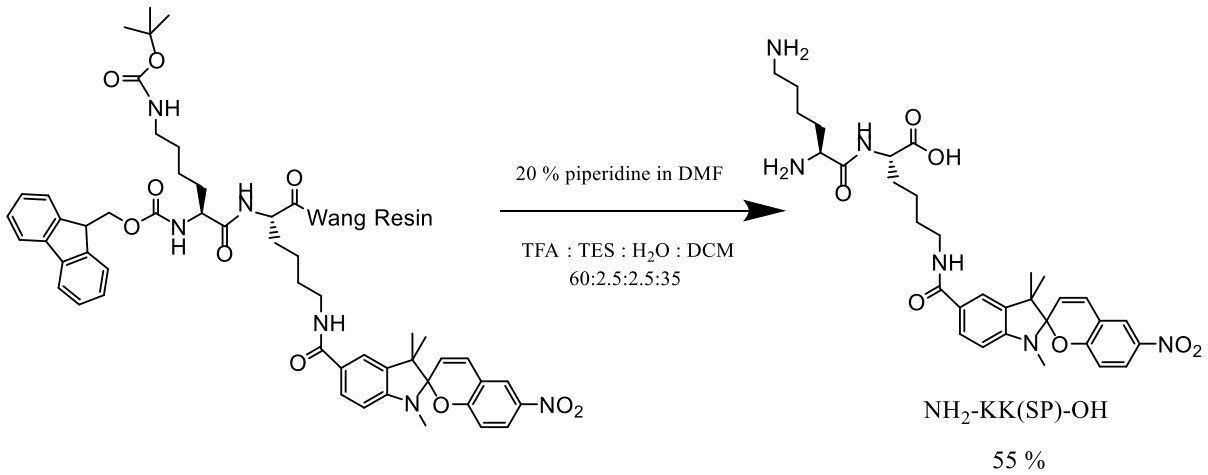

Scheme 6. Synthesis route for NH_2-KK(SP)-OH.

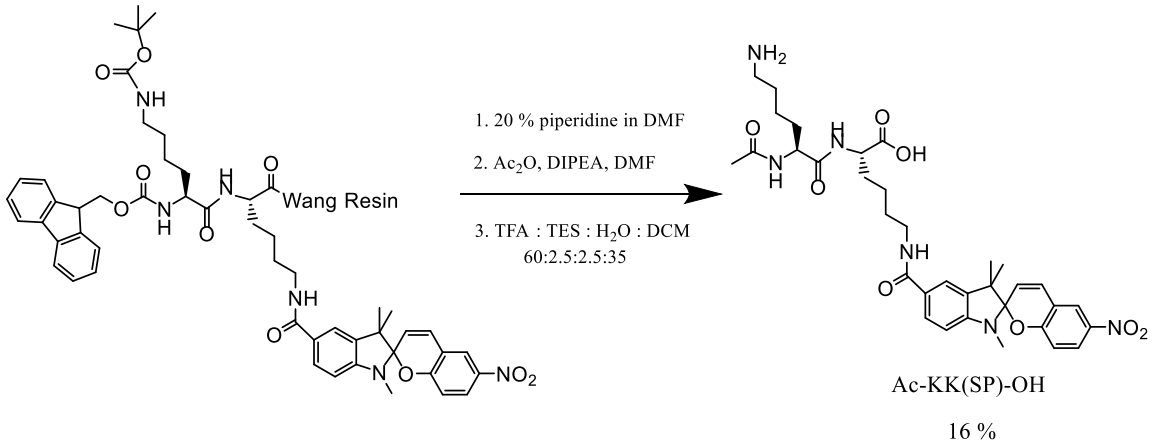

Scheme 7. Synthesis route for Ac-KK(SP)-OH.

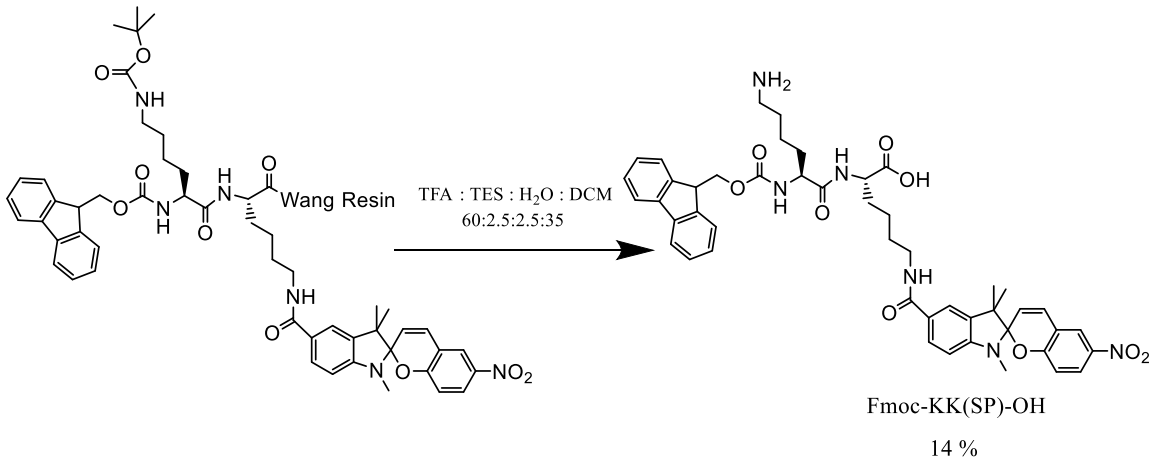

Scheme 8. Synthesis route for Fmoc-KK(SP)-OH.

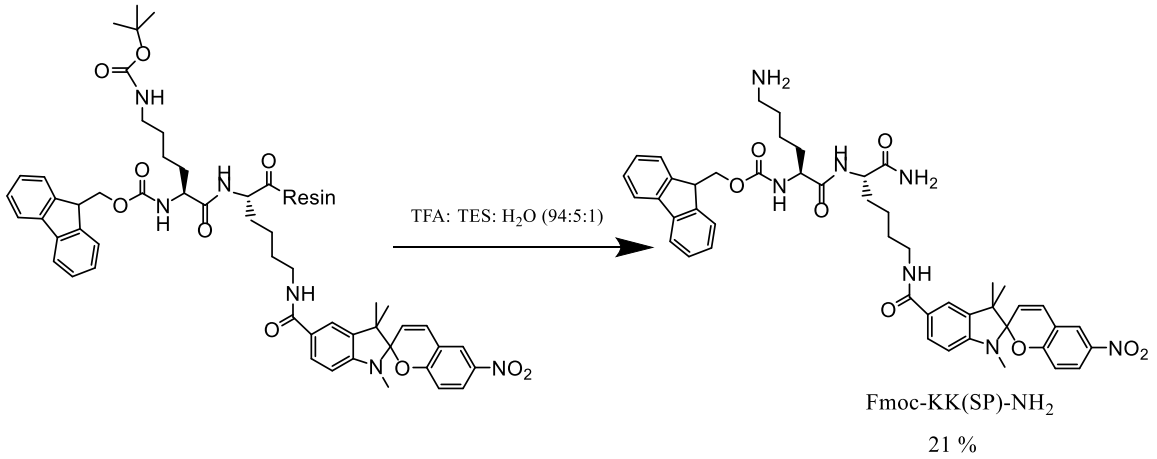

Scheme 9. Synthesis route for Fmoc-KK(SP)-NH_2.

Transmission Electron Microscopy (TEM) Measurement – Negative Stain TEM

10 mM stock sample solution was aged for at least 3 days and diluted to 1 mM before TEM measurement. 10 μL drop of each solution was applied to carbon coated copper grid (Ted Pella, Inc.) for 3 min. The excess solution was removed with filter paper and dried. Then the grid was floated on 10 μL drops of 2 % wt uranyl acetate solution for

negative stain for 1 min. The extra solution was also dried with filtering paper without touching the grid surface.

Ultraviolet-visible (UV-Vis) Spectroscopy Measurement

The UV-Vis spectroscopy studies were conducted using a 1 mm path length quartz cuvette over the range of 200-700 nm. Stock sample solutions were freshly diluted to 1 mM before taking the test.

Circular Dichroism (CD) Spectroscopy Measurement

CD spectra were recorded on a Jasco CD spectrometer under a nitrogen atmosphere. Experiments were performed in a quartz cell with a 1 mm path length over the range of 200-700 nm. Sample solutions were freshly diluted to 1mM from 10 mM aged stock solution before measurements.

Spiropyran Closed and Open Form Measurement

The ratio of the closed (SP) and the protonated open form (MEH) of spiropyran tetrapeptides were measured by analytical reverse-phase HPLC. Solution phase: 0.1% TFA of H_2O and Acetonitrile mixed solution.

References

1. Whitesides, G. M.; Grzybowski, B., Self-assembly at all scales. *Science* **2002,** *295* (5564), 2418-21.
2. Lehn, J.-M., Supramolecular Chemistry—Scope and Perspectives Molecules, Supermolecules, and Molecular Devices(Nobel Lecture). *Angew Chem Int Ed* **1988,** *27* (1), 89-112.
3. Maginn, S. J., Crystal engineering:the design of organic solidsby G. R. Desiraju. *J Appl Crystallogr* **1991,** *24* (3), 265-265.
4. Isaacs, L.; Chin, D. N.; Bowden, N.; Xia, Y.; Whitesides, G. M., Self-Assembling Systems on Scales from Nanometers to Millimeters: Design and Discovery. **1999,** *4*, 1-46.
5. Jakubith, S.; Rotermund, H. H.; Engel, W.; von Oertzen, A.; Ertl, G., Spatiotemporal concentration patterns in a surface reaction: Propagating and standing waves, rotating spirals, and turbulence. *Phys Rev Lett* **1990,** *65* (24), 3013-3016.
6. Hess, B., Periodic patterns in biology. *Naturwissenschaften* **2000,** *87* (5), 199-211.
7. Lehn, J.-M., Perspectives in Supramolecular Chemistry—From Molecular Recognition towards Molecular Information Processing and Self-Organization. *Angew Chem Int Ed* **1990,** *29* (11), 1304-1319.
8. Lehn, J.-M., **1995**.
9. Saini, R.; Saini, S.; Sharma, S., Nanotechnology: the future medicine. *J Cutan Aesthet Surg* **2010,** *3* (1), 32-3.
10. Shetty, R. C., Potential pitfalls of nanotechnology in its applications to medicine: immune incompatibility of nanodevices. *Med Hypotheses* **2005,** *65* (5), 998-9.
11. Gazit, E., Self-assembled peptide nanostructures: the design of molecular building blocks and their technological utilization. *Chem Soc Rev* **2007,** *36* (8), 1263-9.
12. Farokhzad, O. C.; Langer, R., Impact of nanotechnology on drug delivery. *ACS Nano* **2009,** *3* (1), 16-20.
13. Maynard, A. D.; Aitken, R. J.; Butz, T.; Colvin, V.; Donaldson, K.; Oberdorster, G.; Philbert, M. A.; Ryan, J.; Seaton, A.; Stone, V.; Tinkle, S. S.; Tran, L.; Walker, N. J.; Warheit, D. B., Safe handling of nanotechnology. *Nature* **2006,** *444* (7117), 267-9.
14. Miller, R. E.; Shenoy, V. B., Size-dependent elastic properties of nanosized structural elements. *Nanotechnology* **2000,** *11* (3), 139-147.
15. Russew, M.-M.; Hecht, S., Photoswitches: From Molecules to Materials. *Adv Mater* **2010,** *22* (31), 3348-3360.

16. Cheng, J. Y.; Ross, C. A.; Smith, H. I.; Thomas, E. L., Templated Self-Assembly of Block Copolymers: Top-Down Helps Bottom-Up. *Adv Mater* **2006,** *18* (19), 2505-2521.
17. Srinivasan, S.; Praveen, V. K.; Philip, R.; Ajayaghosh, A., Bioinspired superhydrophobic coatings of carbon nanotubes and linear pi systems based on the "bottom-up" self-assembly approach. *Angew Chem Int Ed Engl* **2008,** *47* (31), 5750-4.
18. Wang, X.; Hu, J.; Liu, G.; Tian, J.; Wang, H.; Gong, M.; Liu, S., Reversibly Switching Bilayer Permeability and Release Modules of Photochromic Polymersomes Stabilized by Cooperative Noncovalent Interactions. *J Am Chem Soc* **2015,** *137* (48), 15262-75.
19. Rösler, A.; Vandermeulen, G. W. M.; Klok, H.-A., Advanced drug delivery devices via self-assembly of amphiphilic block copolymers. *Adv Drug Deliv Rev* **2001,** *53* (1), 95-108.
20. Tyrrell, Z. L.; Shen, Y.; Radosz, M., Fabrication of micellar nanoparticles for drug delivery through the self-assembly of block copolymers. *Prog Polym Sci* **2010,** *35* (9), 1128-1143.
21. Wu, E. C.; Zhang, S.; Hauser, C. A. E., Self-Assembling Peptides as Cell-Interactive Scaffolds. *Adv Funct Mater* **2012,** *22* (3), 456-468.
22. Jayawarna, V.; Ali, M.; Jowitt, T. A.; Miller, A. F.; Saiani, A.; Gough, J. E.; Ulijn, R. V., Nanostructured Hydrogels for Three-Dimensional Cell Culture Through Self-Assembly of Fluorenylmethoxycarbonyl–Dipeptides. *Adv Mater* **2006,** *18* (5), 611-614.
23. Justice, B. A.; Badr, N. A.; Felder, R. A., 3D cell culture opens new dimensions in cell-based assays. *Drug Discov Today* **2009,** *14* (1-2), 102-7.
24. Jakab, K.; Norotte, C.; Marga, F.; Murphy, K.; Vunjak-Novakovic, G.; Forgacs, G., Tissue engineering by self-assembly and bio-printing of living cells. *Biofabrication* **2010,** *2* (2), 022001.
25. Kelm, J. M.; Lorber, V.; Snedeker, J. G.; Schmidt, D.; Broggini-Tenzer, A.; Weisstanner, M.; Odermatt, B.; Mol, A.; Zund, G.; Hoerstrup, S. P., A novel concept for scaffold-free vessel tissue engineering: self-assembly of microtissue building blocks. *J Biotechnol* **2010,** *148* (1), 46-55.
26. Lutolf, M. P.; Hubbell, J. A., Synthetic biomaterials as instructive extracellular microenvironments for morphogenesis in tissue engineering. *Nat Biotechnol* **2005,** *23* (1), 47-55.
27. Zang, L.; Che, Y.; Moore, J. S., One-dimensional self-assembly of planar pi-conjugated molecules: adaptable building blocks for organic nanodevices. *Acc Chem Res* **2008,** *41* (12), 1596-608.
28. Kumar, R. J.; MacDonald, J. M.; Singh, T. B.; Waddington, L. J.; Holmes, A. B., Hierarchical self-assembly of semiconductor functionalized peptide alpha-helices and optoelectronic properties. *J Am Chem Soc* **2011,** *133* (22), 8564-73.
29. Diegelmann, S. R.; Gorham, J. M.; Tovar, J. D., One-dimensional optoelectronic nanostructures derived from the aqueous self-assembly of pi-conjugated oligopeptides. *J Am Chem Soc* **2008,** *130* (42), 13840-1.

30. Lee, Y. S., **2008**.
31. Mendes, A. C.; Baran, E. T.; Reis, R. L.; Azevedo, H. S., Self-assembly in nature: using the principles of nature to create complex nanobiomaterials. *Wiley Interdiscip Rev Nanomed Nanobiotechnol* **2013,** *5* (6), 582-612.
32. Jorgensen, W. L.; Pranata, J., Importance of secondary interactions in triply hydrogen bonded complexes: guanine-cytosine vs uracil-2,6-diaminopyridine. *J Am Chem Soc* **1990,** *112* (5), 2008-2010.
33. Kwak, K.; Rosenfeld, D. E.; Chung, J. K.; Fayer, M. D., Solute-solvent complex switching dynamics of chloroform between acetone and dimethylsulfoxide-two-dimensional IR chemical exchange spectroscopy. *J Phys Chem B* **2008,** *112* (44), 13906-15.
34. Murray, T. J.; Zimmerman, S. C., New triply hydrogen bonded complexes with highly variable stabilities. *J Am Chem Soc* **1992,** *114* (10), 4010-4011.
35. Grzybowski, B. A.; Wilmer, C. E.; Kim, J.; Browne, K. P.; Bishop, K. J. M., Self-assembly: from crystals to cells. *Soft Matter* **2009,** *5* (6), 1110.
36. Hoeben, F. J.; Jonkheijm, P.; Meijer, E. W.; Schenning, A. P., About supramolecular assemblies of pi-conjugated systems. *Chem Rev* **2005,** *105* (4), 1491-546.
37. Chandler, D., Interfaces and the driving force of hydrophobic assembly. *Nature* **2005,** *437* (7059), 640-7.
38. Silverstein, T. P., The Real Reason Why Oil and Water Don't Mix. *J Chem Educ* **1998,** *75* (1), 116.
39. Haselmeier, R.; Holz, M.; Marbach, W.; Weingaertner, H., Water Dynamics near a Dissolved Noble Gas. First Direct Experimental Evidence for a Retardation Effect. *J Phys Chem* **1995,** *99* (8), 2243-2246.
40. Nitschke, J. R.; Hutin, M.; Bernardinelli, G., The Hydrophobic Effect as a Driving Force in the Self-Assembly of a [2×2] Copper(I) Grid. *Angew Chem* **2004,** *116* (48), 6892-6895.
41. Sanchez-Iglesias, A.; Grzelczak, M.; Altantzis, T.; Goris, B.; Perez-Juste, J.; Bals, S.; Van Tendeloo, G.; Donaldson, S. H., Jr.; Chmelka, B. F.; Israelachvili, J. N.; Liz-Marzan, L. M., Hydrophobic interactions modulate self-assembly of nanoparticles. *ACS Nano* **2012,** *6* (12), 11059-65.
42. Balakrishnan, K.; Datar, A.; Oitker, R.; Chen, H.; Zuo, J.; Zang, L., Nanobelt self-assembly from an organic n-type semiconductor: propoxyethyl-PTCDI. *J Am Chem Soc* **2005,** *127* (30), 10496-7.
43. Battaglia, M. R.; Buckingham, A. D.; Williams, J. H., The electric quadrupole moments of benzene and hexafluorobenzene. *Chem Phys Lett* **1981,** *78* (3), 421-423.
44. Martinez, C. R.; Iverson, B. L., Rethinking the term “pi-stacking”. *Chem Sci* **2012,** *3* (7), 2191.
45. van der Waals forces. **2009**.
46. Satake, M. S. S. M., *Chemical Bonding*. Discovery Publishing House Pvt. Limited: 2010.

47. Caplan, M. R.; Moore, P. N.; Zhang, S.; Kamm, R. D.; Lauffenburger, D. A., Self-Assembly of a β-Sheet Protein Governed by Relief of Electrostatic Repulsion Relative to van der Waals Attraction. *Biomacromolecules* **2000,** *1* (4), 627-631.
48. Gribbon, C.; Channon, K. J.; Zhang, W.; Banwell, E. F.; Bromley, E. H.; Chaudhuri, J. B.; Oreffo, R. O.; Woolfson, D. N., MagicWand: a single, designed peptide that assembles to stable, ordered alpha-helical fibers. *Biochemistry* **2008,** *47* (39), 10365-71.
49. Potekhin, S. A.; Melnik, T. N.; Popov, V.; Lanina, N. F.; Vazina, A. A.; Rigler, P.; Verdini, A. S.; Corradin, G.; Kajava, A. V., De novo design of fibrils made of short α-helical coiled coil peptides. *Chemistry & Biology* **2001,** *8* (11), 1025-1032.
50. Wagner, D. E.; Phillips, C. L.; Ali, W. M.; Nybakken, G. E.; Crawford, E. D.; Schwab, A. D.; Smith, W. F.; Fairman, R., Toward the development of peptide nanofilaments and nanoropes as smart materials. *Proc Natl Acad Sci U S A* **2005,** *102* (36), 12656-61.
51. Woolfson, D. N., Building fibrous biomaterials from alpha-helical and collagen-like coiled-coil peptides. *Biopolymers* **2010,** *94* (1), 118-27.
52. Zimenkov, Y.; Conticello, V. P.; Guo, L.; Thiyagarajan, P., Rational design of a nanoscale helical scaffold derived from self-assembly of a dimeric coiled coil motif. *Tetrahedron* **2004,** *60* (34), 7237-7246.
53. Lupas, A. N.; Gruber, M., The Structure of α-Helical Coiled Coils. **2005,** *70*, 37-38.
54. Pandya, M. J.; Spooner, G. M.; Sunde, M.; Thorpe, J. R.; Rodger, A.; Woolfson, D. N., Sticky-End Assembly of a Designed Peptide Fiber Provides Insight into Protein Fibrillogenesis†. *Biochemistry* **2000,** *39* (30), 8728-8734.
55. Kojima, S. K., Y.; Yoshida, T.; Yazaki, K.; Miura, K., *Proc Jpn Acad Ser B: Phys Biol Sci* **1997,** *73*, 7-11.
56. Rele, S.; Song, Y.; Apkarian, R. P.; Qu, Z.; Conticello, V. P.; Chaikof, E. L., D-periodic collagen-mimetic microfibers. *J Am Chem Soc* **2007,** *129* (47), 14780-7.
57. Fallas, J. A.; O'Leary, L. E.; Hartgerink, J. D., Synthetic collagen mimics: self-assembly of homotrimers, heterotrimers and higher order structures. *Chem Soc Rev* **2010,** *39* (9), 3510-27.
58. O'Leary, L. E.; Fallas, J. A.; Bakota, E. L.; Kang, M. K.; Hartgerink, J. D., Multi-hierarchical self-assembly of a collagen mimetic peptide from triple helix to nanofibre and hydrogel. *Nat Chem* **2011,** *3* (10), 821-8.
59. Ghadiri, M. R.; Granja, J. R.; Milligan, R. A.; McRee, D. E.; Khazanovich, N., Self-assembling organic nanotubes based on a cyclic peptide architecture. *Nature* **1993,** *366* (6453), 324-7.
60. Ghadiri, M. R.; Granja, J. R.; Buehler, L. K., Artificial transmembrane ion channels from self-assembling peptide nanotubes. *Nature* **1994,** *369* (6478), 301-4.
61. Horne, W. S.; Ashkenasy, N.; Ghadiri, M. R., Modulating charge transfer through cyclic D,L-alpha-peptide self-assembly. *Chemistry* **2005,** *11* (4), 1137-44.

62. Zhang, S.; Holmes, T.; Lockshin, C.; Rich, A., Spontaneous assembly of a self-complementary oligopeptide to form a stable macroscopic membrane. *Proc Natl Acad Sci* **1993,** *90* (8), 3334-3338.
63. Zhang, S.; Holmes, T. C.; DiPersio, C. M.; Hynes, R. O.; Su, X.; Rich, A., Self-complementary oligopeptide matrices support mammalian cell attachment. *Biomaterials* **1995,** *16* (18), 1385-1393.
64. Semino, C. E., Self-assembling peptides: from bio-inspired materials to bone regeneration. *J Dent Res* **2008,** *87* (7), 606-16.
65. Holmes, T. C.; de Lacalle, S.; Su, X.; Liu, G.; Rich, A.; Zhang, S., Extensive neurite outgrowth and active synapse formation on self-assembling peptide scaffolds. *Proc Natl Acad Sci* **2000,** *97* (12), 6728-6733.
66. Maude, S.; Tai, L. R.; Davies, R. P.; Liu, B.; Harris, S. A.; Kocienski, P. J.; Aggeli, A., Peptide synthesis and self-assembly. *Top Curr Chem* **2012,** *310*, 27-69.
67. Aggeli, A.; Bell, M.; Carrick, L. M.; Fishwick, C. W.; Harding, R.; Mawer, P. J.; Radford, S. E.; Strong, A. E.; Boden, N., pH as a trigger of peptide beta-sheet self-assembly and reversible switching between nematic and isotropic phases. *J Am Chem Soc* **2003,** *125* (32), 9619-28.
68. Rajagopal, K.; Lamm, M. S.; Haines-Butterick, L. A.; Pochan, D. J.; Schneider, J. P., Tuning the pH responsiveness of beta-hairpin peptide folding, self-assembly, and hydrogel material formation. *Biomacromolecules* **2009,** *10* (9), 2619-25.
69. Rajagopal, K.; Ozbas, B.; Pochan, D. J.; Schneider, J. P., Probing the importance of lateral hydrophobic association in self-assembling peptide hydrogelators. *Eur Biophys J* **2006,** *35* (2), 162-9.
70. Schneider, J. P.; Pochan, D. J.; Ozbas, B.; Rajagopal, K.; Pakstis, L.; Kretsinger, J., Responsive Hydrogels from the Intramolecular Folding and Self-Assembly of a Designed Peptide. *J Am Chem Soc* **2002,** *124* (50), 15030-15037.
71. Veiga, A. S.; Sinthuvanich, C.; Gaspar, D.; Franquelim, H. G.; Castanho, M. A.; Schneider, J. P., Arginine-rich self-assembling peptides as potent antibacterial gels. *Biomaterials* **2012,** *33* (35), 8907-16.
72. Pochan, D. J.; Schneider, J. P.; Kretsinger, J.; Ozbas, B.; Rajagopal, K.; Haines, L., Thermally reversible hydrogels via intramolecular folding and consequent self-assembly of a de novo designed peptide. *J Am Chem Soc* **2003,** *125* (39), 11802-3.
73. Ozbas, B.; Kretsinger, J.; Rajagopal, K.; Schneider, J. P.; Pochan, D. J., Salt-Triggered Peptide Folding and Consequent Self-Assembly into Hydrogels with Tunable Modulus. *Macromolecules* **2004,** *37* (19), 7331-7337.
74. Haines-Butterick, L.; Rajagopal, K.; Branco, M.; Salick, D.; Rughani, R.; Pilarz, M.; Lamm, M. S.; Pochan, D. J.; Schneider, J. P., Controlling hydrogelation kinetics by peptide design for three-dimensional encapsulation and injectable delivery of cells. *Proc Natl Acad Sci U S A* **2007,** *104* (19), 7791-6.
75. Yanlian, Y.; Ulung, K.; Xiumei, W.; Horii, A.; Yokoi, H.; Shuguang, Z., Designer self-assembling peptide nanomaterials. *Nano Today* **2009,** *4* (2), 193-210.

76. Vauthey, S.; Santoso, S.; Gong, H.; Watson, N.; Zhang, S., Molecular self-assembly of surfactant-like peptides to form nanotubes and nanovesicles. *Proc Natl Acad Sci U S A* **2002,** *99* (8), 5355-60.
77. Santoso, S.; Hwang, W.; Hartman, H.; Zhang, S., Self-assembly of Surfactant-like Peptides with Variable Glycine Tails to Form Nanotubes and Nanovesicles. *Nano Lett* **2002,** *2* (7), 687-691.
78. von Maltzahn, G.; Vauthey, S.; Santoso, S.; Zhang, S., Positively Charged Surfactant-like Peptides Self-assemble into Nanostructures. *Langmuir* **2003,** *19* (10), 4332-4337.
79. Yaghmur, A.; Laggner, P.; Zhang, S.; Rappolt, M., Tuning curvature and stability of monoolein bilayers by designer lipid-like peptide surfactants. *PLoS One* **2007,** *2* (5), e479.
80. Khoe, U.; Yang, Y.; Zhang, S., Synergistic effect and hierarchical nanostructure formation in mixing two designer lipid-like peptide surfactants Ac-A6D-OH and Ac-A6K-NH2. *Macromol Biosci* **2008,** *8* (11), 1060-7.
81. Khoe, U.; Yang, Y.; Zhang, S., Self-assembly of nanodonut structure from a cone-shaped designer lipid-like peptide surfactant. *Langmuir* **2009,** *25* (7), 4111-4.
82. Corin, K.; Baaske, P.; Ravel, D. B.; Song, J.; Brown, E.; Wang, X.; Wienken, C. J.; Jerabek-Willemsen, M.; Duhr, S.; Luo, Y.; Braun, D.; Zhang, S., Designer lipid-like peptides: a class of detergents for studying functional olfactory receptors using commercial cell-free systems. *PLoS One* **2011,** *6* (11), e25067.
83. Cui, H.; Webber, M. J.; Stupp, S. I., Self-assembly of peptide amphiphiles: from molecules to nanostructures to biomaterials. *Biopolymers* **2010,** *94* (1), 1-18.
84. Niece, K. L.; Czeisler, C.; Sahni, V.; Tysseling-Mattiace, V.; Pashuck, E. T.; Kessler, J. A.; Stupp, S. I., Modification of gelation kinetics in bioactive peptide amphiphiles. *Biomaterials* **2008,** *29* (34), 4501-9.
85. Behanna, H. A.; Donners, J. J.; Gordon, A. C.; Stupp, S. I., Coassembly of amphiphiles with opposite peptide polarities into nanofibers. *J Am Chem Soc* **2005,** *127* (4), 1193-200.
86. Bull, S. R.; Guler, M. O.; Bras, R. E.; Meade, T. J.; Stupp, S. I., Self-assembled peptide amphiphile nanofibers conjugated to MRI contrast agents. *Nano Lett* **2005,** *5* (1), 1-4.
87. Bull, S. R.; Guler, M. O.; Bras, R. E.; Venkatasubramanian, P. N.; Stupp, S. I.; Meade, T. J., Magnetic resonance imaging of self-assembled biomaterial scaffolds. *Bioconjug Chem* **2005,** *16* (6), 1343-8.
88. Guler, M. O.; Pokorski, J. K.; Appella, D. H.; Stupp, S. I., Enhanced oligonucleotide binding to self-assembled nanofibers. *Bioconjug Chem* **2005,** *16* (3), 501-3.
89. Guler, M. O.; Claussen, R. C.; Stupp, S. I., Encapsulation of pyrene within self-assembled peptide amphiphile nanofibers. *J Mater Chem* **2005,** *15* (42), 4507.
90. Sone, E. D.; Stupp, S. I., Semiconductor-encapsulated peptide-amphiphile nanofibers. *J Am Chem Soc* **2004,** *126* (40), 12756-7.

91. Cui, H.; Muraoka, T.; Cheetham, A. G.; Stupp, S. I., Self-assembly of giant peptide nanobelts. *Nano Lett* **2009,** *9* (3), 945-51.
92. Guler, M. O.; Hsu, L.; Soukasene, S.; Harrington, D. A.; Hulvat, J. F.; Stupp, S. I., Presentation of RGDS epitopes on self-assembled nanofibers of branched peptide amphiphiles. *Biomacromolecules* **2006,** *7* (6), 1855-63.
93. Sargeant, T. D.; Oppenheimer, S. M.; Dunand, D. C.; Stupp, S. I., Titanium foam-bioactive nanofiber hybrids for bone regeneration. *J Tissue Eng Regen Med* **2008,** *2* (8), 455-62.
94. Sargeant, T. D.; Guler, M. O.; Oppenheimer, S. M.; Mata, A.; Satcher, R. L.; Dunand, D. C.; Stupp, S. I., Hybrid bone implants: self-assembly of peptide amphiphile nanofibers within porous titanium. *Biomaterials* **2008,** *29* (2), 161-71.
95. Hoffman, R. A. G. a. W. F., Note. *J Am Chem Soc* **1921,** *43* (10), 2199-2202.
96. Menger, F. M.; Caran, K. L., Anatomy of a Gel. Amino Acid Derivatives That Rigidify Water at Submillimolar Concentrations. *J Am Chem Soc* **2000,** *122* (47), 11679-11691.
97. Menger, F. M.; Yamasaki, Y.; Catlin, K. K.; Nishimi, T., X-Ray Structure of a Self-Assembled Gelating Fiber. *Angew Chem Int Ed* **1995,** *34* (5), 585-586.
98. Orbach, R.; Mironi-Harpaz, I.; Adler-Abramovich, L.; Mossou, E.; Mitchell, E. P.; Forsyth, V. T.; Gazit, E.; Seliktar, D., The rheological and structural properties of Fmoc-peptide-based hydrogels: the effect of aromatic molecular architecture on self-assembly and physical characteristics. *Langmuir* **2012,** *28* (4), 2015-22.
99. Reches, M.; Gazit, E., Casting metal nanowires within discrete self-assembled peptide nanotubes. *Science* **2003,** *300* (5619), 625-7.
100. Mahler, A.; Reches, M.; Rechter, M.; Cohen, S.; Gazit, E., Rigid, Self-Assembled Hydrogel Composed of a Modified Aromatic Dipeptide. *Adv Mater* **2006,** *18* (11), 1365-1370.
101. Smith, A. M.; Williams, R. J.; Tang, C.; Coppo, P.; Collins, R. F.; Turner, M. L.; Saiani, A.; Ulijn, R. V., Fmoc-Diphenylalanine Self Assembles to a Hydrogel via a Novel Architecture Based on π–π Interlocked β-Sheets. *Adv Mater* **2008,** *20* (1), 37-41.
102. Ryan, D. M.; Nilsson, B. L., Self-assembled amino acids and dipeptides as noncovalent hydrogels for tissue engineering. *Polym. Chem.* **2012,** *3* (1), 18-33.
103. Shao, H.; Parquette, J. R., Controllable peptide-dendron self-assembly: interconversion of nanotubes and fibrillar nanostructures. *Angew Chem Int Ed Engl* **2009,** *48* (14), 2525-8.
104. Kim, S. H.; Sun, Y.; Kaplan, J. A.; Grinstaff, M. W.; Parquette, J. R., Photo-crosslinking of a self-assembled coumarin-dipeptide hydrogel. *New J Chem* **2015,** *39* (5), 3225-3228.
105. Shao, H.; Gao, M.; Kim, S. H.; Jaroniec, C. P.; Parquette, J. R., Aqueous Self-Assembly of L-Lysine-Based Amphiphiles into 1D n-Type Nanotubes. *Chem Eur J* **2011,** *17* (46), 12882-12885.
106. Shao, H.; Parquette, J. R., A [small pi]-conjugated hydrogel based on an Fmoc-dipeptide naphthalene diimide semiconductor. *Chem Commun* **2010,** *46* (24), 4285-4287.

107. Shao, H.; Seifert, J.; Romano, N. C.; Gao, M.; Helmus, J. J.; Jaroniec, C. P.; Modarelli, D. A.; Parquette, J. R., Amphiphilic Self-Assembly of an n-Type Nanotube. *Angew Chem Int Ed* **2010,** *49* (42), 7688-7691.
108. Kim, S. H.; Parquette, J. R., A model for the controlled assembly of semiconductor peptides. *Nanoscale* **2012,** *4* (22), 6940-7.
109. Tu, S.; Kim, S. H.; Joseph, J.; Modarelli, D. A.; Parquette, J. R., Proton-coupled self-assembly of a porphyrin-naphthalenediimide dyad. *Chemphyschem* **2013,** *14* (8), 1609-17.
110. Shao, H.; Lockman, J. W.; Parquette, J. R., Coupled conformational equilibria in beta-sheet peptide-dendron conjugates. *J Am Chem Soc* **2007,** *129* (7), 1884-5.
111. Sofos, M.; Stone, D. A.; Goswami, D. K.; Okasinski, J. S.; Jin, H.; Bedzyk, M. J.; Stupp, S. I., Nanoscale Structure of Self-Assembling Hybrid Materials of Inorganic and Electronically Active Organic Phases. *J Phys Chem C* **2008,** *112* (8), 2881-2887.
112. Song, B.; Wei, H.; Wang, Z.; Zhang, X.; Smet, M.; Dehaen, W., Supramolecular Nanofibers by Self-Organization of Bola-amphiphiles through a Combination of Hydrogen Bonding and π–π Stacking Interactions. *Adv Mater* **2007,** *19* (3), 416-420.
113. Guo, Y.; Yui, H.; Minamikawa, H.; Masuda, M.; Kamiya, S.; Sawada, T.; Ito, K.; Shimizu, T., FT-IR Study of the Interlamellar Water Confined in Glycolipid Nanotube Walls. *Langmuir* **2005,** *21* (10), 4610-4614.
114. Ratna, B. R.; Baral-Tosh, S.; Kahn, B.; Schnur, J. M.; Rudolph, A. S., Effect of alcohol chain length on tubule formation in 1,2-bis(10,12-tricosadiynoyl)-sn-glycero-3-phosphocholine. *Chem Phys Lipids* **1992,** *63* (1-2), 47-53.
115. Lipowsky, R., The conformation of membranes. *Nature* **1991,** *349* (6309), 475-81.
116. Kim, S. H.; Kaplan, J. A.; Sun, Y.; Shieh, A.; Sun, H. L.; Croce, C. M.; Grinstaff, M. W.; Parquette, J. R., The self-assembly of anticancer camptothecin-dipeptide nanotubes: a minimalistic and high drug loading approach to increased efficacy. *Chemistry* **2015,** *21* (1), 101-5.
117. Sun, Y.; Shieh, A.; Kim, S. H.; King, S.; Kim, A.; Sun, H. L.; Croce, C. M.; Parquette, J. R., The self-assembly of a camptothecin-lysine nanotube. *Bioorg Med Chem Lett* **2016,** *26* (12), 2834-8.
118. Sun, Y.; Kaplan, J. A.; Shieh, A.; Sun, H. L.; Croce, C. M.; Grinstaff, M. W.; Parquette, J. R., Self-assembly of a 5-fluorouracil-dipeptide hydrogel. *Chem Commun (Camb)* **2016,** *52* (30), 5254-7.
119. Balzani, V.; Credi, A.; Raymo, F. M.; Stoddart, J. F., Artificial Molecular Machines. *Angew Chem* **2000,** *39* (19), 3348-3391.
120. Aida, T.; Meijer, E. W.; Stupp, S. I., Functional Supramolecular Polymers. *Science* **2012,** *335* (6070), 813-817.
121. Rotzler, J.; Mayor, M., Molecular daisy chains. *Chem Soc Rev* **2013,** *42* (1), 44-62.
122. Nakahata, M.; Takashima, Y.; Hashidzume, A.; Harada, A., Redox-Generated Mechanical Motion of a Supramolecular Polymeric Actuator Based on Host–Guest Interactions. *Angew Chem Int Ed* **2013,** *52* (22), 5731-5735.

123. Li, L.; Zhang, H.-Y.; Zhao, J.; Li, N.; Liu, Y., Self-Sorting of Four Organic Molecules into a Heterowheel Polypseudorotaxane. *Chem Eur J* **2013,** *19* (20), 6498-6506.
124. Niu, Z.; Huang, F.; Gibson, H. W., Supramolecular AA−BB-Type Linear Polymers with Relatively High Molecular Weights via the Self-Assembly of Bis(m-phenylene)-32-Crown-10 Cryptands and a Bisparaquat Derivative. *J Am Chem Soc* **2011,** *133* (9), 2836-2839.
125. Gröger, G.; Meyer-Zaika, W.; Böttcher, C.; Gröhn, F.; Ruthard, C.; Schmuck, C., Switchable Supramolecular Polymers from the Self-Assembly of a Small Monomer with Two Orthogonal Binding Interactions. *J Am Chem Soc* **2011,** *133* (23), 8961-8971.
126. Fang, R.; Liu, Y.; Wang, Z.; Zhang, X., Water-soluble supramolecular hyperbranched polymers based on host-enhanced π–π interaction. *Polym Chem* **2013,** *4* (4), 900.
127. Ma, X.; Sun, R.; Li, W.; Tian, H., Novel electrochemical and pH stimulus-responsive supramolecular polymer with disparate pseudorotaxanes as relevant unimers. *Polym Chem* **2011,** *2* (5), 1068-1070.
128. Sun, R.; Xue, C.; Ma, X.; Gao, M.; Tian, H.; Li, Q., Light-Driven Linear Helical Supramolecular Polymer Formed by Molecular-Recognition-Directed Self-Assembly of Bis(p-sulfonatocalix[4]arene) and Pseudorotaxane. *J Am Chem Soc* **2013,** *135* (16), 5990-5993.
129. Sun, R.; Zhang, Q.; Wang, Q.; Ma, X., Novel supramolecular CT polymer employing disparate pseudorotaxanes as relevant monomers. *Polymer* **2013,** *54* (10), 2506-2510.
130. Zhang, Q.; Qu, D.-H.; Ma, X.; Tian, H., Sol-gel conversion based on photoswitching between noncovalently and covalently linked netlike supramolecular polymers. *Chem Commun* **2013,** *49* (84), 9800-9802.
131. Zhu, L.; Lu, M.; Zhang, Q.; Qu, D.; Tian, H., Construction of Polypseudorotaxane from Low-Molecular Weight Monomers via Dual Noncovalent Interactions. *Macromolecules* **2011,** *44* (11), 4092-4097.
132. Irie, M.; Fukaminato, T.; Sasaki, T.; Tamai, N.; Kawai, T., Organic chemistry: A digital fluorescent molecular photoswitch. *Nature* **2002,** *420* (6917), 759-760.
133. Kato, T., Self-Assembly of Phase-Segregated Liquid Crystal Structures. *Science* **2002,** *295* (5564), 2414-2418.
134. Vollmer, M. S.; Clark, T. D.; Steinem, C.; Ghadiri, M. R., Photoswitchable Hydrogen-Bonding in Self-Organized Cylindrical Peptide Systems. *Angew Chem Int Ed* **1999,** *38* (11), 1598-1601.
135. Yagai, S.; Karatsu, T.; Kitamura, A., Photocontrollable Self-Assembly. *Chem Eur J* **2005,** *11* (14), 4054-4063.
136. Chen, S. H.; Chen, H. M. P.; Geng, Y.; Jacobs, S. D.; Marshall, K. L.; Blanton, T. N., Novel Glassy Nematic Liquid Crystals for Non-destructive Rewritable Optical Memory and Photonic Switching. *Adv Mater* **2003,** *15* (13), 1061-1065.

137. Olson, C. E.; Previte, M. J. R.; Fourkas, J. T., Efficient and robust multiphoton data storage in molecular glasses and highly crosslinked polymers. *Nat Mater* **2002,** *1* (4), 225-228.
138. Uchida, K.; Saito, M.; Murakami, A.; Kobayashi, T.; Nakamura, S.; Irie, M., Three Bits Eight States Photochromic Recording and Nondestructive Readout by Using IR Light. *Chem Eur J* **2005,** *11* (2), 534-542.
139. Aldred, M. P.; Contoret, A. E. A.; Farrar, S. R.; Kelly, S. M.; Mathieson, D.; O'Neill, M.; Tsoi, W. C.; Vlachos, P., A Full-Color Electroluminescent Device and Patterned Photoalignment Using Light-Emitting Liquid Crystals. *Adv Mater* **2005,** *17* (11), 1368-1372.
140. Abraham, S.; Mallia, V. A.; Ratheesh, K. V.; Tamaoki, N.; Das, S., Reversible Thermal and Photochemical Switching of Liquid Crystalline Phases and Luminescence in Diphenylbutadiene-Based Mesogenic Dimers. *J Am Chem Soc* **2006,** *128* (23), 7692-7698.
141. Zhang, X.; Wen, Y.; Li, Y.; Li, G.; Du, S.; Guo, H.; Yang, L.; Jiang, L.; Gao, H.; Song, Y., Molecularly Controlled Modulation of Conductance on Azobenzene Monolayer-Modified Silicon Surfaces. *J Phys Chem C* **2008,** *112* (22), 8288-8293.
142. Chan, Y.-H.; Gallina, M. E.; Zhang, X.; Wu, I. C.; Jin, Y.; Sun, W.; Chiu, D. T., Reversible Photoswitching of Spiropyran-Conjugated Semiconducting Polymer Dots. *Anal Chem* **2012,** *84* (21), 9431-9438.
143. Feng, G.; Ding, D.; Li, K.; Liu, J.; Liu, B., Reversible photoswitching conjugated polymer nanoparticles for cell and ex vivo tumor imaging. *Nanoscale* **2014,** *6* (8), 4141-4147.
144. Bouas-Laurent, H.; Dürr, H., Organic photochromism (IUPAC Technical Report). *Pure Appl Chem* **2001,** *73* (4).
145. Ghavidast, A.; Mahmoodi, N. O., A comparative study of the photochromic compounds incorporated on the surface of nanoparticles. *J Mol Liq* **2016,** *216*, 552-564.
146. Irie, M.; Fukaminato, T.; Matsuda, K.; Kobatake, S., Photochromism of Diarylethene Molecules and Crystals: Memories, Switches, and Actuators. *Chem Rev* **2014,** *114* (24), 12174-12277.
147. Minkin, V. I., Photo-, Thermo-, Solvato-, and Electrochromic Spiroheterocyclic Compounds. *Chem Rev* **2004,** *104* (5), 2751-2776.
148. Willner, I.; Rubin, S.; Shatzmiller, R.; Zor, T., Reversible light-stimulated activation and deactivation of .alpha.-chymotrypsin by its immobilization in photoisomerizable copolymers. *J Am Chem Soc* **1993,** *115* (19), 8690-8694.
149. Chen, C.-T.; Chou, Y. C., C2-Symmetric Dibenzosuberane-Based Helicenes as Potential Chirochromic Optical Switches. *J Am Chem Soc* **2000,** *122* (32), 7662-7672.
150. Cook, M. J.; Nygård, A.-M.; Wang, Z.; Russell, D. A., An evanescent field driven mono-molecular layer photoswitch: coordination and release of metallated macrocycles. *Chem Commun* **2002,** (10), 1056-1057.
151. Mativetsky, J. M.; Pace, G.; Elbing, M.; Rampi, M. A.; Mayor, M.; Samori, P., Azobenzenes as light-controlled molecular electronic switches in nanoscale metal-molecule-metal junctions. *J Am Chem Soc* **2008,** *130* (29), 9192-3.

152. Liu, D.; Xie, Y.; Shao, H.; Jiang, X., Using azobenzene-embedded self-assembled monolayers to photochemically control cell adhesion reversibly. *Angew Chem Int Ed Engl* **2009,** *48* (24), 4406-8.
153. Wand, A.; Rozin, R.; Eliash, T.; Jung, K. H.; Sheves, M.; Ruhman, S., Asymmetric toggling of a natural photoswitch: ultrafast spectroscopy of Anabaena sensory rhodopsin. *J Am Chem Soc* **2011,** *133* (51), 20922-32.
154. Denekamp, C.; Feringa, B. L., Optically Active Diarylethenes for Multimode Photoswitching Between Liquid-Crystalline Phases. *Adv Mater* **1998,** *10* (14), 1080-1082.
155. Zacharias, P.; Gather, M. C.; Kohnen, A.; Rehmann, N.; Meerholz, K., Photoprogrammable organic light-emitting diodes. *Angew Chem Int Ed Engl* **2009,** *48* (22), 4038-41.
156. Angiolini, L.; Benelli, T.; Bicciocchi, E.; Giorgini, L.; Raymo, F. M., Synthesis and photoresponsive behavior of optically active methacrylic homopolymers containing side-chain spiropyran chromophores. *React Funct Polym* **2012,** *72* (7), 469-477.
157. Berkovic, G.; Krongauz, V.; Weiss, V., Spiropyrans and Spirooxazines for Memories and Switches. *Chem Rev* **2000,** *100* (5), 1741-1754.
158. Crano, J. C.; Guglielmetti, R. J., *Organic photochromic and thermochromic compounds*. Kluwer Academic/Plenum Publishers: New York, 1999.
159. Durr, H.; Kranz, C.; Schulz, C.; Kilburg, H.; Jonsson, H. P., Molecular and supramolecular systems in photochromism: Dihydroindolizines - New versatile molecules. *Proceedings of the Indian Academy of Sciences-Chemical Sciences* **1995,** *107* (6), 314–466， 855–878.
160. Guo, X.; Zhang, D.; Yu, G.; Wan, M.; Li, J.; Liu, Y.; Zhu, D., Reversible Photoregulation of the Electrical Conductivity of Spiropyran-Doped Polyaniline for Information Recording and Nondestructive Processing. *Adv Mat* **2004,** *16* (7), 636-640.
161. McArdle, C. B., *Applied Photochromic Polymer Systems*. 1 ed.; Springer Netherlands: 1992.
162. Raymo, F. M.; Giordani, S., Signal Communication between Molecular Switches. *Org Let* **2001,** *3* (22), 3475-3478.
163. Raymo, F. M.; Giordani, S., Multichannel Digital Transmission in an Optical Network of Communicating Molecules. *J Am Chem Soc* **2002,** *124* (9), 2004-2007.
164. Wang, X.; Hu, J.; Liu, G.; Tian, J.; Wang, H.; Gong, M.; Liu, S., Reversibly Switching Bilayer Permeability and Release Modules of Photochromic Polymersomes Stabilized by Cooperative Noncovalent Interactions. *J Am Chem Soc* **2015,** *137* (48), 15262-15275.
165. Krebs, M. R.; Bromley, E. H.; Donald, A. M., The binding of thioflavin-T to amyloid fibrils: localisation and implications. *J Struct Biol* **2005,** *149* (1), 30-7.
166. Hudson, S. A.; Ecroyd, H.; Kee, T. W.; Carver, J. A., The thioflavin T fluorescence assay for amyloid fibril detection can be biased by the presence of exogenous compounds. *FEBS J* **2009,** *276* (20), 5960-72.
167. Biancalana, M.; Koide, S., Molecular mechanism of Thioflavin-T binding to amyloid fibrils. *Biochim Biophys Acta* **2010,** *1804* (7), 1405-12.

168. Nelson, R.; Sawaya, M. R.; Balbirnie, M.; Madsen, A. O.; Riekel, C.; Grothe, R.; Eisenberg, D., Structure of the cross-beta spine of amyloid-like fibrils. *Nature* **2005,** *435* (7043), 773-8.
169. Howie, A. J.; Brewer, D. B.; Howell, D.; Jones, A. P., Physical basis of colors seen in Congo red-stained amyloid in polarized light. *Lab Invest* **2008,** *88* (3), 232-42.
170. Elghetany, M. T.; Saleem, A., Methods for Staining Amyloid in Tissues: A Review. *Stain Technol* **2009,** *63* (4), 201-212.
171. Stsiapura, V. I.; Maskevich, A. A.; Kuzmitsky, V. A.; Turoverov, K. K.; Kuznetsova, I. M., Computational study of thioflavin T torsional relaxation in the excited state. *J Phys Chem A* **2007,** *111* (22), 4829-35.
172. Voropai, E. S.; Samtsov, M. P.; Kaplevskii, K. N.; Maskevich, A. A.; Stepuro, V. I.; Povarova, O. I.; Kuznetsova, I. M.; Turoverov, K. K.; Fink, A. L.; Uverskii, V. N., Spectral Properties of Thioflavin T and Its Complexes with Amyloid Fibrils. *J Appl Spectrosc* **2003,** *70* (6), 868-874.
173. Dzwolak, W.; Pecul, M., Chiral bias of amyloid fibrils revealed by the twisted conformation of Thioflavin T: an induced circular dichroism/DFT study. *FEBS Lett* **2005,** *579* (29), 6601-3.
174. Khurana, R.; Coleman, C.; Ionescu-Zanetti, C.; Carter, S. A.; Krishna, V.; Grover, R. K.; Roy, R.; Singh, S., Mechanism of thioflavin T binding to amyloid fibrils. *J Struct Biol* **2005,** *151* (3), 229-38.
175. Khurana, R.; Ionescu-Zanetti, C.; Pope, M.; Li, J.; Nielson, L.; Ram ŕez-Alvarado, M.; Regan, L.; Fink, A. L.; Carter, S. A., A General Model for Amyloid Fibril Assembly Based on Morphological Studies Using Atomic Force Microscopy. *Biophys J* **2003,** *85* (2), 1135-1144.
176. Sabate, R.; Lascu, I.; Saupe, S. J., On the binding of Thioflavin-T to HET-s amyloid fibrils assembled at pH 2. *J Struct Biol* **2008,** *162* (3), 387-96.
177. Biancalana, M.; Makabe, K.; Koide, A.; Koide, S., Molecular mechanism of thioflavin-T binding to the surface of beta-rich peptide self-assemblies. *J Mol Biol* **2009,** *385* (4), 1052-63.
178. Wu, C.; Wang, Z.; Lei, H.; Duan, Y.; Bowers, M. T.; Shea, J. E., The binding of thioflavin T and its neutral analog BTA-1 to protofibrils of the Alzheimer's disease Abeta(16-22) peptide probed by molecular dynamics simulations. *J Mol Biol* **2008,** *384* (3), 718-29.
179. Biancalana, M.; Makabe, K.; Koide, A.; Koide, S., Aromatic cross-strand ladders control the structure and stability of beta-rich peptide self-assembly mimics. *J Mol Biol* **2008,** *383* (1), 205-13.
180. Greenfield, N. J., Applications of circular dichroism in protein and peptide analysis. *Trends Anal Chem* **1999,** *18* (4), 236-244.
181. Klajn, R., Spiropyran-based dynamic materials. *Chem Soc Rev* **2014,** *43* (1), 148-84.
182. Jonsson, F.; Beke-Somfai, T.; Andreasson, J.; Norden, B., Interactions of a photochromic spiropyran with liposome model membranes. *Langmuir* **2013,** *29* (7), 2099-103.

183. Tomasulo, M.; Kaanumal, S. L.; Sortino, S.; Raymo, F. M., Synthesis and Properties of Benzophenone−Spiropyran and Naphthalene−Spiropyran Conjugates. *J Org Chem* **2007,** *72* (2), 595-605.
184. Crano, J. C.; Guglielmetti, R. J., **2002**.
185. Irie, M., *Photo-reactive materials for ultrahigh density optical memory: MITI research and development program on basic technologies for future industries*. Elsevier: 1994.
186. Finch, C. A., Photochemistry and polymeric systems. Edited by J. M. Kelly, C. B. McArdle and M. J. de Maunder. *Polym Int* **1994,** *35* (2), 215-215.
187. photochromism. **2009**.
188. Abe, J., Fast Photochromism of Bridged Imidazole Dimers. **2013**, 161-181.
189. Horii, T.; Abe, Y.; Nakao, R., Theoretical quantum chemical study of spironaphthoxazines and their merocyanines. *J. Photochem. Photobiol. A* **2001,** *144* (2-3), 119-129.
190. Schaus, S. E.; Brandes, B. D.; Larrow, J. F.; Tokunaga, M.; Hansen, K. B.; Gould, A. E.; Furrow, M. E.; Jacobsen, E. N., Highly Selective Hydrolytic Kinetic Resolution of Terminal Epoxides Catalyzed by Chiral (salen)CoIIIComplexes. Practical Synthesis of Enantioenriched Terminal Epoxides and 1,2-Diols. *J Am Chem Soc* **2002,** *124* (7), 1307-1315.
191. Nakamura, S.; Uchida, K.; Murakami, A.; Irie, M., Ab initio MO and proton NMR NOE studies of photochromic spironaphthoxazine. *J Org Chem.* **1993,** *58* (20), 5543-5545.
192. Cottone, G.; Noto, R.; La Manna, G.; Fornili, S. L., Ab initio study on the photoisomers of a nitro-substituted spiropyran. *Chem Phys Lett* **2000,** *319* (1-2), 51-59.
193. Lee, D.-H.; Lee, M.; Chung, C.; Lee, W.-H.; Lee, I.-J., Low-temperature NMR and IR Spectra of Photomerocyanine Form of Spirophenanthrooxazine. *Chem Lett* **2003,** *32* (7), 578-579.
194. Kainthan, R. K.; Janzen, J.; Kizhakkedathu, J. N.; Devine, D. V.; Brooks, D. E., Hydrophobically derivatized hyperbranched polyglycerol as a human serum albumin substitute. *Biomaterials* **2008,** *29* (11), 1693-704.
195. Son, S.; Shin, E.; Kim, B. S., Light-responsive micelles of spiropyran initiated hyperbranched polyglycerol for smart drug delivery. *Biomacromolecules* **2014,** *15* (2), 628-34.
196. Parrot, A.; Izzet, G.; Chamoreau, L. M.; Proust, A.; Oms, O.; Dolbecq, A.; Hakouk, K.; El Bekkachi, H.; Deniard, P.; Dessapt, R.; Mialane, P., Photochromic properties of polyoxotungstates with grafted spiropyran molecules. *Inorg Chem* **2013,** *52* (19), 11156-63.
197. Chu, Y.; Saad, A.; Yin, P.; Wu, J.; Oms, O.; Dolbecq, A.; Mialane, P.; Liu, T., Light- and Solvent-Controlled Self-Assembly Behavior of Spiropyran-Polyoxometalate-Alkyl Hybrid Molecules. *Chemistry* **2016,** *22* (33), 11756-62.

Appendix A: NMR Spectrum

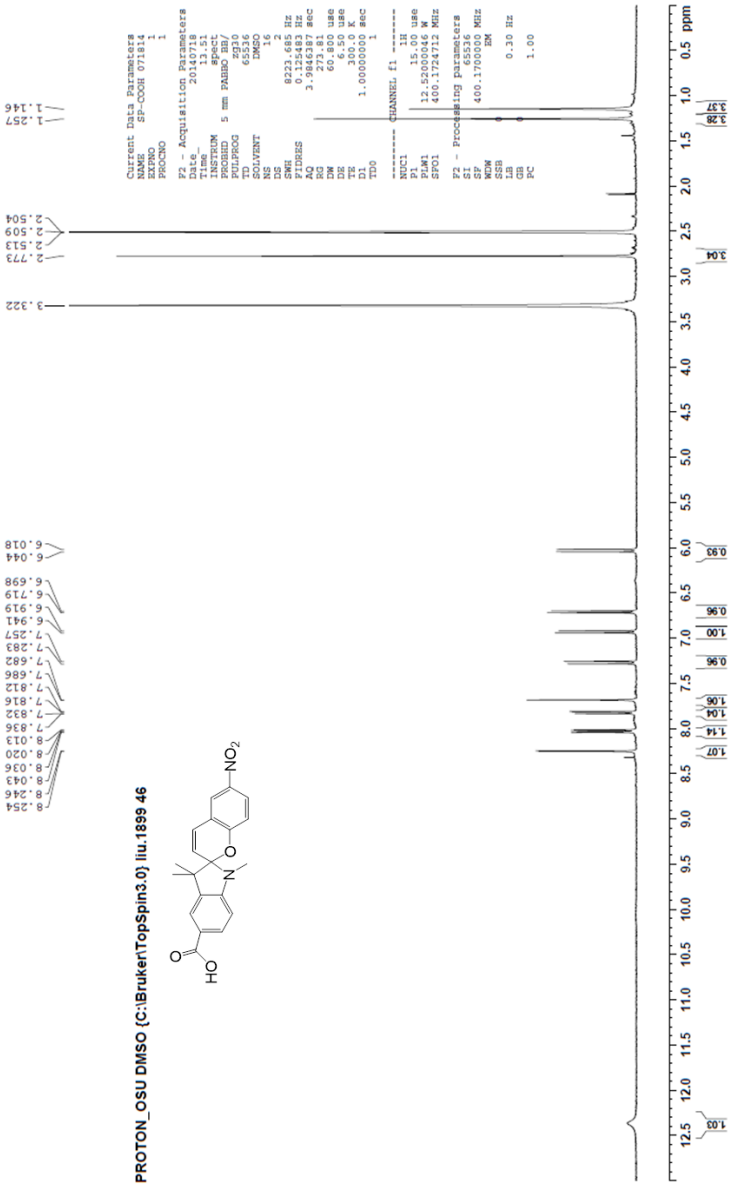

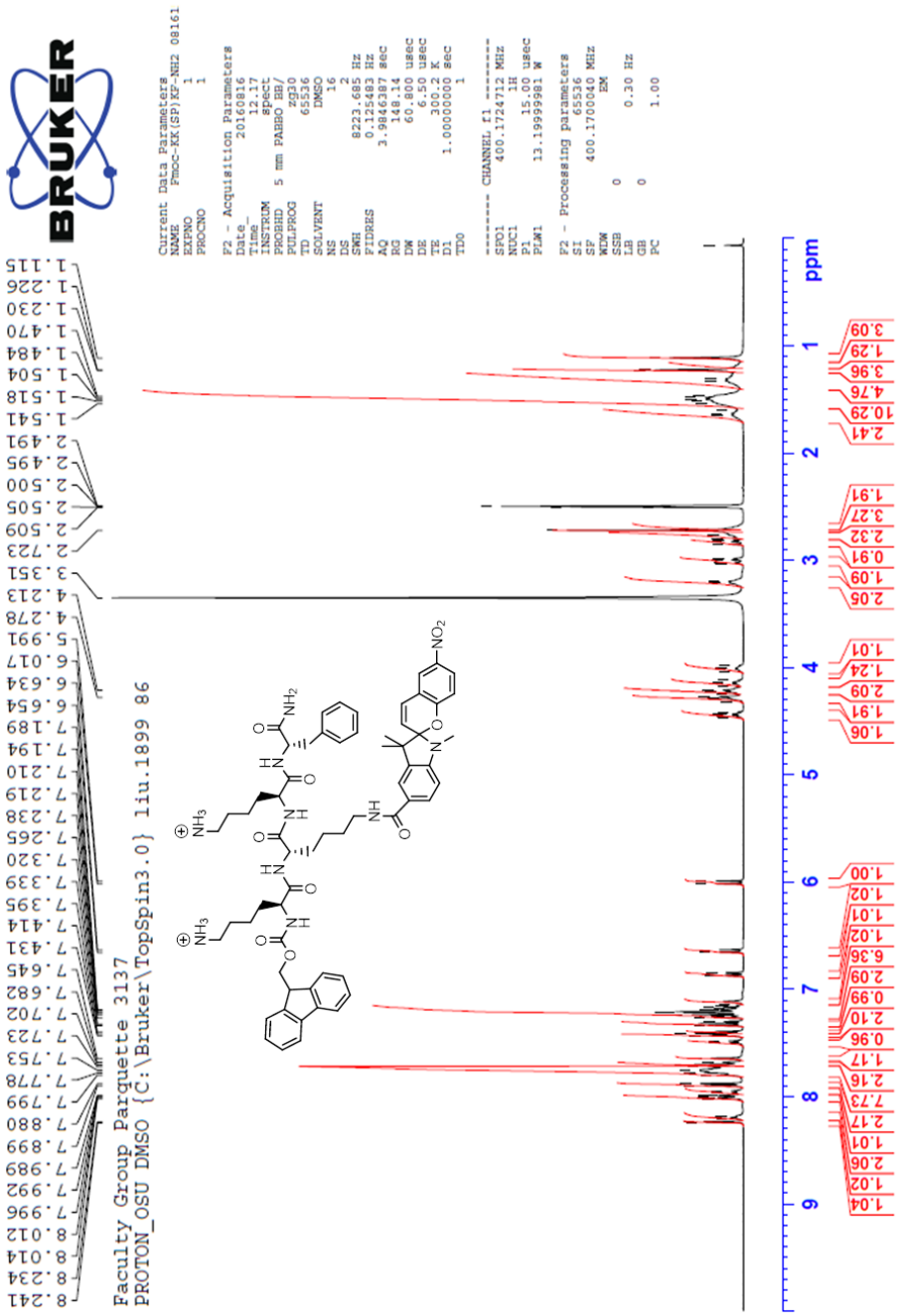
Faculty Group Parquette 3137
PROTON_OSU DMSO {C:\Bruker\TopSpin3.0} liu.1899 86
ppm

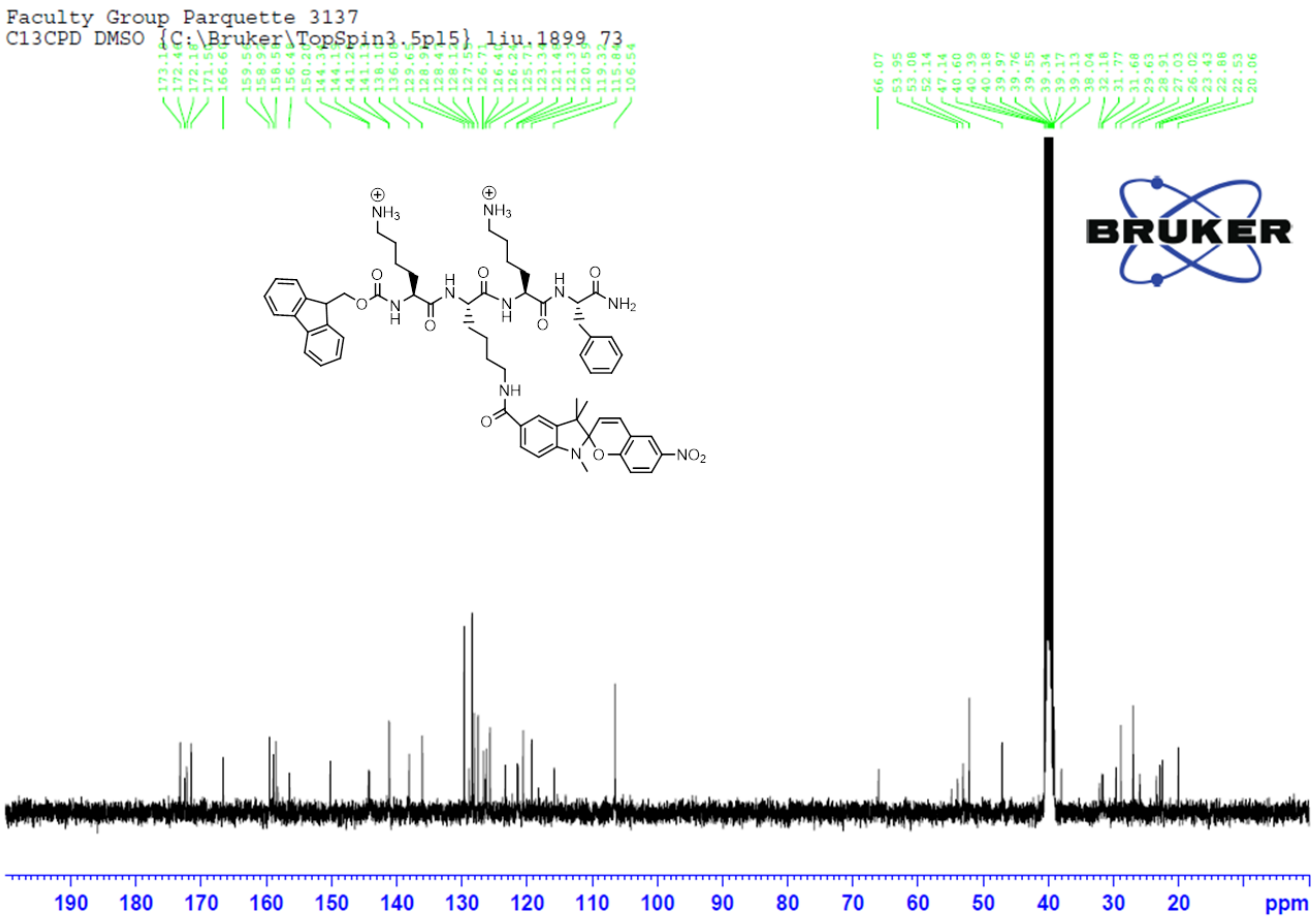
Faculty Group Parquette 3137
C13CPD DMSO {C:\Bruker\TopSpin3.5pl5} liu.1899 73
BRUKER
190 180 170 160 150 140 130 120 110 100 90 80 70 60 50 40 30 20 ppm

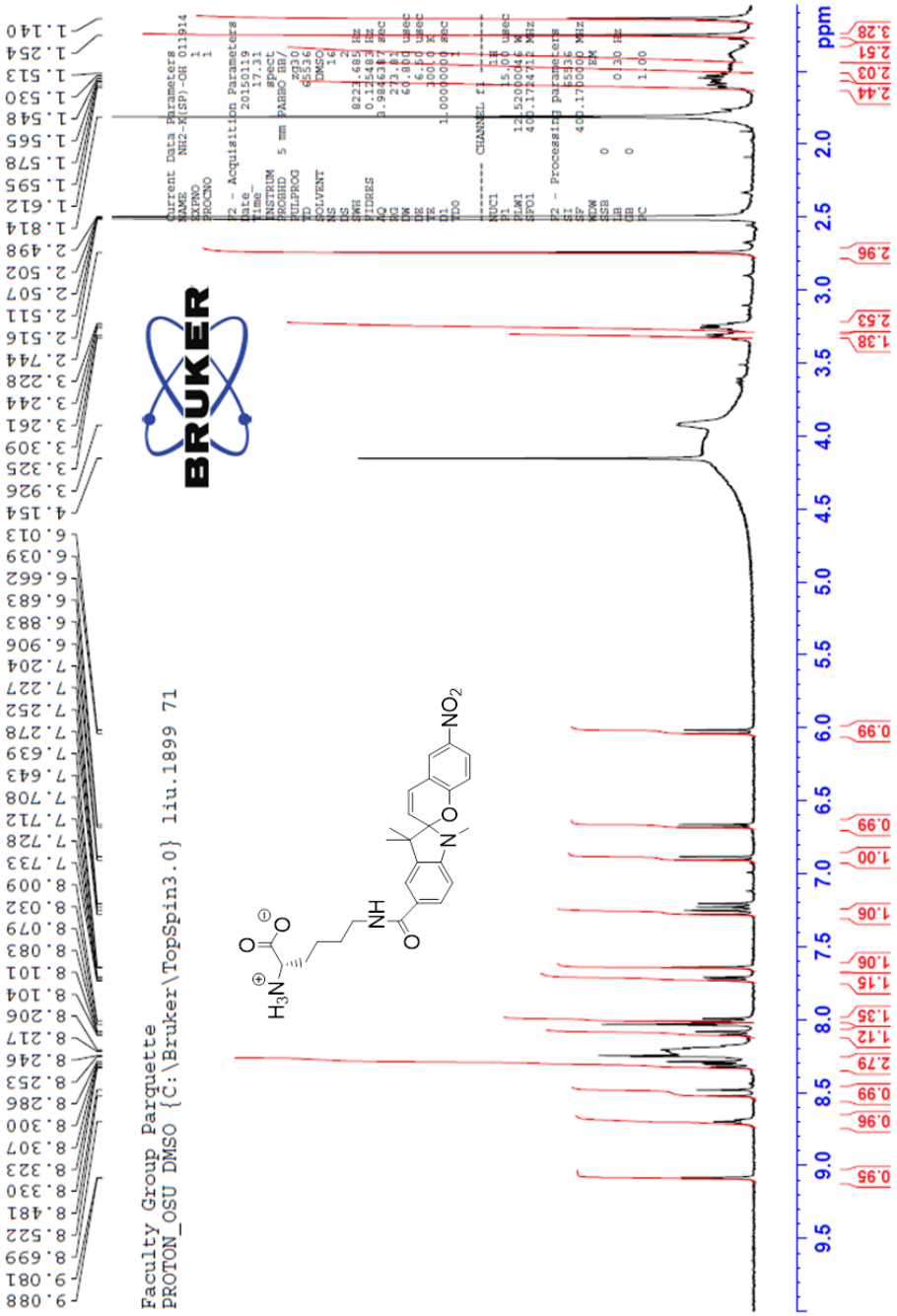
Faculty Group Parquette
PROTON_OSU DMSO {C:\Bruker\TopSpin3.0} liu.1899 71
BRUKER
ppm

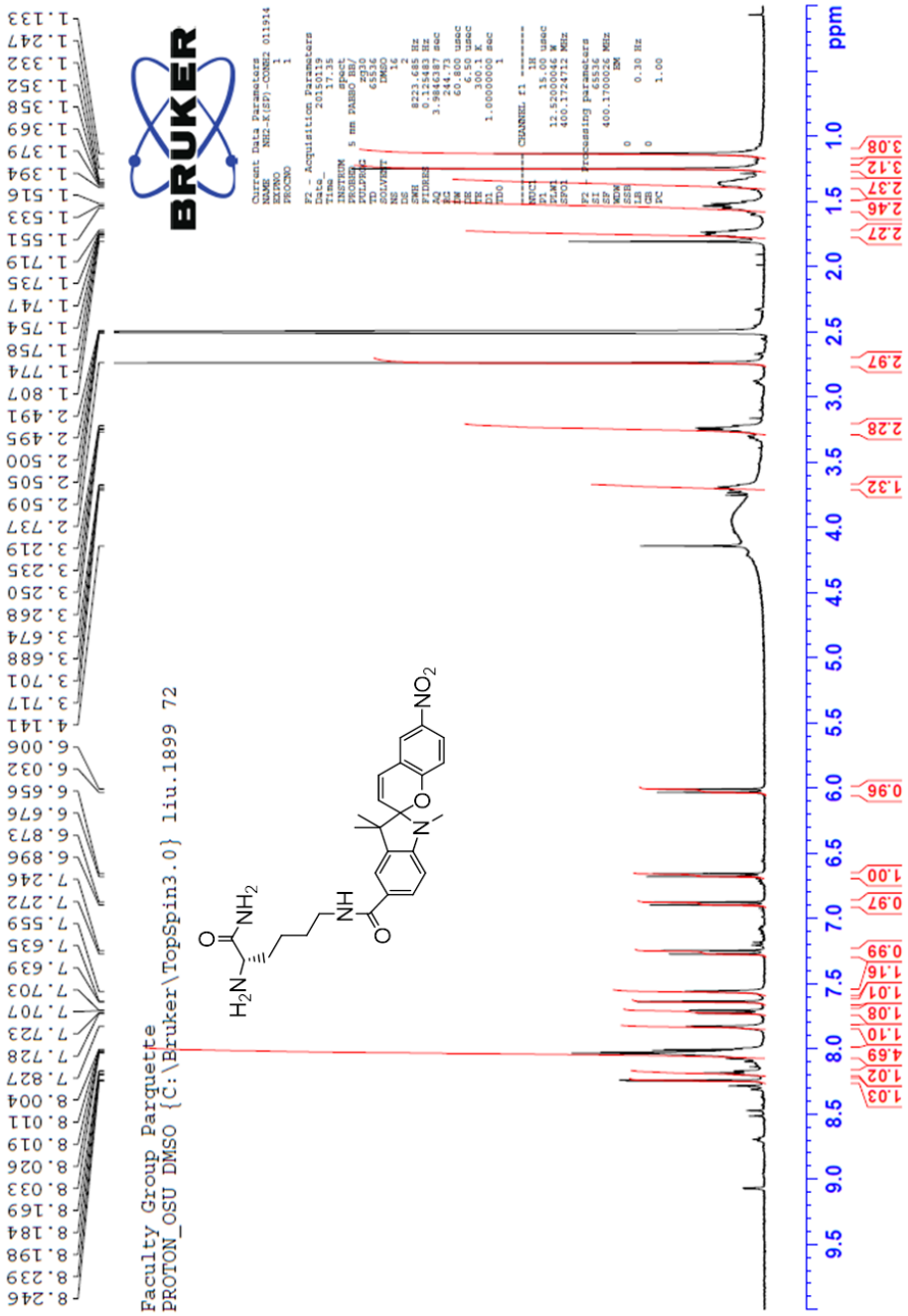
Faculty Group Parquette
PROTON_OSU DMSO {C:\Bruker\TopSpin3.0} liu.1899 72
ppm

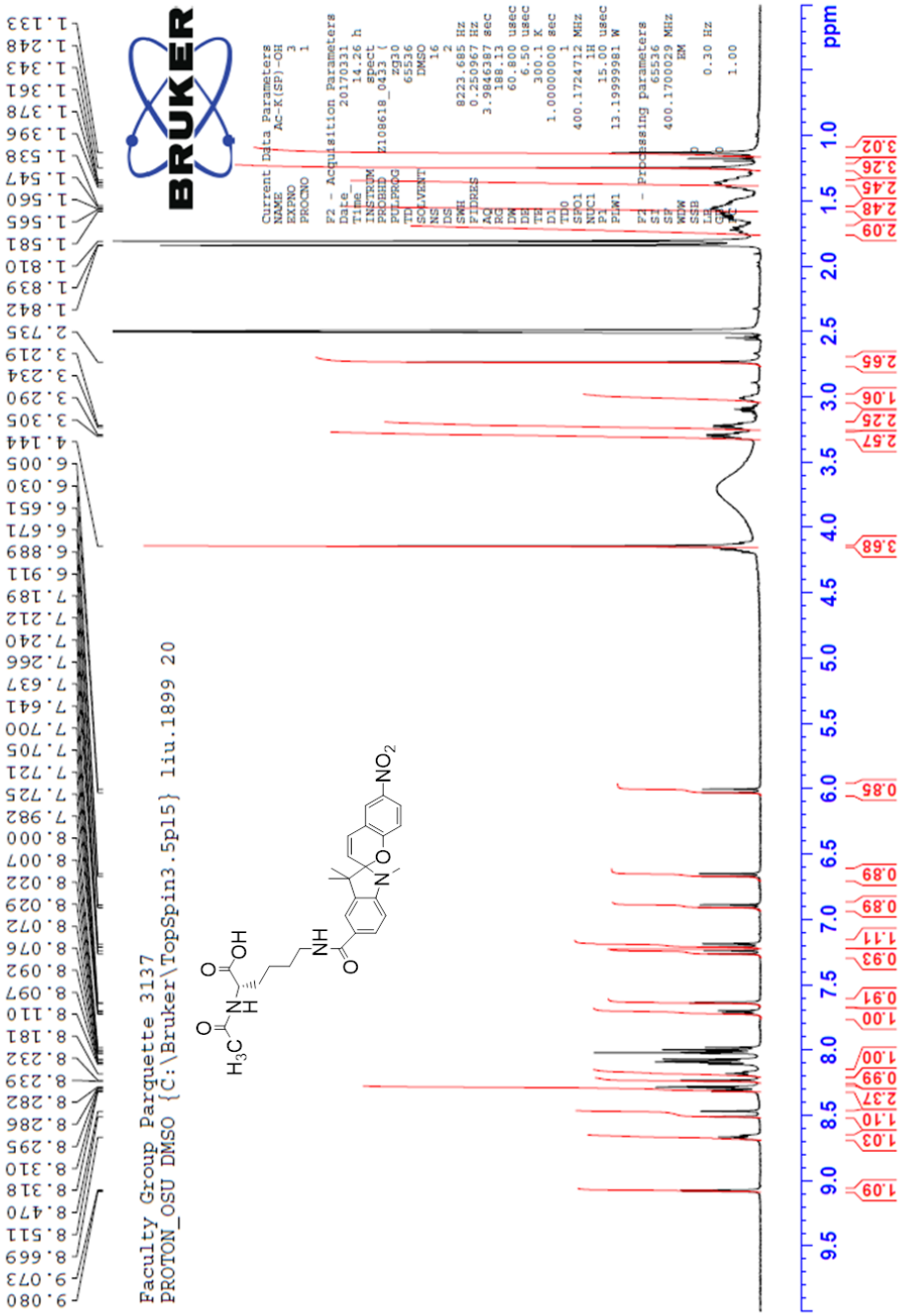
Faculty Group Parquette 3137
PROTON_OSU DMSO {C:\Bruker\TopSpin3.5pl5} liu.1899 20
ppm

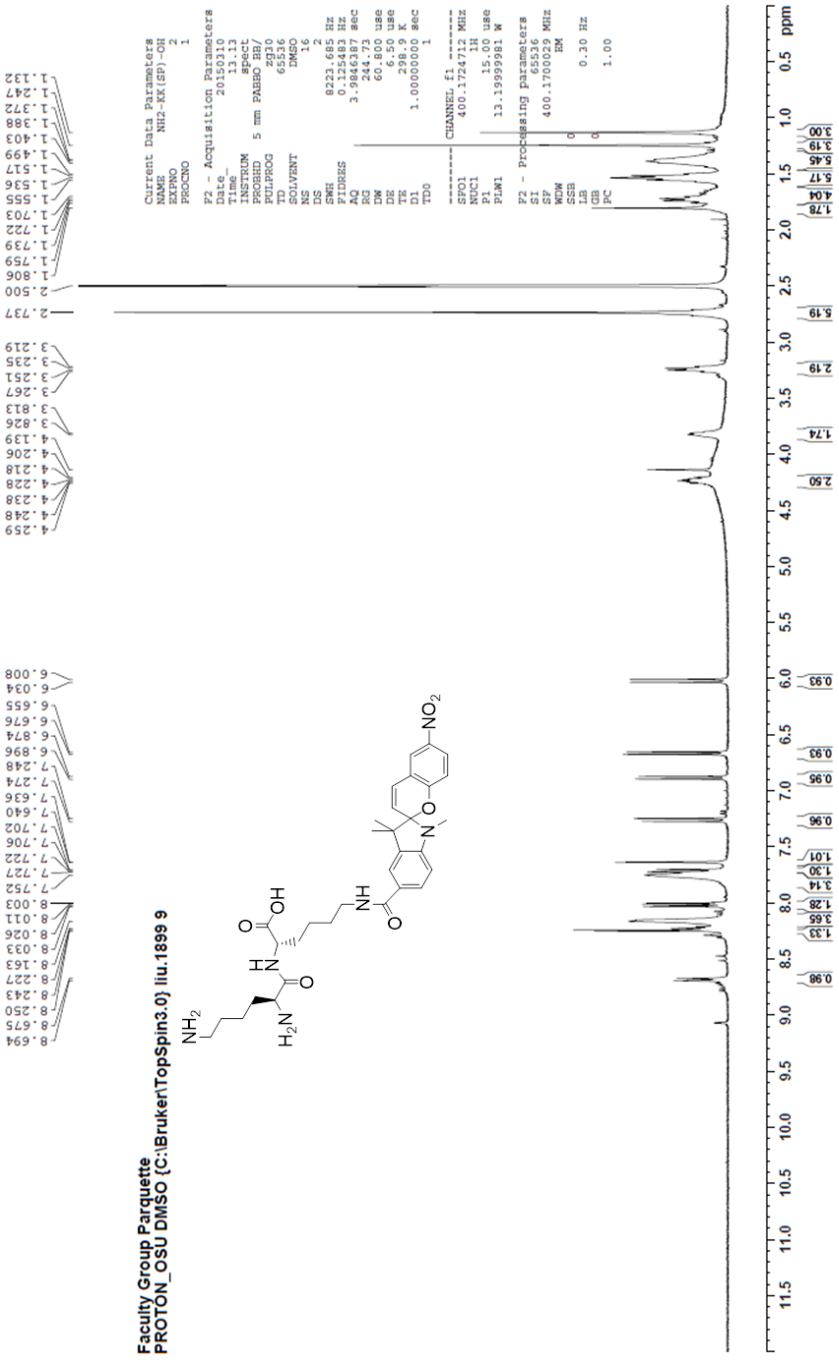
Faculty Group Parquette
PROTON_OSU DMSO (C:\Bruker\TopSpin3.0) liu.1899 9
Current Data Parameters
NAME NH2-KK(SP)-OH
EXPNO 2
PROCNO 1
F2 - Acquisition Parameters
Date_ 20151210
Time 13.13
INSTRUM spect
PROBHD 5 mm PABBO BB/
PULPROG zg30
TD 65536
SOLVENT DMSO
NS 16
DS 2
SWH 8223.685 Hz
FIDRES 0.125483 Hz
AQ 3.9846387 sec
RG 244.73
DW 60.800 usec
DE 6.50 usec
TE 298.9 K
D1 1.00000001 sec
TD0 1
CHANNEL f1
SFO1 400.1724712 MHz
NUC1 1H
P1 15.00 usec
PLW1 13.19999981 W
F2 - Processing parameters
SI 65536
SF 400.1700029 MHz
WDW EM
SSB 0
LB 0.30 Hz
GB 0
PC 1.00
NH2
H2N
O
OH
N
H
O
NH
O
O
N
NO2
ppm

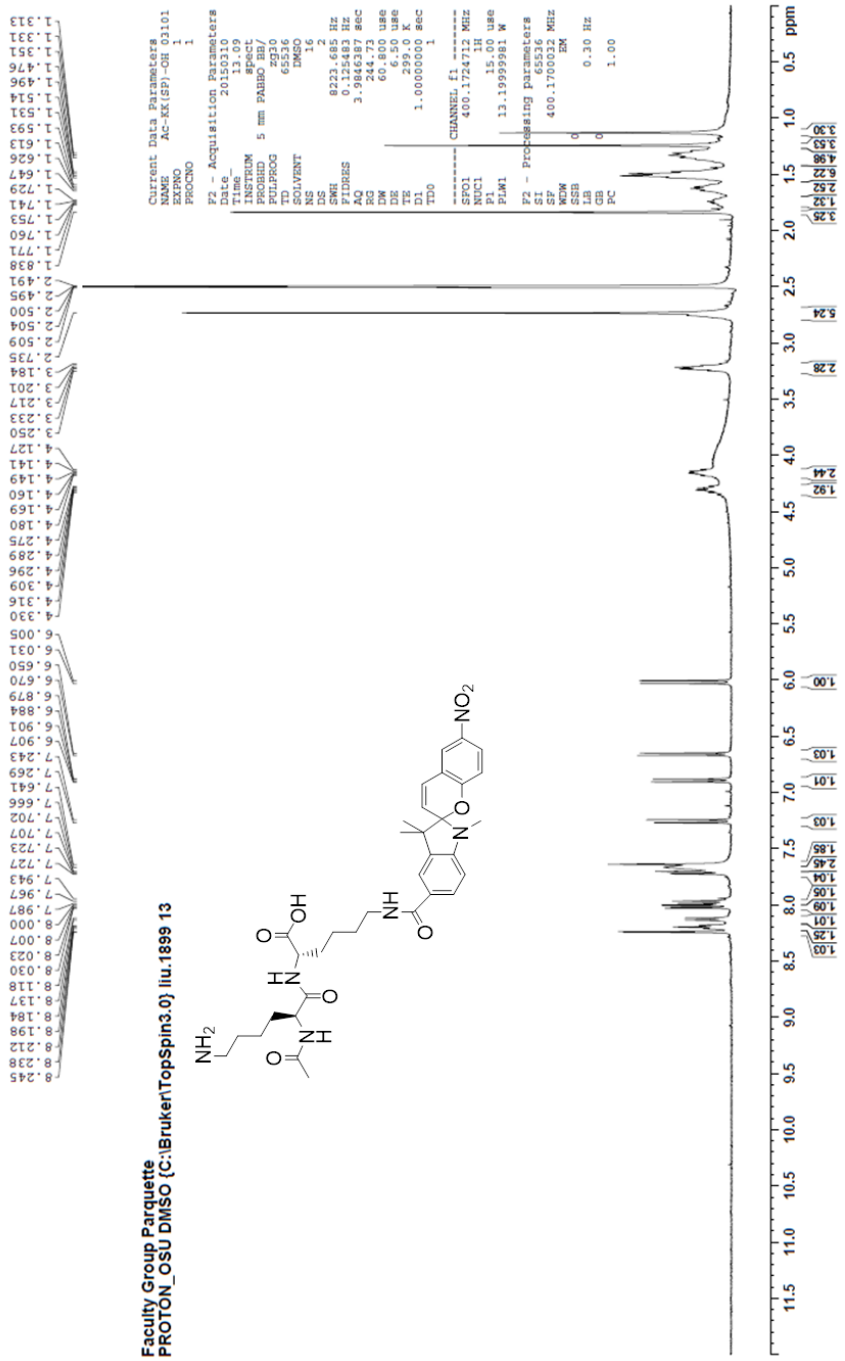
Faculty Group Parquette
PROTON_OSU DMSO (C:\Bruker\TopSpin3.0) liu.1899 13
Current Data Parameters
NAME Ac-KK(SP)-OH 03101
EXPNO 1
PROCNO 1
F2 - Acquisition Parameters
Time 20:51:10
INSTRUM spect
PROBHD 5 mm PABBO BB/
PULPROG zg30
TD 65536
SOLVENT DMSO
NS 16
DS 2
SWH 8223.685 Hz
FIDRES 0.125483 Hz
AQ 3.9846387 sec
RG 244.73
DW 60.800 usec
DE 6.50 usec
TE 298.0 K
D1 1.00000001 sec
TD0 1
CHANNEL f1
SFO1 400.1724712 MHz
NUC1 1H
P1 15.00 usec
PLW1 13.19999981 W
F2 - Processing parameters
SI 65536
SF 400.1700032 MHz
WDW EM
SSB 0
LB 0.30 Hz
GB 0
PC 1.00
ppm

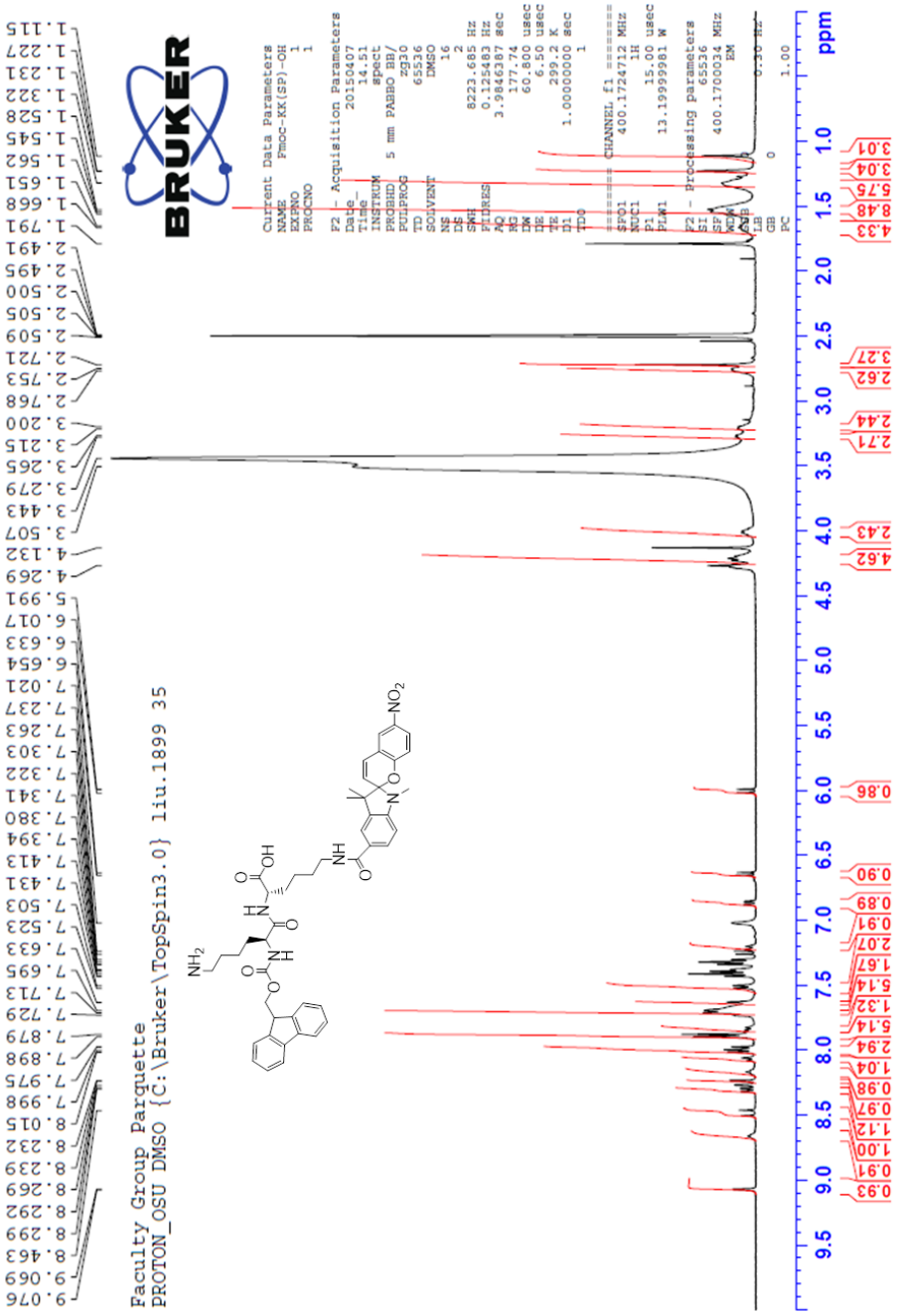
Faculty Group Parquette
PROTON_OSU DMSO {C:\Bruker\TopSpin3.0} liu.1899 35
Current Data Parameters
NAME Fmoc-KK(SP)-OH
EXPNO 1
PROCNO 1
F2 - Acquisition Parameters
Date_ 20150407
Time 14.51
INSTRUM spect
PROBHD 5 mm PABBO BB/
PULPROG zg30
TD 65536
SOLVENT DMSO
NS 16
DS 2
SWH 8223.685 Hz
FIDRES 0.125403 Hz
AQ 3.9846387 sec
RG 177.74
DW 60.800 usec
DE 6.50 usec
TE 299.2 K
D1 1.00000000 sec
TD0 1
======== CHANNEL f1 ========
SFO1 400.1724712 MHz
NUC1 1H
P1 15.00 usec
PLW1 13.19999981 W
F2 - Processing parameters
SI 65536
SF 400.1700034 MHz
WDW EM
SSB 0
LB 0.30 Hz
GB
PC 1.00
ppm

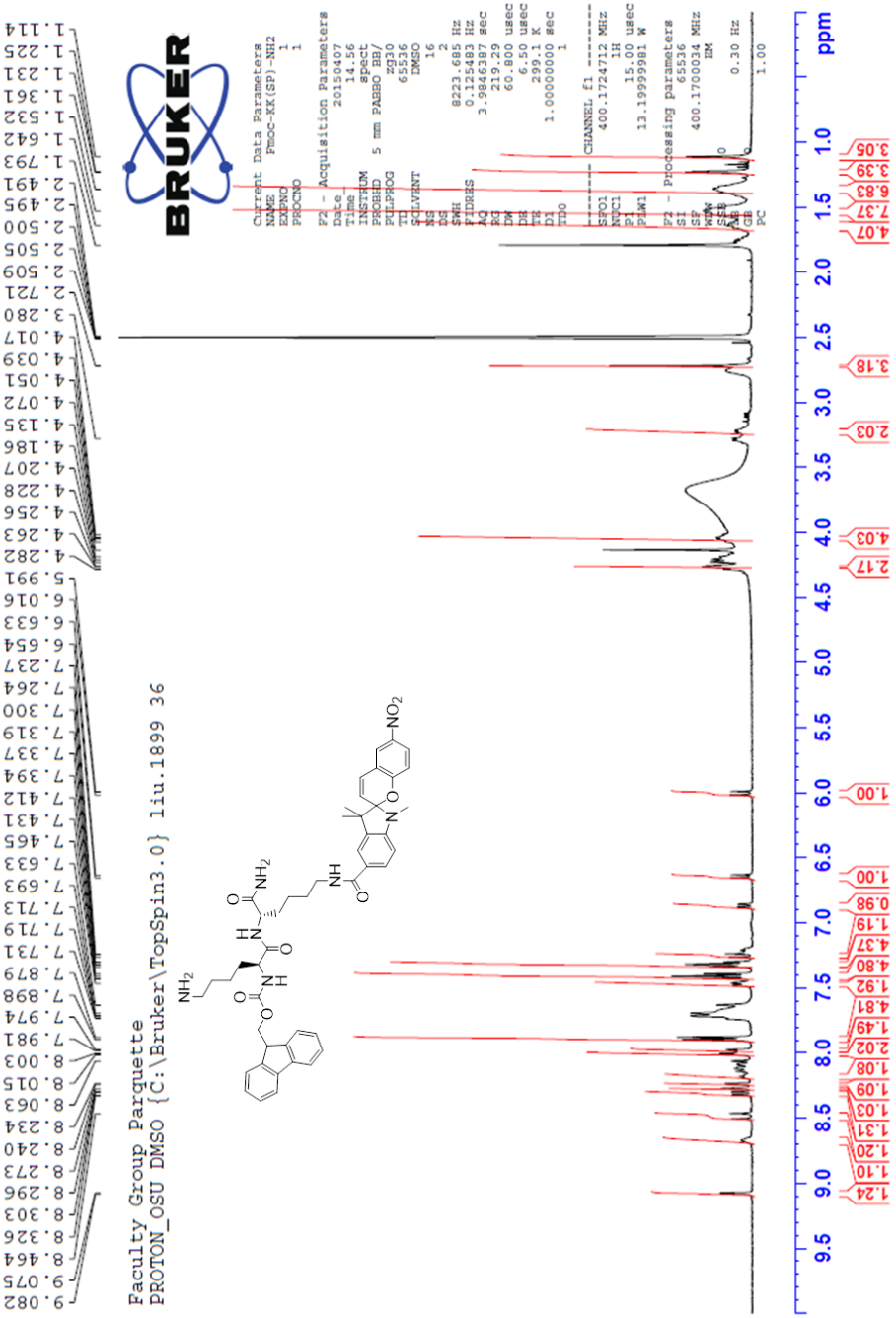
Faculty Group Parquette
PROTON_OSU DMSO {C:\Bruker\TopSpin3.0} liu.1899 36
ppm

Appendix B: ESI and HPLC Purity Analysis

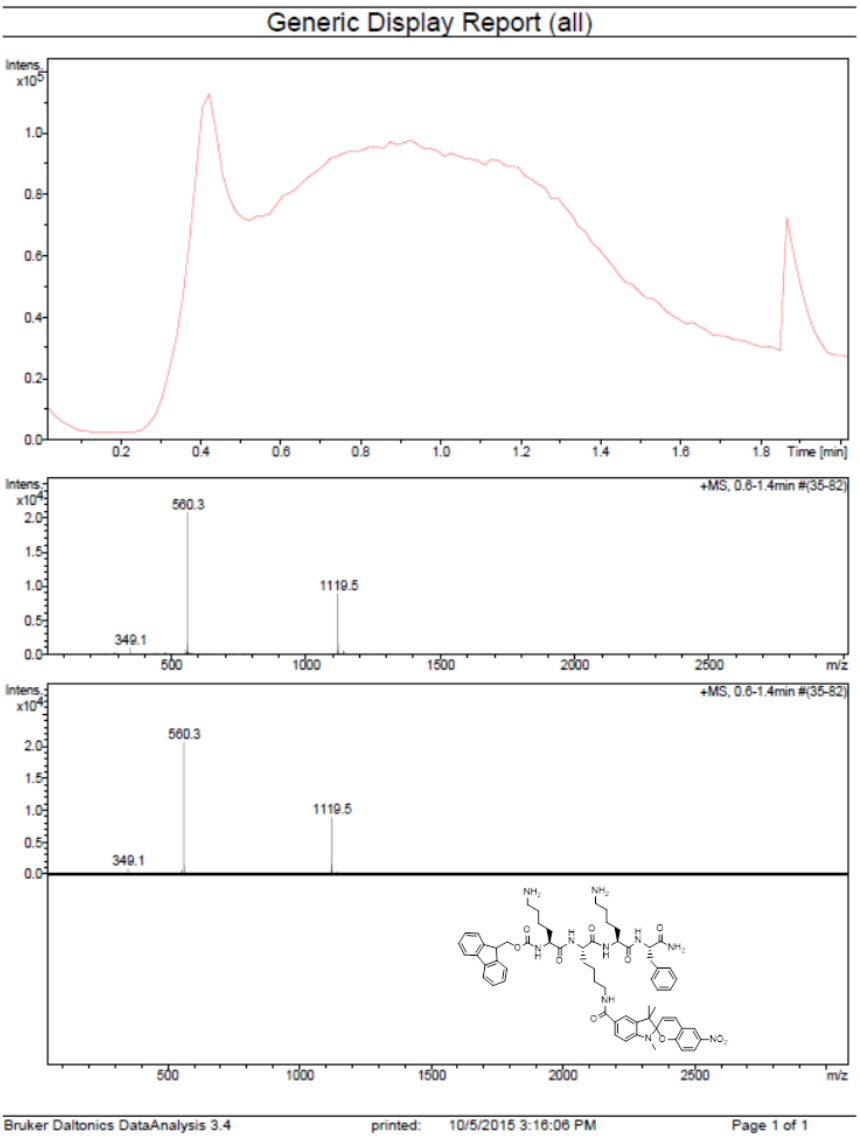

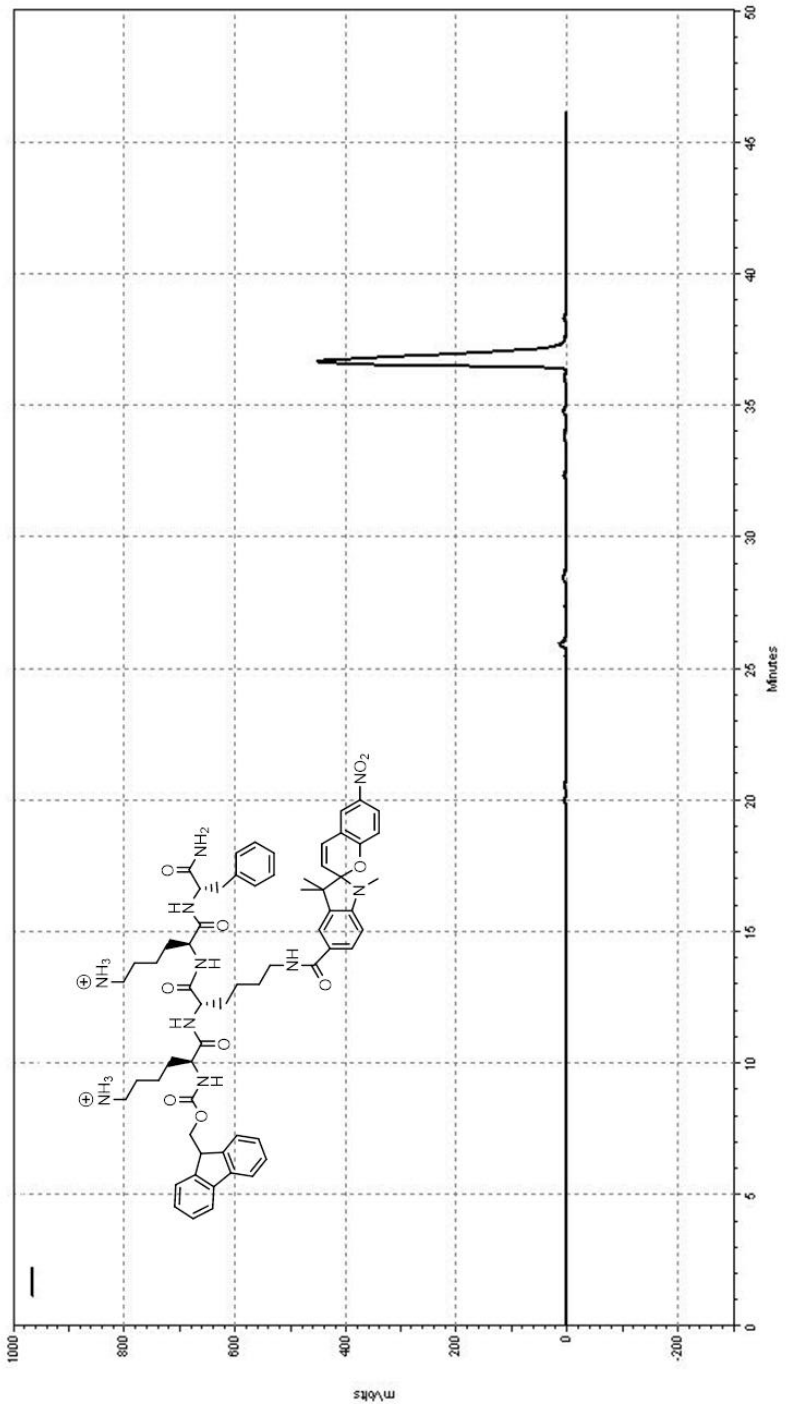
mVolts
1000
800
600
400
200
0
-200
0
5
10
15
20
25
30
35
40
45
50
Minutes
NO2
NH2
NH3
NH3